



UNIVERSITY OF CATANIA

DEPARTMENT OF CHEMICAL SCIENCES

INTERNATIONAL PhD IN CHEMICAL SCIENCES – XXXIII CYCLE

The INCIPIT-COFUND project co-funded by HORIZON 2020/Marie Skłodowska Curie

Ikhlas Mohamed Mohamud Ahmed

Getting Insight into the Molecular Determinants of Foldopathies

PhD Thesis

CNR Tutor: Dr. Francesco Bellia

University Tutor: Prof.ssa Graziella Vecchio

PhD Coordinator:

Prof. Salvatore Sortino

To all the members of my family, specifically to my lovely father, my kind mother and to the one who saved me from 3 years of loneliness; my amazing sister Fatma.

Table of Contents

Aim of the Research.....	6
Chapter 1	7
Introduction.....	7
1.1. Foldopathies and aggregation	7
1.2. The interplay between α -Syn, Copper(II) and Acrolein.....	9
1.2.1. α -Syn and metal ions.....	11
1.2.2. α -Syn and RCS.....	13
1.2.2.1. α -Syn and acrolein	15
1.3. Interplay between amyloid beta, proteasome 20S and Ubiquitin.....	16
1.3.1. Clearance system and Amyloid beta	16
1.3.2. A β and metal ions	20
1.4. Interplay between Alzheimer's disease and Diabetes mellitus	20
1.4.1. Cross seeding	20
1.4.2. Alzheimer's and Diabetes	24
1.4.3. Insulin degrading enzyme and nociceptin/orphanin FQ	24
1.5. Therapeutic compounds	26
1.5.1. Proteomic approach for mass spectrometry.....	26
1.5.2. Anti-aggregation Compounds.....	28
1.6. Overview.....	29
Chapter 2.....	31
Material and Methods	31
2.1. α -Syn purification.....	34
2.2. α -Syn carbonylation assay	35
2.2.1. Dynamic light scattering.....	35
2.2.2. Circular dichroism.....	36
2.2.3. Aggregation assay	36
2.2.4. MDA and α -Syn.....	36
2.3. α -Syn interactions with compounds.....	37
2.3.1. Native mass spectrometry.....	37
2.3.2. Aggregation assay	37

2.3.3. Influence of citicoline on 20S proteasome	37
2.4. α -Syn and Amyloid beta	38
2.4.1. IDE, α -Syn and Amyloid beta	38
2.4.2. Aggregation assay	38
2.5. Proteasome 20S action on A β	38
2.5.1. 20S mediated A β ₁₋₄₀ hydrolysis	38
2.5.2. A β ₁₋₄₀ hydrolysis and Ub role	39
2.5.3. 20S mediated A β ₁₆₋₂₈ hydrolysis.....	39
2.5.4. The effect of A β ₁₋₄₀ on 20S mediated A β ₁₆₋₂₈ hydrolysis	39
2.5.5. 20S mediated A β ₁₋₂₈ hydrolysis	39
2.5.6. The effect of AP on 20S mediated A β ₁₋₂₈ hydrolysis	40
2.6. Insulin degrading enzyme.....	40
2.6.1. IDE and nociceptin/orphanin FQ	40
2.6.2. Mutant IDE hydrolysis of amyloid beta.....	40
2.7. Supplementary experiments.....	40
2.7.1. PICUP.....	41
2.7.2. SPR experiment.....	41
Chapter 3.....	42
Results and Discussion.....	42
3.1. The interplay between α -Syn's carbonylation, aggregation and metal ions	43
3.1.1. α -Syn carbonylation by ACR.....	43
3.1.2. DLS and CD measurements	49
3.1.3. Aggregation assay syn-ACR	52
3.1.4. P2 peptide and ACR	53
3.1.5. MDA and α -Syn.....	55
3.2. α -Syn interaction with compounds.....	59
3.2.1. Native mass spectrometry.....	59
3.2.2. Aggregation assay	69
3.2.3. Citicoline and 20S proteasome	71
3.3. α -Syn and amyloid beta.....	72
3.3.1. IDE, α -Syn and amyloid beta	72

3.3.2. Aggregation assay	78
3.4. Proteasome 20S action on Aβ: effect of Ub and AP	79
3.4.1. 20S mediated Aβ₁₋₄₀ hydrolysis	79
3.4.2. Aβ₁₋₄₀ hydrolysis and Ub role	80
3.4.3. The effect of Aβ₁₋₄₀ on 20S mediated Aβ₁₆₋₂₈ hydrolysis	82
3.4.4. 20S mediated Aβ₁₋₂₈ hydrolysis	83
3.4.5. The effect of AP on 20S mediated Aβ₁₋₂₈ hydrolysis	84
3.5. Insulin degrading enzyme and its studies	86
3.5.1. Insulin degrading enzyme and nociceptin/orphanin FQ	86
3.5.2. Insulin degrading enzyme mutation and the role of metal ion	92
Concluding remarks	95
Acknowledgment.....	97
List of abbreviations	99
References	102
Scientific activities.....	107
Supplementary material.....	110

Aim of the Research

The general aim of this project is to inspect the molecular determinants of foldopathies. These widespread diseases, including Parkinson's and Alzheimer's disorders, are characterized by the misfolding of targeted proteins. In this project, we aim to tackle some common factors that could trigger the onset of these disorders. Since the protein aggregation is a common pathological pathway, we are investigating biochemical events that may affect this process, either singularly or in combination.

In particular, the experimental activities carried out during the three years of the PhD program were mainly focused on the optimization of protein purification protocol for the protein α -synuclein and subsequently studying this protein using different techniques. Moreover, the protein amyloid beta was also recruited in these studies. The effect of reactive carbonyl species, clearance systems and therapeutic compounds were also investigated. Mass spectrometry techniques were heavily enlisted throughout this project. The in-depth understanding of the factors involved in the early stages of the disorders could represent an important achievement for the development of customized therapeutic approaches.

Chapter 1

Introduction

In this Chapter, there is a brief introduction about diseases associated with protein disorder/aggregation. Then, the bulk of the introduction constitute factors that play part in protein aggregation and subsequently in these diseases. They include oxidative stress, metal ions, post-translational modifications and reactive carbonyl species among others. The interplay between each of these factors and two proteins that are aggregation prone (α -Syn and A β) is explained in the following sections with a major emphasis on the protein α -Syn. Moreover, clearance systems and enzymes involved in getting rid of excess protein before a pathological consequence are explored. Cross seeding as a factor contributing to protein aggregation and as a mean to link different protein conformational diseases is touched upon. The chapter is concluded with a small focus on native mass spectrometry and some therapeutic approaches, which are employed in this study.

1.1. Foldopathies and aggregation

Proteopathies, proteinopathies, protein conformational disorders or protein misfolding diseases (PMD) all refer to diseases that result from improperly folded proteins. Consequently, soluble oligomers, protein aggregates and insoluble fibrils are formed leading to toxicity. The main players in PMD are Intrinsically Disordered Proteins (IDPs) which are highly capable of fibril formation due to their unstructured nature. Briefly, IDPs are proteins with a high content of disorder promoting amino acids (charged amino acids in addition to glycine and proline), while possessing a reduced content of order promoting amino acids (hydrophobic and aromatic amino acids)¹. Proteins can have Intrinsically Disordered Regions (IDRs) of various amino acid lengths or completely disordered regions as seen in Figure 1.1. For this reason, any protein (including globular “highly structured” proteins) is capable of aggregation and/or fibril formation. The accumulation of protein aggregates in tissues, such as amyloid beta (A β) and alpha synuclein (α -Syn) fibrils, is the main histological hallmark of Alzheimer’s and Parkinson’s diseases,

respectively. Both A β and α -Syn are IDPs, and their structural and functional investigation is the main focus of this thesis ¹.

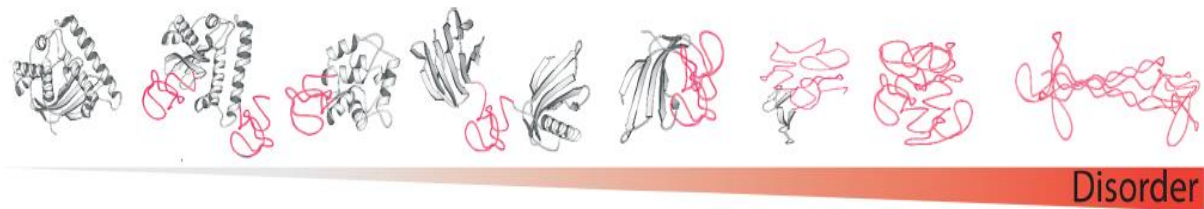


Figure 1.1 Continuum of a Protein Conformational Disorder. From Left: “no disorder/completely ordered” to Right: “completely disordered protein”. Corresponding disordered regions are shown in red. Copyright 2005 John Wiley and Sons, Inc¹.

Typically for amyloidogenic proteins (A β , α -Syn), the aggregation starts with monomer and proceeds to oligomers (most toxic species), protofibrils, protofilaments and finally fibrils (Figure 1.2). There is a link between protein aggregation and PMD and several methods are involved in the detection of these species. Usually, the oligomer forms are spotted by antibody assays, whereas the formation of fibril species can be followed by a thioflavin T (ThT) fluorescence assay where the fluorescence signal is directly proportional to fibril formation as a function of time (Figure 1.3A). Moreover, these aggregates take up different shapes when observed under a microscope (Figure 1.3B). Amorphous aggregates can also form in an off-pathway aggregation process. Larger aggregates can be detected via transmission electron microscopy (TEM). Oligomers, on the other hand, require atomic force microscopy (AFM) for visualization².

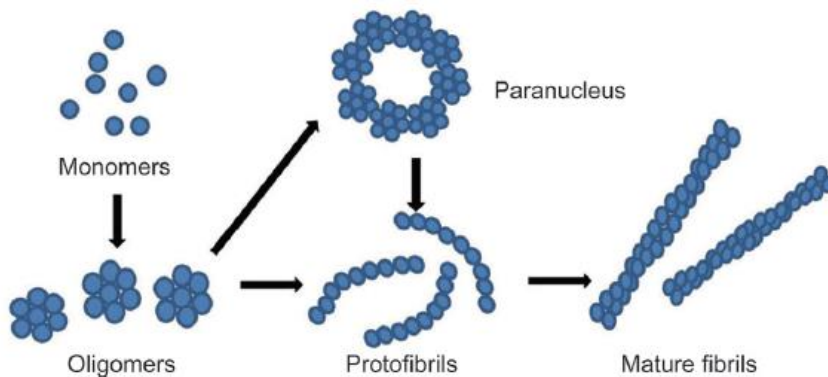


Figure 1.2. Fibril formation process for A β , from monomers to mature fibrils³.

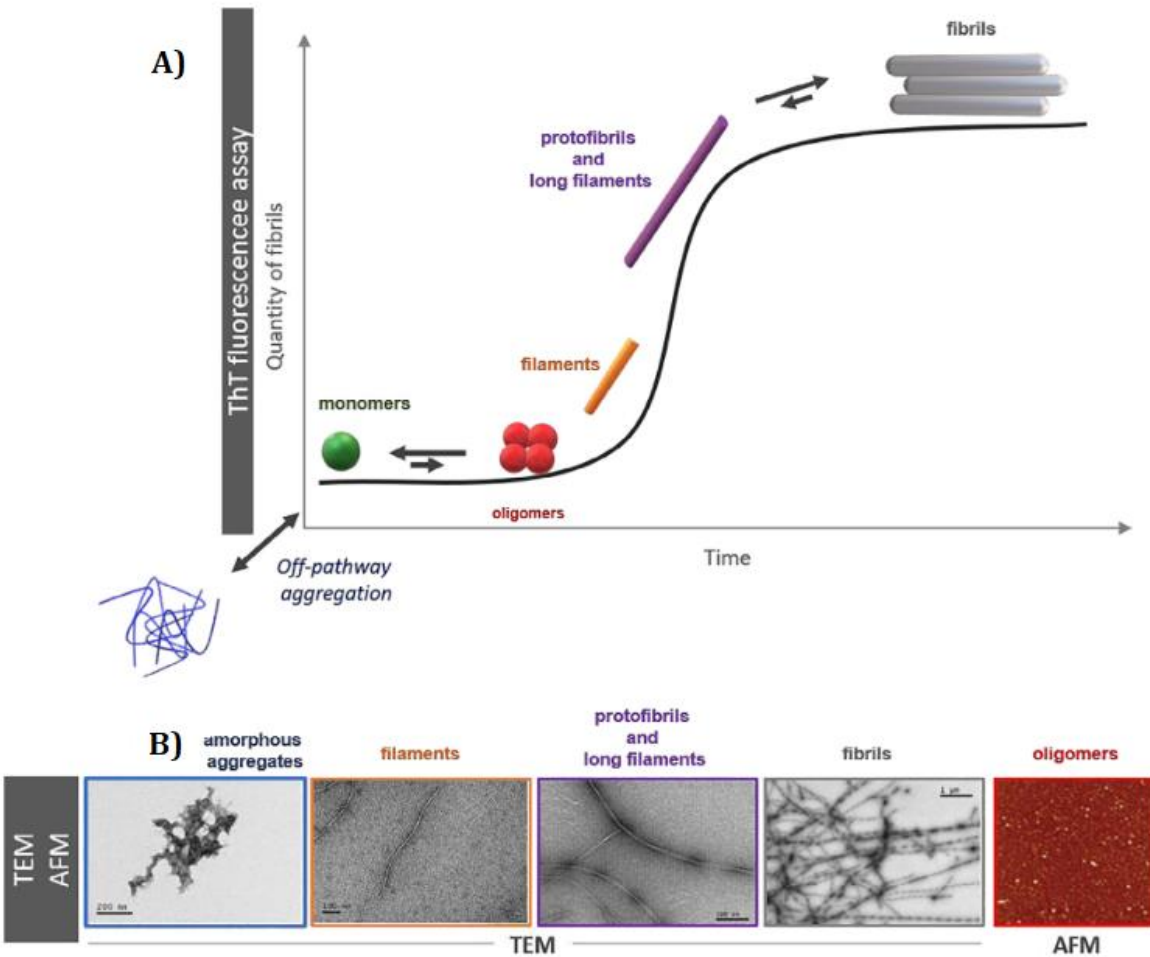


Figure 1.3. The different stages of fibril formation and the monitoring mechanisms by means of different techniques, A) ThT Fluorescence assay and B) TEM/AFM ².

1.2. The interplay between α -Syn, Copper(II) and Acrolein

Synucleinopathies are neurodegenerative disorders characterized by the misfolding of α -Syn. The main histological hallmark is the abnormal accumulation of α -Syn aggregates in Lewy Body (LB)⁴ deposits within neurons, nerve fibers or glial cells. Synucleinopathies include Parkinson's disease (PD) and Parkinson's disease with dementia (PDD)⁵. Notwithstanding the efforts that the scientists have been spending to understand the mechanism of the disease, there is no treatment yet for PD. Mutations of SNCA (the α -Syn gene) were found in PD patients⁵. So far, six mutations of SNCA were detected: A53T, A30P, E46K, H50Q, G51D, and A53E6. α -Syn function, although largely unknown, should be mainly related to the presynaptic terminal⁵.

α -Syn is an IDP containing 140 amino acids (MW 14 kDa, Figure 1.4 were the primary sequence is displayed). N-terminus (residues 1-60) is rich in lysine residues and involved in the membrane interaction; it contains six conserved sequences similarly to lipid-binding lipoprotein motifs⁶. Moreover, when the protein is mutated at A30P, α -Syn does not bind to lipid vesicles which points to a potential α -Syn function. The relationship between lipids and α -Syn is further proved by the involvement of α -Syn in lipid transport⁷. The disordered C-terminus (residues 96-140) is negatively charged and interacts with small molecules and other proteins.

The non-amyloid β component (NAC, residues 61-95, underlined Figure 1.4) is the hydrophobic central region responsible for aggregation; in particular, residues 71-82 of NAC are prone to form β -sheet structures. β -synuclein (β -Syn) does not aggregate as it lacks 11 amino acids (residues 73-83) in the NAC region in comparison to α -Syn. Therefore, β -Syn could play a role in preventing α -Syn aggregation⁶. Due to the extended disordered form, α -Syn has a flexible structure and hence a broad spectrum of potential functions^{5,6}.

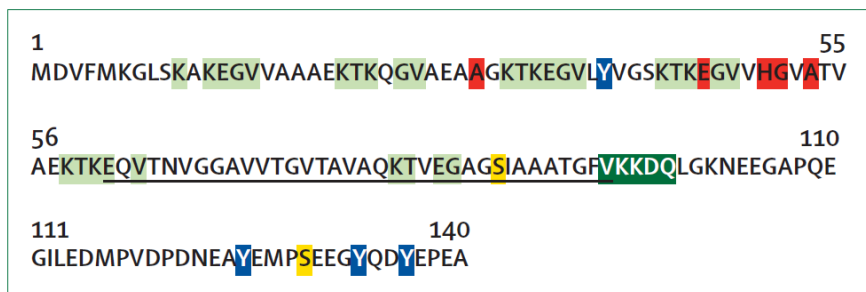


Figure 1.4. Primary structure of α -Syn. Color code: light green = N-terminal repeats, red = mutation sites, blue=nitration sites, yellow=phosphorylation sites, Dark green= autophagy recognition sites and underlined is NAC region².

Post-translation modifications (PTMs, some of which are highlighted in Figure 1.4) of α -Syn related to LB and/or synucleinopathies include: 1. Phosphorylation⁸ at S87 and S129, the latter being especially abundant in LB. 2. Nitration⁹ at Y39, Y125 and Y133. 3. Oxidation by dopamine⁴ derivatives. 4. Truncation¹⁰ at C-terminal region near amino acid D121. Typically, the presence of PTMs, the coordination of metal ion (copper and zinc)

or increased protein concentration lead to aggregation and toxicity. The formation of oligomers and aggregates increases α -Syn permeability across different membranes, (the mitochondrial, lysosomal and vesicular membrane), which subsequently increases intracellular calcium levels leading to cell death^{5,6}.

1.2.1. α -Syn and metal ions

A high concentration of the metal ions (copper, zinc and iron) is found in AD and PD aggregates². Metal ions are key players in PMD because: 1) metals interact with proteins which might lead to a) aggregation b) reactive oxygen species (ROS) production and c) toxicity and cell death; 2) metal homeostasis levels change in PMD. The modification of homeostasis is a telling sign for PD. In the presence of oxygen and ascorbic acid, the binding of α -Syn to metal ions leads to ROS which consequently leads to faster onset of neurodegeneration and damage to cells¹¹.

A link between α -Syn interaction with metal ions and an increased aggregation rate of α -syn have been thoroughly investigated^{2,11}. The protein coordination with divalent metal ions, such as copper(II) and zinc(II), facilitates the transition of α -Syn to a partially folded structure which is more prone to form aggregated species in comparison to monomeric form of α -Syn. *In vitro* studies have shown that several divalent metal ions in millimolar concentrations play a role in the oligomerization process, whereas only Cu^{2+} had an active role on the formation of protein fibrils when the metal ions were tested in the micromolar range¹², which is the relevant concentration in a physiological environment. Cu^{2+} - α -Syn forms at least three complex species, involving the N-terminal and the C-terminal regions (Figure 1.5). The N-terminal sequence has the higher affinity to Cu^{2+} (due to the first two amino acids M1 and D2). The formation of this species is abolished when the N-terminal residue is acetylated (a common PTM of α -Syn). Acetylated α -Syn is bound to Cu^{2+} via its unique His50 residue, albeit in lower affinity compared to the masked N-terminal site. Although there is accordant about the binding sites, the coordination mechanism is still unknown, as shown in Figure 1.6². C-terminal also coordinates Cu^{2+} , but its low binding affinity makes the complex species involving the N-terminal sequence more relevant to

physiological studies¹². The formation of different α -Syn - Cu²⁺ species could be attributed to the pH value and the metal ion concentration (Figure 1.7)².

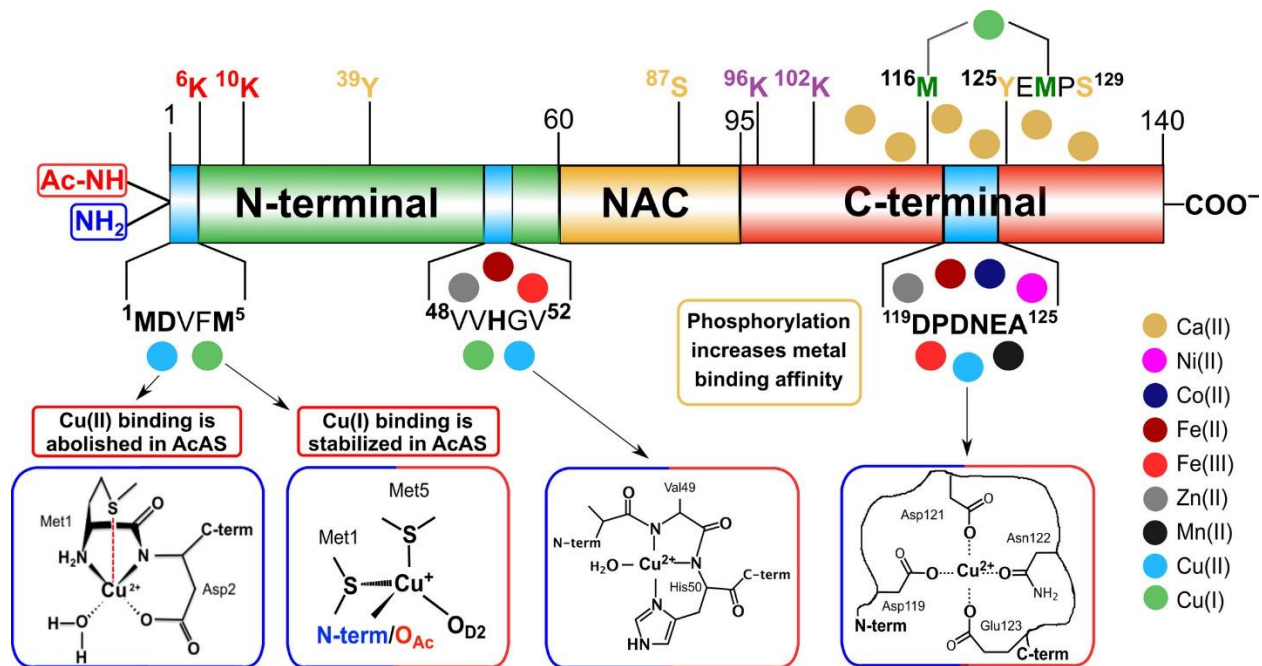


Figure 1.5. The binding sites of different metal ions on α -Syn¹².

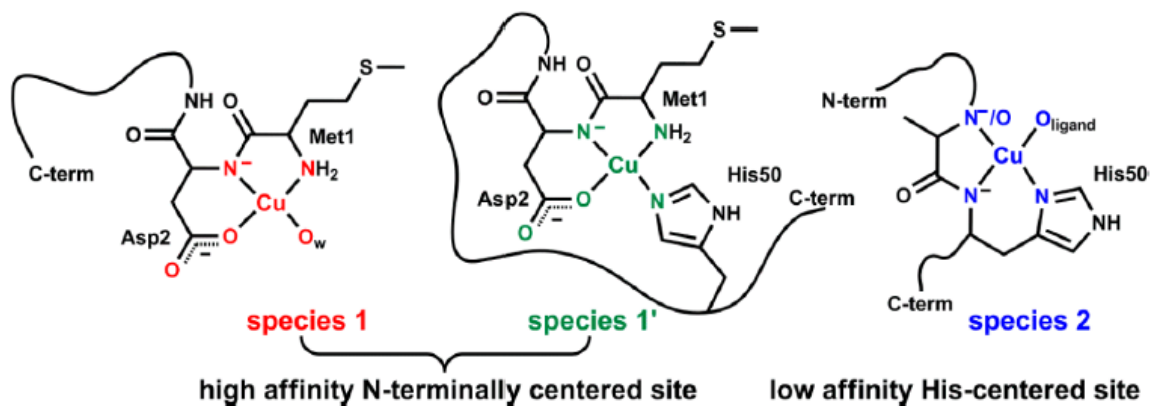


Figure 1.6. The low and the high affinity coordination of copper with α -Syn¹¹.

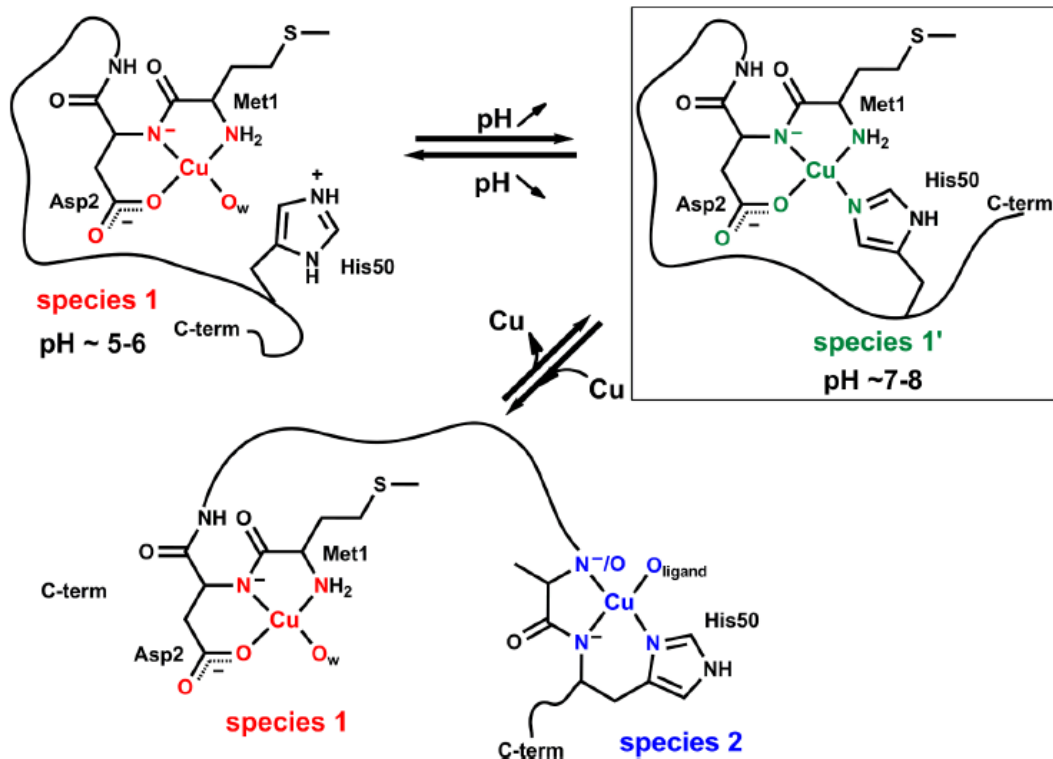


Figure 1.7. The effect of pH on copper coordination with α-Syn¹¹.

The unclear equilibrium between the Cu²⁺-α-Syn complex species notwithstanding, the unique His residue could play an important role on the copper coordination in the physiological environment. Histidine (his50) acts as the main N-terminal binding site for acetylated α-Syn which are increasingly present *in vivo*⁵. Moreover, the change of pH plays a major role in whether his50 binds Cu²⁺ or not. As seen in Figure 1.7, the coordination of α-Syn with Cu²⁺ is demonstrated in the presence and/or absence of his50 at pH 7-8, pH 5-6 respectively¹¹. Hence, the study of his50 coordination with Cu²⁺ under different conditions is essential. On the other hand, Zn²⁺ coordination for α-Syn is not well studied, although His50 and D121 could be involved².

1.2.2. α-Syn and RCS

α-Syn adopts different folding states depending on the chemical environment: the random coil content predominates in solution, the α-helix structure is preferred when the protein

is bound to phospholipids, whereas β -sheet layers form in amyloid-type fibrils. The N-terminal short repeats are linked to α -Syn-lipid interaction, which, in turn, could be involved in cell death. A30P mutation inhibits α -Syn from binding to lipids, which consequently contributes to α -Syn aggregation due to imbalance in lipid-bound-to-free α -Syn ratio. Hence the interaction of α -Syn with lipids and their derived products should be taken into account when studying the structural and functional features of α -Syn⁷.

Lipid peroxidation significantly contribute to the oxidative stress in the central nervous system (CNS)¹³. Lipid metabolism and lipid peroxidation produce Reactive Carbonyl Species (RCS), the most reactive of which are α,β -unsaturated aldehydes (Figure 1.8)¹⁴. These species normally form adducts with the side chain of few amino acids (Cys, Lys, His, and Arg). 4-hydroxy-2-nonenal (HNE, Figure 1.8) is one of the most reactive species and targets several proteins, including α -Syn. his50 is the main reactive site at low HNE concentrations (50-200 μ M)¹⁵; it is the driving force for HNE-induced α -Syn oligomerization¹⁵. The carbonylation of lysine side chains are also involved when the HNE dose increases. It leads to faster α -Syn aggregation and a severer toxic effect¹⁵.

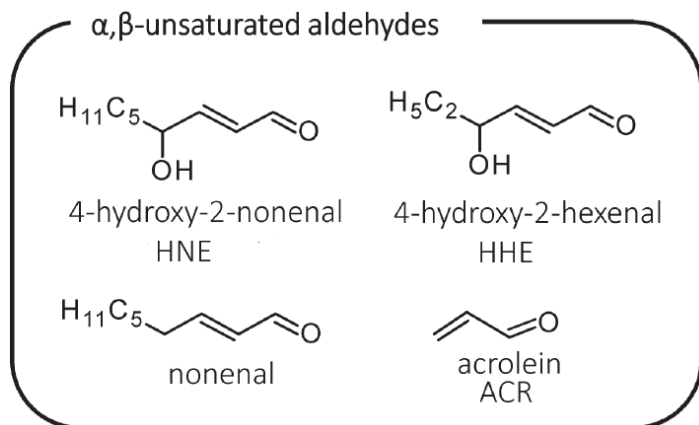


Figure 1.8. The structure of α,β saturated aldehydes¹⁴.

Malondialdehyde (MDA) belongs to the di-aldehyde group of short-chain RCS alongside glyoxal (Figure 1.9). It is the most copious aldehyde product of lipid peroxidation. MDA can interact with another MDA molecule, moreover it is generally less reactive than other RCS due to proton loss and formation of enolate salts at neutral pH. MDA binds the amino group of Lys and the guanidine group of Arg¹⁴.

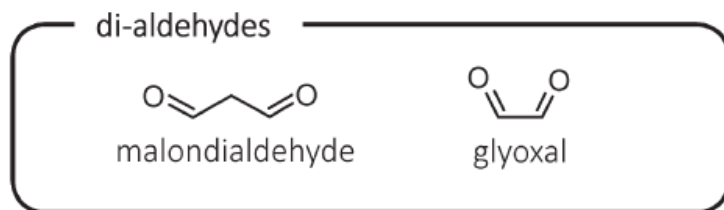


Figure 1.9. The structure of di-aldehydes¹⁴.

1.2.2.1. α -Syn and acrolein

Another α,β -unsaturated aldehyde is Acrolein (ACR, Figure 1.8), much more abundant than HNE¹⁶. Moreover, HNE mainly has an endogenous source, while ACR comes also from food and environmental sources (fume and combustion)^{14,17}. ACR and HNE target the same amino acids, but ACR is more reactive than HNE. Such a difference implies that ACR exhibits a lesser regioselectivity towards his50¹⁶ than that produced by HNE. The covalent linkage between α -Syn and ACR could be due to the formation of Base Schiff or Michael adducts (Figure 1.10)¹⁴. ACR is a major contributor to oxidative stress linked to PD. ACR-based protein carbonylation changes the physic-chemical properties and the physiological function of the targeted protein. Remarkably, the half-life of ACR is even longer than that of toxic radical species, like hydroxyl oxide and superoxide anion¹³.

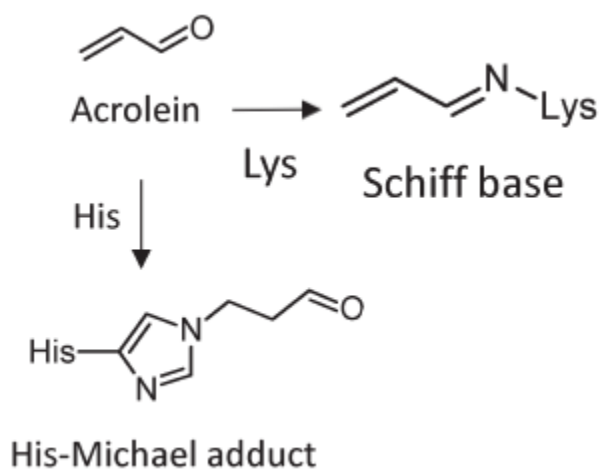


Figure 1.10. Michael adduct formation with histidine, and Schiff base formation with lysine¹⁴.

The incubation of ACR with α -Syn clearly affects the protein aggregation, whereas the addition of hydralazine to the reaction mixture halts the same process. Aggregation of α -Syn also depends on the levels of tyrosine hydroxylase (TH), an enzyme involved in dopamine synthesis¹³. Moreover, it is also linked to the dopaminergic cells' destruction in substantia nigra (SN)¹³. What distinguishes ACR from other peroxidation products is that the modification process occurs in a short time; ACR in the micromolar range promotes the α -Syn oligomerization⁷. Therefore, investigating the formation of α -Syn-ACR adducts represents an important goal because low levels of ACR in cells can cause severe damage¹⁶ and, then, it has the potential to be toxic in a chronic exposure. Hence, ACR would be an interesting target for a PD therapeutic approach.

In recent studies, ACR modification of α -Syn was investigated *in vitro*¹³. More interestingly, the α -Syn-ACR covalent adducts accumulate into the brain of PD patients⁷. As for animal models with an induced PD by damaging dopaminergic neurons with 6-hydroxydopamine, levels of ACR remained elevated for 14 days following the injury¹⁶. Moreover, the chronic injection of ACR induces the formation of high molecular weight species of α -Syn (~37 KDa), probably due to the presence of a dimer¹⁶. Therefore, ACR causes both a dose- and time- dependent toxicity.

1.3. Interplay between amyloid beta, proteasome 20S and Ubiquitin

1.3.1. Clearance system and Amyloid beta

The proteolytic cleavage of Amyloid Precursor Protein (APP) by two secretases (Figure 1.11) produces the peptide A β (39-43 residues, Figure 1.12)³. Residues 17-21 and the last ten C-terminal residues mainly contribute to the hydrophobic feature of the peptide. A β is involved in Alzheimer's disease (AD). Although the biochemical processes that trigger the onset of this devastating disorders are unknown yet, several hypotheses have been proposed, including the Amyloid cascade hypothesis that connects the A β deposits to the progress of AD. Therefore, A β should play a pivotal role in AD: the aggregated forms of the peptide accumulate into the brain plaques of the AD patients³.

There is a growing consensus that the dysfunction of the A β clearance systems, rather than an increase of the A β production, has a prominent effect on the AD progression^{18,19}. A 30% decline in the A β removal rate from the brain of AD patients clearly supports this

hypothesis¹⁹. The degradation systems involved in the A β clearance include specific enzymes such as Insulin degrading enzyme (IDE), Nepilysin (NEP), matrix metalloproteinases (MMPs), as well as multifunctional systems, like the Ubiquitin-Proteasome system (UPS) and the Autophagy-lysosomal pathway (ALP).

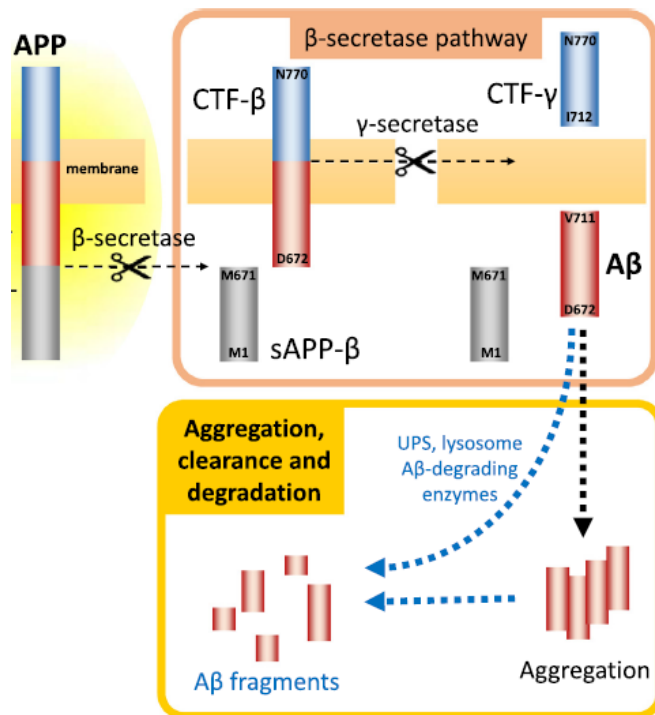


Figure 1.11. The release of A β from APP by the action of two enzymes¹⁸.

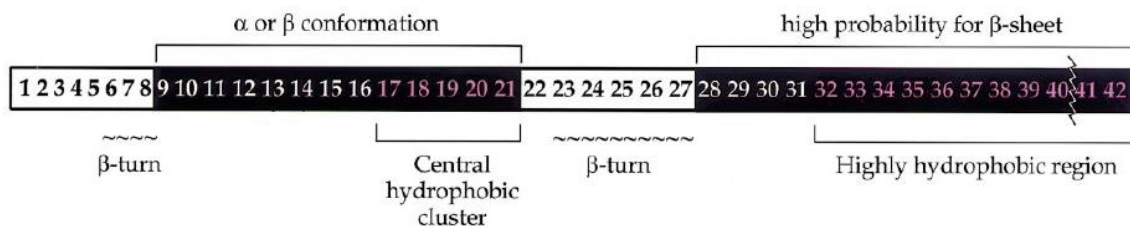


Figure 1.12. The primary sequence of A β ²⁰.

Protein unfolding and misfolding, also related to several diseases, are major reasons of imbalanced protein homeostasis (proteostasis). When those proteins fail to refold or start to aggregate, clearance systems are involved to regulate their levels. Clearance systems

include UPS and ALP^{21,22}. UPS and ALP experience a decline in their own function in aging and several diseases²². UPS targets small misfolded proteins, while ALP handles large protein aggregates. Briefly, UPS tags the protein with ubiquitin (Ub) and degrades it by mean of the proteasome; as for ALP, proteins are dispatched towards lysosome for degradation. In both procedures, Ub is covalently linked to the lysine or N-terminal residues of the targeted protein through the synergic function of three enzymes: E1 (activating enzyme), E2 (conjugating enzyme) and E3 (ligase enzyme). Upon the linkage of Ub, a growing chain of multiple Ub unit forms on the degradation-fated protein. Depending on the lysis residue involved in the formation of these multi-Ub chain, the targeted protein follows a specific clearance pathway. For example, UPS targets K48-labeled chains, whereas ALP marks K60 chains, even though it was recently found that ALP also targets K48-linked Ub chains²².

Several players are involved in A β degradation, among which is the 26S proteasome. The regulatory particle 19S (RP) acts as a lid for both ends of the cylindrical core particle 20S (CP) where the protein degradation occurs (Figure 1.13)^{21,22}. 20S combine several protease-like activities to generate peptides 2-24 residues long. Specifically, caspase-like (β 1 subunit), trypsin-like (β 2 subunit) and chymotrypsin-like (β 5 subunit) activities of 20S are the major players in protein degradation²¹. 20S proteasome degrades proteins in oxidizing conditions. Free CP is prevalent in human cell extract, and it constitute 66% of other cell types. Typically, proteins degraded by free 20S lack a folded structure and contain some unfolded regions. Therefore, Intrinsically Disordered Proteins are targeted by 20S proteasome as well as aged and/or oxidative damaged proteins which turned unfolded and participate in aggregation²³.

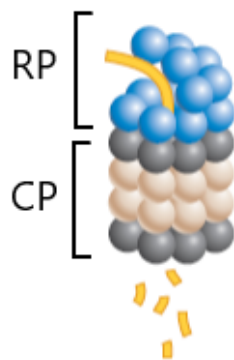


Figure 1.13. The regulatory particle (RP, 19S) and the core particle (CP, 20S)²¹.

IDPs tend to aggregate and cause diseases generally due to a disruption of their synthesis-degradation mechanism, which could serve as a therapeutic target. The two systems involved in the clearance are UPS, that handles soluble forms, and ALP, that deals with complex forms. The clearance systems are targeted in therapeutic studies/strategies. These strategies include (Figure 1.14): 1. enhancing the activity of the clearance system (UPS and ALP); 2. interfering with PTMs that are disease associated; 3. disbanding protein aggregation. All these strategies aim to decrease aggregation prone IDP levels. However, tackling PMD is a goal very difficult to achieve because it requires to know the native structural composition of IDPs *in vivo*. As a general statement, dissociating or preventing the formation of toxic oligomer species as well as securing the monomer forms of the target IDP are main therapeutic approaches. The unpredictable behavior of proteins that lack a fixed 3D structure is both the reason PMD are threatening and the hurdle to overcome in order to succeed^{5,6}.

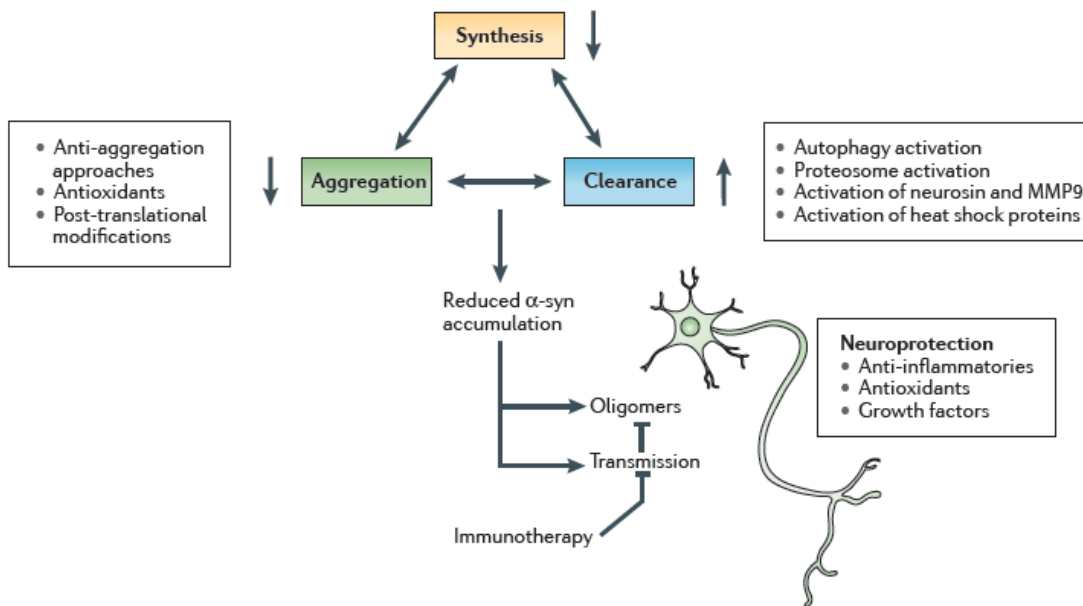


Figure 1.14. IDPs general therapeutic strategies involving the clearance systems ⁵.

1.3.2. A β and metal ions

The interaction between transition metal ions and A β leads several consequences. Some of them include: 1) zinc speeds up the aggregation process and 2) Cu²⁺ leads to the formation of toxic aggregates². Metal ions interact with A β at high affinity at N-terminal region (1-16 residues). A β is similar to α -syn as it also has 2 different binding modes to Cu²⁺ depending on pH. Both components coordinate using D1 residue (the N-terminal amine group). As reported in Figure 1.15, component I coordinate at low pH, while component II coordinates at high pH. However, other studies suggested different amino acid residues to be involved in the coordination of component II^{2,24}. In Zn²⁺ coordination with A β , the site is located at the N-terminal and involves several histidine residues².

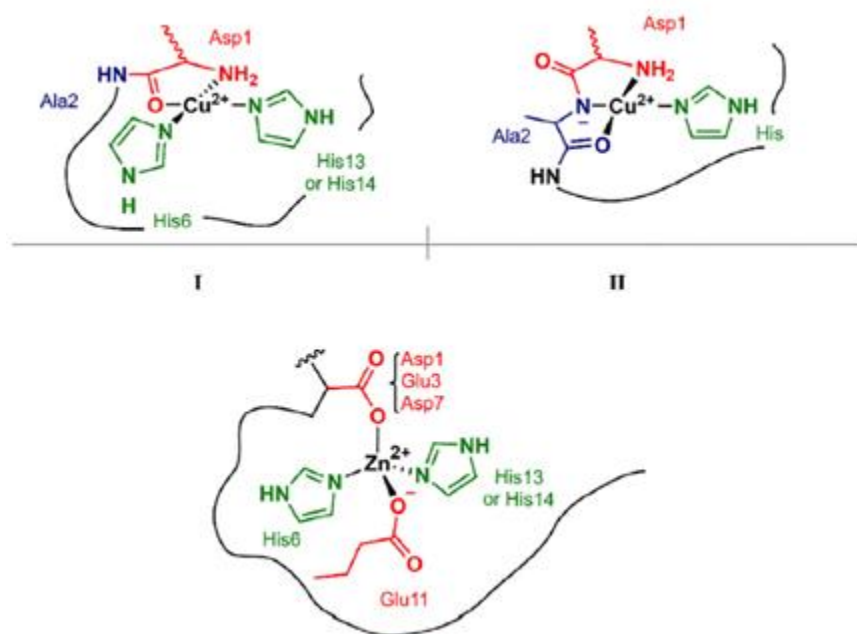


Figure 1.15. A β coordination with copper and zinc, components I and II².

1.4. Interplay between Alzheimer's disease and Diabetes mellitus

1.4.1. Cross seeding

AD and PD among other PMD are characterized by the presence of β -sheet aggregates and toxic amyloid accumulation in organs. These aggregates either form from a single misfolded protein aggregate, or the addition of the seeds of the same (homologous) or a different (heterologous) protein. Such a process is known as the seeding-nucleation

polymerization model (Figure 1.16, upper image). The model includes: 1) the nucleation phase (lag phase) where several molecules (partially denatured monomers, unstable oligomers) come together in a thermodynamically unfavorable manner, followed by 2) the Polymerization stage, i.e. the rapid addition of folded protein to form oligomers and/or fibrils. Adding seeds decrease lag phase; the reduction is higher in the presence of homologous rather than heterologous seed (Figure 1.16, lower image)²⁵.

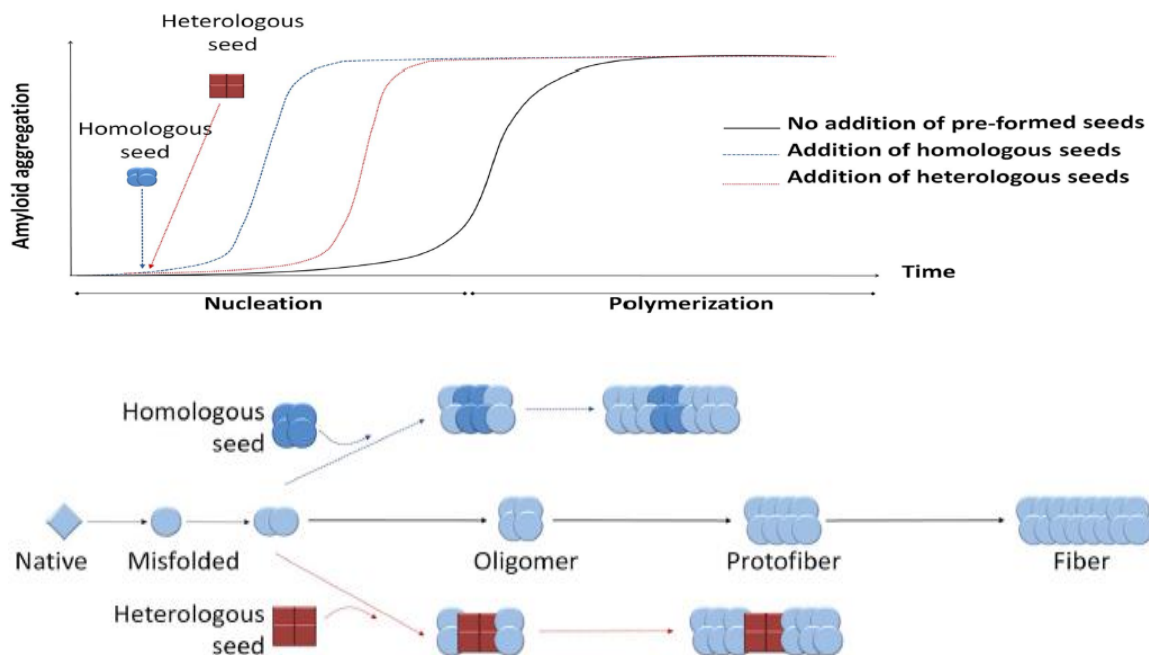


Figure 1.16. The seeding-nucleation polymerization model for disease linked proteins²⁵.

Cross-seeding is the addition of a heterologous seed to speed up the nucleation process of a different protein. Cross-seeding depends, among others, on both the seed's and the protein partner's conformation. The process does not follow a specific mechanism; for example, A β cross-seed α -Syn and vice versa, however, the two-way seeding effect is not a rule. Islet amyloid polypeptide (IAPP) protein can be seeded by A β , and it has no effect on A β aggregation²⁵. Experimentally, the incubation of NAC with A β lead to A β aggregation²⁶ and NAC speeds up A β aggregation by 50%²⁷. Additionally, different fragments of A β does seed NAC, however NAC's homologous seed is much more competent in speeding up NAC's aggregation. Both NAC and A β bind to the same site

on α -Syn. Moreover, α -Syn increases the polymerization level of $A\beta$ compared to aggregation levels of $A\beta$ without a seed²⁸. The NAC hydrophobic region has an important driving role in the fibril formation. Its fibril formation delay time can speed up by the addition of a seed (NAC fibrils)²⁷. Several factors play a role in the NAC aggregation, for example concentration and temperature: high protein concentration and/or high temperature promote faster aggregation, whereas the process is quite slow at 4°C. Aggregation of NAC is a two thermodynamic step process: favorable, when the monomer NAC is added to nucleus, and unfavorable, i.e. nucleation²⁷.

Further studies revealed $A\beta_{1-38}$ and $A\beta_{25-35}$ as α -Syn binding partners; however, α -Syn can't bind $A\beta_{1-28}$. The inability to bind some but not all $A\beta$ forms indicated the importance of amino acids 25-35 of $A\beta$ to the binding. In the presence of α -Syn, $A\beta_{1-38}$ can aggregate at the ratio of 1:125 α -Syn / $A\beta_{1-38}$. The interaction between both proteins and the promotion of aggregation is suggesting that α -Syn possibly plays a role in AD²⁹. Moreover, α -Syn favors the interaction with the more toxic form of $A\beta$, as it's aggregation accelerates in the presence of $A\beta_{42}$ but not $A\beta_{40}$ ³⁰. An indirect interaction between $A\beta$ and α -Syn is in the IDE ($A\beta$ degrading enzyme) α -Syn interaction, because it seems that IDE- α -Syn form a complex *in vitro*. The interaction is beneficial for both parties; α -Syn doesn't form fibrils and IDE is much more active on its substrate. α -Syn seized to form fibrils upon the addition of IDE and remained in the oligomeric state. However, the addition of IDE to c-truncated α -Syn did not stop the formation of fibrils³¹. The catalytic activity of IDE increases up to 30% in the presence of α -Syn C-terminal³¹.

Cross-seeding and/or the cooperative involvement of several IDPs in a single disease are a poor-studied area. It is vital to focus on it since it can account for experimental evidences. 1) the presence of several misfolded proteins in a single disease (Figure 1.17). 2) It could also explain the presence of more than one form of PMD in some patients. 3) It also explains why patients with a PMD are more prone to getting another PMD. 4) Worsen symptoms in people with heterologous protein aggregation. α -Syn is available in 50% of AD patients and it leads to worse symptoms, while 81% of AD patients have type 2 diabetes or impaired glucose function. Moreover, mice, with both α -Syn and $A\beta$ aggregate, have a severe decline in health in comparison to mice with a single form of

protein aggregates. Furthermore, the presence of α -Syn and $A\beta$ together equals a faster decline of brain function²⁵. Lewy body variant with Alzheimer's disease (AD-LBV) patients have higher mortality rates in comparison to other AD patients. In some brain areas of AD-LBV patients, both LB and plaques occur simultaneously, which is an unfamiliar event. It pointed out to the possibility that these proteins (α -Syn, $A\beta$) might promote each other's accumulation. Therefore, cross-seeding should be taken into account when designing therapeutic approaches for PMD³⁰.

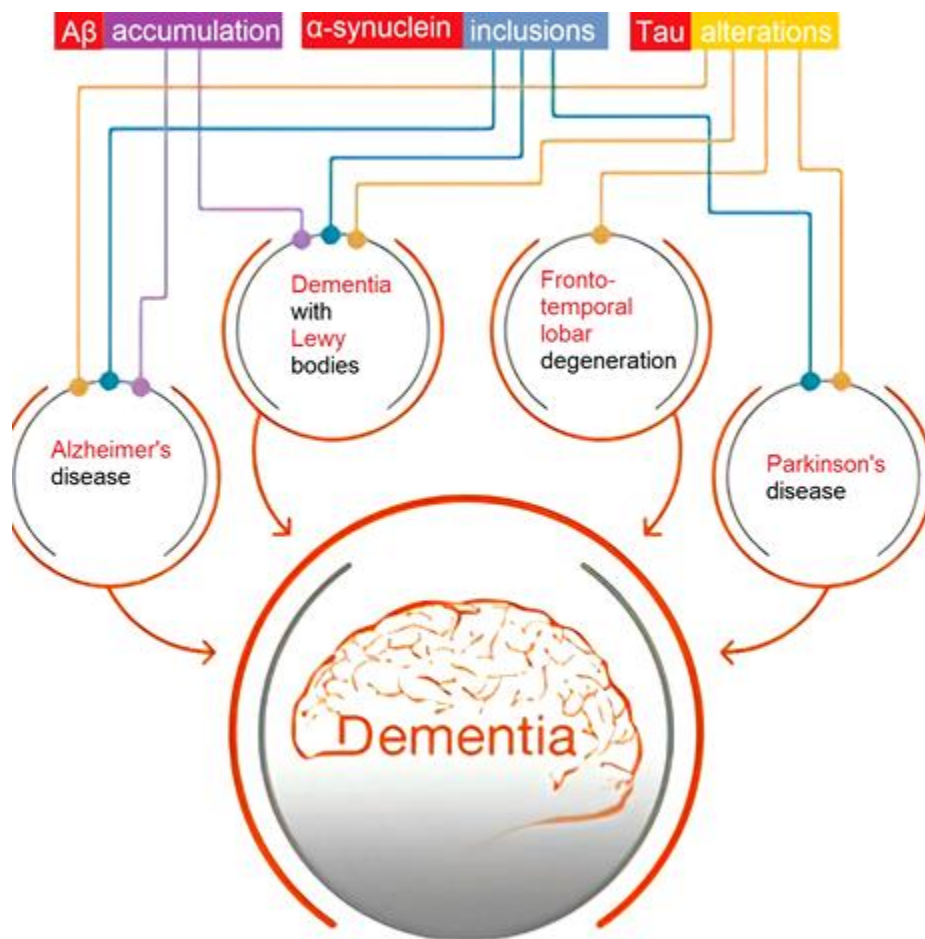


Figure 1.17. Cross-seeding, the center of dementia and other diseases³².

1.4.2. Alzheimer's and Diabetes

It is common for neurodegenerative disorders to be somehow linked one to each other. Similarly, a linkage was established between AD and Diabetes mellitus (DM), both of which are prevalent in elderly. The quality of life is continuously improved for diabetic patient; however, this disease imposes a huge burden on the healthcare system. Dementia is a symptom of multiple illnesses of which AD is predominant. Studies have shown the increased prevalence of dementia in diabetic versus nondiabetic patients. Cognitive dysfunction is associated with hyperglycemia, hypoglycemia and insulin resistance, all of which are factors associated with DM³³.

AD and DM share multiple similarities, thus prompting scientists and clinicians alike to tackle both simultaneously. Specifically, type-two DM (T2DM) and AD are age-associated diseases that increase risk for cardiac conditions, oxidative stress and inflammation. A β deposits, which are the histological hallmark of AD, are also found in T2DM in association with IAPP. Interestingly, IAPP share a structural similarity with APP (the precursor for A β). Moreover, neuron loss in AD and pancreatic β cell loss in T2DM is also observed³⁴. Additionally, glucose levels and A β are also linked. Increase in blood glucose levels impose a risk for AD development³⁵. Moreover, A β accumulates in case of hyperglycemia due to the inhibitory effect of high glucose levels on APP degradation³⁵. Moreover, the same degradation enzyme (IDE) targets both insulin (Ins) and A β . These observations provide an indirect evidence of the association of both diseases.

1.4.3. Insulin degrading enzyme and nociceptin/orphanin FQ

IDE is a multi-substrate enzyme targeting proteins with a size limit of ~40-50 residues in total^{31,36}. It is a zinc metallopeptidase that has 2 domains (IDE-N, IDE-C, Figure 1.18) with a central chamber that takes an open state for the substrate binding³⁷. The active site is on IDE-N, while IDE-C has an exosite (positively charged) which can bind specific sequence of peptides³⁶. The substrate binding on the exosite increases the activity of IDE-N. Furthermore, since the exosite is blocked, substrates reach the active site more readily^{36,37}. As IDE degradation is limited to small-sized substrates both Ins and A β are targeted. This fact as well as the observed shortage of zinc³⁸, which is required for IDE function, in both disorders extends the connection between AD and DM.

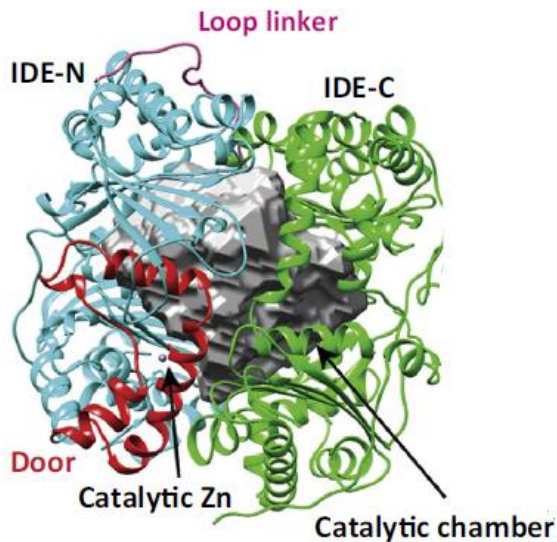


Figure 1.18. The subunits of insulin degrading enzyme³⁷.

Pathological disorders are associated with different levels of pain. A possible pain regulator is nociceptin/orphanin FQ, a 17 amino acid neuropeptide that binds to opioid receptor. The peptide was discovered by two groups, both contributing to its nomenclature. Meunier et al. called it Nociceptin (N) due to its pronociceptive activity³⁹, while Reinscheid et al. named it orphanin because of the binding capabilities to the orphan opioid receptor⁴⁰; F (phenylalanine) and Q (glutamine) are the N- and C- terminal residues, respectively, hence it's abbreviated as OFQ/N peptide. The binding of OFQ/N to its receptor triggers number of responses including anxiety, food intake, pain signaling, memory and cardiovascular functions. A recent study⁴¹ has shown the effect of OFQ/N on Ins release in a dose-dependent manner. It is possible to establish an indirect link between DM, AD and OFQ/N, since both the disorders are connected and targeted by IDE while OFQ/N is involved in memory, Ins release and as a small peptide could be potentially targeted by IDE.

1.5. Therapeutic compounds

One of the strategies for the cure or prevent the onset of neurodegenerative disorders is the research about potential therapeutic compounds. The compounds can be natural, chemically synthesized and/or modified. Different techniques are recruited to carry out these studies and approve the possibility of each of these compounds in the fight against neurodegeneration. Mass spectrometry is a technique heavily relied upon in these studies.

1.5.1. Proteomic approach for mass spectrometry

The transition of a charged protein or peptide from the solution to the gas phase is the basis of protein Mass Spectrometry (MS). The advances in soft ionization techniques made it possible to study proteins and other macromolecules using mass spectrometry as these approaches do not damage the protein during the experimental measurements. Soft ionization techniques include electrospray ionization (ESI) and matrix assisted laser desorption/ionization (MALDI). Each of these soft ionization techniques has precise features and specifications; for example, MALDI gives mainly mono-charged species while ESI produces multi-charged adducts making ESI the preferred method for studying complex protein systems including IDPs. Typically, proteins display a variety of charged species in the mass spectrum, whose range is indicative of the protein structure. Globular compacted protein displays a small range of charges as opposed to less compacted and/or disordered proteins (such as IDPs) as can be seen in Figure 1.18. The unfolded regions of the protein are susceptible to protonation which aids in signal detection for mass spectrometry. increasing its charge. Hence, mass spectrometry is an excellent aqueous label-free technique for studying the compactness differences between entire proteins and/or different protein regions⁴².

One of the most famous MS methods is the bottom-up proteomics. It simply means starting the analysis of protein samples from the fragments (peptides) all the way up to the full protein. It is a widely used technique for the analysis of protein, protein mixture and/or the quantification of samples. Initially for protein mixtures a fractionation step by which proteins are separated based on their molecular weight using a gel is employed to reduce the complexity of the sample. The previous step is ignored in the analysis of a

single protein which is simply digested via trypsin and introduced into liquid chromatography coupled with MS (LC-MS) for analysis. Isolated proteins from the mixture are then digested with trypsin inside the gel into their peptide components and extracted analysis. It is also possible to employ a gel-free approach for a complex protein mixture by starting with enzymatic digestion into peptides and then separating them using a multidimensional liquid chromatography where the separation is based on charge (strong cation exchange chromatography (SCX) followed by reversed-phase (RP) LC-MS). The fractionation methods are known as GeLC-MS for gel-based fractionation and multidimensional protein identification technology (MudPIT) for gel-free fractionation. It is important to monitor each step as it can greatly impact the reproducibility of the MS results. The fractionation into different molecular weight zones and getting rid of small impurities by means of gel-separation makes GeLC-MS a technique with a superior reproducing capability⁴³.

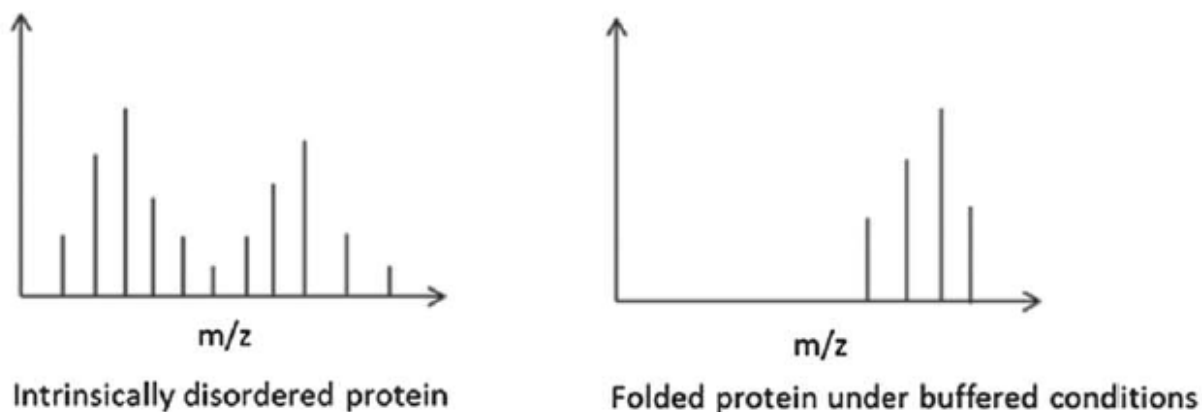


Figure 1.18. Charge state distribution difference between an IDP and a globular protein⁴².

The study of full-length protein is easier using the native MS. Macromolecules are normally subjected to enzyme cleavage, as previously mentioned, for the study of the smaller fragments. The action of the enzyme is un-needed in native MS as it is equipped with a wide m/z scale. General conditions for an MS experiment include sample purity and buffer compatibility. Ammonium acetate is an attractive choice for native MS as it provides minimal background interference and good volatility. Background interference

is due to elevated salt concentrations especially in case of directly injecting the sample into the ionization source (direct infusion). In order to avoid salt-associated problems, MS instruments for proteomic approaches are usually coupled with liquid chromatography by which the sample and the salt are separated at the initial stages⁴⁴.

1.5.2. Anti-aggregation Compounds

The use of compounds which inhibit the aggregation of proteins involved in neurodegeneration is one of the therapeutic methods exploited in the neurodegeneration research. A wealth of studies are already done on the anti-aggregation ability of some compounds against A β aggregation including as 8-hydroxyquinoline⁴⁵, cyclodextrin⁴⁶ and trehalose⁴⁷. Compounds tested against the aggregation of α -Syn⁴⁸ include Rifampicin also which is an antibiotic. Rifampicin slows down and/or inhibits the aggregation of the protein in a concentration dependent manner using the fluorescent dye ThT. Moreover, α -Syn was mostly in a soluble form in the presence of Rifampicin as opposed to the insoluble protein content in the control experiment⁴⁸. In order to enhance the anti-aggregate effect, conjugates of some compounds already tested against A β were synthesized (Figure 1.19) and used against α -Syn aggregation as a potential therapeutic target.

Hydroxyquinoline (HQ) and its derivatives have chelating property, particularly towards Cu²⁺ and Zn²⁺. There is a wide interest in HQ in the pharmaceutical industry for its neuroprotective effect. HQ delays the formation of amyloid aggregates, but does not inhibit it, hence its properties could be emphasized by its derivatives. Cyclodextrin (CD), a cyclic oligosaccharide, conjugated to HQ enhances water solubility which is vital for *in vitro* experiments as higher concentrations can be utilized. The antiaggregant properties are also increased due to CD role in reducing oxidative stress as well as interfering with aggregation inducing protein interactions such as those with other proteins or metals. CD conjugates of HQ have tremendous potential in the fight against neurodegenerative disorders. These properties are efficient against amyloid protein as this conjugate inhibits the aggregation of A β , possibly by interacting with the monomeric specie. Interestingly, CD alone doesn't have an influence on protein aggregation⁴⁹.

Carnosine (Car) is a dipeptide increasingly populating the brain and muscles. It is also involved in antioxidant activities as it chelates Cu²⁺ and quenches radical

species. These properties indicate a potential role of Car against protein aggregation induced by oxidative stress and/or metal dyshomeostasis. Car is effective against A β aggregation and toxicity, however its inhibitor activities are not enough to initiate a perfect inhibition⁵⁰. Therefore, similarly to CD conjugate of HQ, Car inhibition potential could be potentially enhanced.

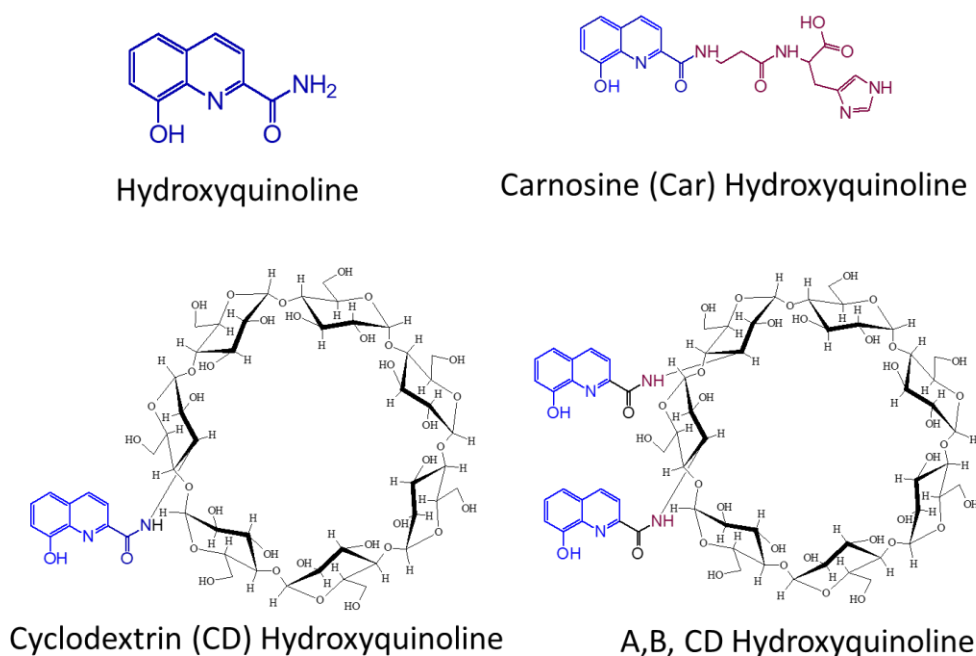
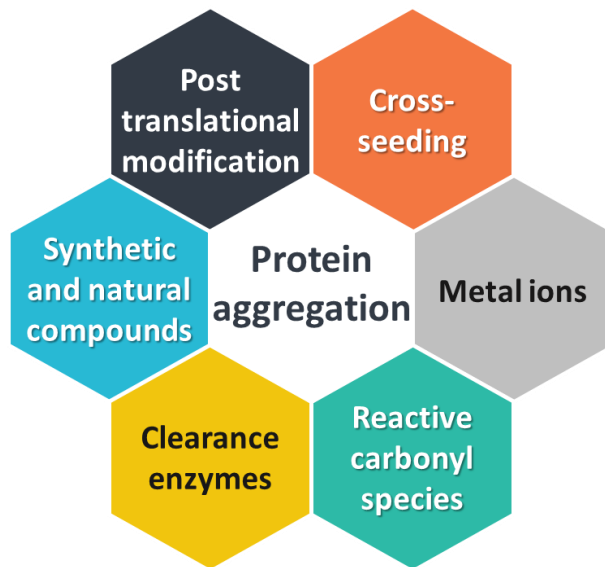


Figure 1.19. Hydroxyquinoline (HQ) and its conjugates.

1.6. Overview

Unlike other diseases, foldopathies are notable for their complexity, which is a major obstacle to find a therapy. Experimental strategies involve the examination of protein aggregation, which is a marker for different foldopathic diseases. The factors that lead to protein aggregation are numerous as seen in the flow diagram. Hence, this project “Getting insights into the molecular determinant of foldopathies” will dissect these factors and apply the experimental approaches to different foldopathies.



The following sections will include the description an interdisciplinary approach to study two proteins involved in neurodegeneration. Initially the focus will be on α -Syn, which has been produced and purified in our laboratories. The experimental data will include carbonylation assays, spectroscopic and spectrometric measurements. The effects of some potential therapeutic compounds and their interactions with α -Syn will also be described. Next, the interaction between α -Syn and $A\beta$ will be presented, investigated in the presence of clearance enzyme, before moving on into studies of $A\beta$ with multiple clearance systems/enzymes. The goal of this project is to highlight the importance of an interdisciplinary study as a preferred approach in tackling neurodegenerative disorders.

Chapter 2

Material and Methods

All the reagents, if not otherwise specified, were analytical grade, used without further purification, and purchased from Sigma-Aldrich.

The amyloid β was purified before any use in order to enrich the sample of monomer species. A β_{1-42} was dissolved to a final concentration 2.5 mg/ml in 6 M guanidinium chloride in phosphate buffer (20 mM), EDTA (0.2 mM), NaN₃ 0.02 %, pH 8.0. The protein purification was performed by Size Exclusion Chromatography (SEC). The sample was injected into a Superdex 200 increase10/30 gel column (0.75 ml/min, 600 psi, injection volume 70 μ l). The eluent was the same used for dissolving the amyloid peptide, except for the absence of guanidinium chloride. The protein content was detected using a UV filter at 280 nm. The concentration of the amyloid peptide was assessed by UV measurements at 280 nm (extinction coefficient 1490 M⁻¹ cm⁻¹).

α -Syn samples in 5 mM Tris pH 7.4 were reconstituted in water to the appropriate concentration. Tris buffer was exchanged to ammonium acetate 100 mM pH 6.9. Amicon® Ultra -0.5 ml centrifugal filters 3 kDa MWCO were prepared for the buffer exchange by running three cycles of 200 μ l ammonium acetate 100 mM at 14100 xg for 10 minutes each. Next, 50 μ l of α -Syn was added and the volume was completed to 200 μ l with ammonium acetate. Five cycles were run at 9100 xg for 10 minutes each, and extra ammonium acetate was added at the end of the first four cycles to restore the volume to 200 μ l while getting rid of the flow through. At the end of the fifth cycle, the filter is inverted into a new vial and centrifuged for 2 minutes at 2000 xg to collect the sample.

Acrolein was obtained by the complete hydrolysis of corresponding diethyl acetal in 0.1 M HCl for 1 hour at room temperature. The sample was diluted to 2mM (α -Syn experiments) or 10 mM (P2 peptide experiments) with water just before use.

The peptide Ac-EGVVH-NH₂ (P2) was synthesized in Peter Faller's laboratory using peptide synthesis techniques. Briefly, a solid phase synthesis was carried out using a standard 9-fluorenylmethoxycarbonyl (Fmoc)/tert-Butyl (tBu) strategy, which requires a

resin Fmoc-Rink amide aminomethyl-polystyrene resin (Fmoc-Rink-Amid AM Resin from Iris Biotech, 0.74 mmol/g loading, 100-200 mesh) a coupling agent HBTU (3-[Bis(dimethylamino) methylumyl]-3H-benzotriazol-1-oxide hexa fluoro phosphate), a base DIEA (N,N-diisopropylethylamine) and a solvent DMF (N,N-dimethyl-formamide). Purity and identity of the peptides were assessed by analytical high-performance liquid chromatography (HPLC) and electron spray ionization-mass spectrometry (ESI-MS).

A Q-Exactive hybrid quadrupole-Orbitrap mass spectrometer (Thermo Scientific) coupled to an Ultimate 3000 HPLC RSLCnano system (Dionex Thermo Scientific) through an EASY-Spray source (Thermo Scientific) was used for the analysis of some of the samples. The experimental setup was as follows: Capillary temperature 300 °C, voltage 2 kV. Full scan mode for MS acquisition (maximum injection time 50 ms , 70,000 resolution, AGC target 1·10⁶, scan range 500 to 2000 m/z).

In MS/MS specific ions are isolated and further fragmented and identified precisely through the collision with high energy inert gas. The fragmentation effect is on the peptide bond: ions formed from the C-terminal are part of the y series while those formed from the N-terminal are part of the b series. Based on the mass of each series the peptide primary sequence can be extracted and identify the location of any covalent modification. In MS/MS mode acquisition, the parameters differ than MS acquisition in the resolution (17,500), AGC target 1·10⁵ and scan range 200 to 2000 m/z. The EASY-Spray PepMap® C18 column was used for separation (75 µm × 150 mm, 3 µm particle size, 100 Å pore size). The solvent system included: solvent A (water with 0.1% formic acid (FA)) and solvent B (80% acetonitrile, 0.1% FA in water) flow rate of 0.3 µL/min. a linear gradient of solvent B (5% to 40%) was used to elute the samples. The extracted ion chromatogram (XIC) of the most abundant charged species of each fragment was enlisted for peak detection. MagTran software⁵¹ deconvoluted mass spectra, while MaxQuant software⁵² identified the MS/MS analyzed tryptic digested peptides through their XIC. Together, data from the MS and MS/MS (HCD) spectra were useful in identifying the peptide fragments and the modified residues.

MALDI-TOF MS experiments were performed using an AB SCIEX MALDI-TOF/TOF 5800 Analyzer (AB SCIEX, Foster City, CA) equipped with a nitrogen UV laser ($\lambda = 337$ nm) pulsed at a 20 Hz frequency. The mass spectrometer operated in one of two modes depending on sample size. Ion Reflector mode for samples 4 kDa and less, while the linear mode is used for larger samples. In each case, experimental parameters and the applied matrix are different. Experimental spectra were analysed using Data Explorer software (Applied Biosystems) and mMass software⁵³.

The mass spectrometer was operated with the ion reflector mode with an accelerating potential of 20 kV and a grid percentage equal to 70%. Mass spectra were recorded with the laser intensity set just above the ionization threshold (3000 in arbitrary units, on our instrument) to avoid fragmentation and labile group losses, to maximize the resolution and to result in a strong analyte signal with minimal matrix interference. Time delay between laser pulse and ion extraction was set to 450 ns. Typically, mass spectra were obtained by accumulation of 1000 laser shots. Saturated solution of α -Cyano-4-hydroxycinnamic acid (CHCA in water:acetonitrile 2.3:1 with 0.3% trifluoroacetic acid (TFA) was used as matrix.

Linear mode consisted of an accelerating potential of 25 kV, a grid percentage of 93% and an extraction delay of 800 ns. Mass spectra were recorded with the laser intensity set just above the ionization threshold (4500 in arbitrary units) to avoid fragmentation and labile group losses, to maximize the resolution, and to result in a strong analyte signal with minimal matrix interference. Mass spectra were obtained by accumulation 800–1000 laser shots. A saturated solution of sinapinic acid in water/acetonitrile 70:30 with 0.1% TFA was used as the matrix.

For ThT aggregation assay, All the amyloid-type kinetic measurements were carried out in duplicates and/or triplicate and the experimental data were fitted to Equation (1):

$$F(t) = F_0 + \frac{F_{max} - F_0}{1 + e^{-\frac{t-t_{1/2}}{k}}} \quad (\text{Eq. 1})$$

in which the fitted parameters are the starting (F_0) and final (F_{max}) fluorescence emissions of the amyloid aggregation process, the elongation rate constant ($1/k$) and the

time at which the amplitude of ThT emission is 50% of the Fmax – F0 value ($t_{1/2}$). The last two parameters contribute to calculate (Equation 2) the lag time (t_{lag}), defined as the intercept between the time axis and the tangent of the curve with slope k from the midpoint of the fitted sigmoidal curve.

$$t_{lag} = t_{1/2} - 2k \quad (\text{Eq. 2})$$

The kinetic parameters of any set of measurements were expressed as mean \pm SD.

2.1. α -Syn purification

The published protocol⁵⁴ was followed in the production of the protein however certain modifications were applied. Briefly, α -Syn DNA was inserted into the protein expression vector pRK172 (from Jennifer C. Lee (NIH-laboratory of molecular biophysics, Bethesda) and Michel Goedert (MRC Laboratory of Molecular Biology, Cambridge) and subsequently transformed into Escherichia coli strain (BL21(DE3), from Francesca Guarino (Department of Biomedical and Biotechnological Sciences, University of Catania)). The cells were grown using 0.5L of LB media in the presence of the antibiotics Ampicillin (0.1 mg/ml, Sigma). Cell growth took place at 37°C for 2-3 hours until OD600 of ~0.6. At this point, Isopropyl β -D-1-thiogalactopyranoside (IPTG, 0.5 mM, Sigma) was added to induce protein production and the growth remained at 37°C for an additional 5 hours. Note that when using glycerol stock as a starting point OD600 = 0.6 is achieved faster. Afterward, the cells were harvested, and the pellet was dissolved in lysis buffer (50mM Tris, 30mM NaCl, 2 mM EDTA, 0.1% Triton-X 100, pH 8.6 in the presence of HaltTM protease and phosphatase single-use inhibitor cocktail 100X (Thermo Scientific). Cells were lysed by the addition of lysozyme (0.3mg/ml, Sigma), incubation at 37°C for 40 min, water bath 37°C for 30 min, -80°C fridge for 20 min and then 37°C incubator until sample thaws. Next, reduce pH to 3.5 and centrifuge the cells (Thermo scientific SL40R centrifuge F15-6X100y rotor, 20,000 xg, 1hr, 4°C). Moreover, FPLC instrument (Bio-Rad Biologic Duo flow with Bio-Rad Biologic Biofrac fraction collector) was used to remove the salt and purify the sample: Hiprep 26/10 desalting column, Hiprep DEAE FF 16/10 column, BioRad UNO Q1 column sequentially. Finally, using Thermo Scientific Pierce concentrator 9KMWCO, the sample was concentrated to the desired concentration

which was monitored by UV spectroscopy at 280 nm and stored at -80°C until use. Dinox Ultimate 3000 HPLC in conjunction with Thermo scientific Q exactive mass spectroscopy and/or Bolt™ 10% Bis-tris plus gel (Thermo Fisher scientific, with Bolt MES SDS running buffer Novex life technologies) were used to check the final product before storage. Using overnight dialysis instead of a desalting column as the initial steps and ending the purification with a size exclusion chromatography (Superdex 200 increase 10/30 gel) increased the yield of the protein, the production accuracy was monitored using nanoLC-HRMS.

2.2. α -Syn carbonylation assay

α -Syn (20 μ M) was incubated with freshly prepared acrolein (200 μ M) in 100 mM MOPS (3-(N-morpholino) propanesulfonic acid) buffer (pH 7.4 or pH 6 at 37 °C). Different concentrations of copper were added to the reaction mixture to reach 1:1, 1:2 or 1:4 α -Syn: copper molar ratios. The reaction was stopped by incubating for 10 minutes at room temperature with NaBH₄ (5 mM). Next digestion with trypsin at 37°C was carried out overnight a 1:20 trypsin/ α -Syn molar ratio. The reaction was stopped by diluting the sample ten-fold with 5% Acetonitrile and 0.05% TFA in water. Finally, samples were further diluted 10 times with 5% acetonitrile, 0.05% TFA in water for nanoLC-HRMS analysis.

A short synthetic peptide (P2) which mimics the binding site of α -syn on acrolein (ACR) was produced. P2 peptide (20 μ M) was incubated with freshly prepared acrolein (1 mM) in 50 mM MOPS (3-(N-morpholino)propanesulfonic acid) buffer (pH 7.4 or pH 6 at 37 °C) in a 1:50 molar ratio. Different concentrations of Cu²⁺ were added to the reaction mixture to reach for α -syn: Cu²⁺ molar ratios of 1:1, 1:2 or 1:4. The addition of NaBH₄ (5 mM) for 10 minutes at room temperature terminated the reaction. The sample was diluted ten-fold with 5% Acetonitrile and 0.05% TFA in water and the dilution was carried out twice for nanoLC-HRMS analysis.

2.2.1. Dynamic light scattering

In dynamic light scattering (DLS) measurements the samples were analyzed on a Zetasizer Nano ZS (Malvern Instruments Ltd., UK) at Catania University. The DLS instrument was equipped with a λ =633 nm He-Ne laser and a Peltier temperature controller set at 37°C temperature for a total incubation time of 144 hours. The protein

samples were prepared at 100 μM (α -syn monomer equivalents) and buffered in MOPS (pH 7.4). The effect of ACR and/or Cu^{2+} on the aggregation of α -syn was evaluated adding a freshly prepared ACR and/or a standardized $\text{CuSO}_4 \cdot 5\text{H}_2\text{O}$ solution to obtain α -syn/ACR 1:10 and/or α -syn/ Cu^{2+} 1:2 molar ratios. Disposable, solvent resistant microcuvettes were used for size measurements, which were conducted at a scattering angle of 173° . Each DLS measurement was run by using automated, optimal measurement times and laser attenuation settings. All samples were measured 5-10 times using 15–40 accumulated scans to give averaged d_H values.

2.2.2. Circular dichroism

In circular dichroism (CD) measurement α -syn (20 μM) samples were prepared by adding a freshly prepared ACR and/or a standardized $\text{CuSO}_4 \cdot 5\text{H}_2\text{O}$ solution to obtain α -syn/ACR 1:10 and/or α -syn/ Cu^{2+} 1:2 molar ratios and incubated at 37°C for a total of 52 hours. The samples were diluted to a final concentration of 1.5 μM in 100 mM MOPS, pH 7.4. The far-UV CD spectra (between 260 and 195 nm) were recorded on a Jasco J-1500 spectrometer (Jasco, Easton, MD, USA) using a cuvette with a 1-cm path length. Each scan was repeated 5-10 times, and the background value of the MOPS buffer was subtracted for all samples.

2.2.3. Aggregation assay

The role of the α -syn carbonylation on the protein aggregation was also studied via ThT assay. α -syn (70 μM) was incubated with acrolein (70 μM) at 37°C for 1 hour without shaking. Next, NaBH_4 (4.75mM) was added to the sample at room temperature for 15 min. Then the α -syn aggregation was monitored by ThT assay. All the samples were run on black 96-well plate (Nalge–Nunc, Rochester, NY).

2.2.4. MDA and α -Syn

MDA was prepared by the complete hydrolysis of dimethyl acetal (MDA-acetal). MDA acetal was diluted to a final concentration of 50 mM with 0.1M HCL solution and the hydrolysis was carried out at 37°C per for 40 minutes. The conversion rate from MDA-acetal to MDA is assumed to be 100% according to the literature concerning similar reaction towards another RCS⁵⁵, and the solution is ready for use.

α -Syn was diluted to 20 μ M in phosphate buffer (50 mM, pH 7.4) in the presence of 200 μ M MDA. The sample was incubated at 37 $^{\circ}$ C and aliquots were retrieved at time intervals: 1,30,60 and 90 minutes. Next the aliquots were subjected to trypsin enzymatic digestion for 24 hrs. at 37 $^{\circ}$ C at a ratio of 1:30 trypsin to α -Syn. The reaction mixture was inhibited by a 1:1 dilution with a 1:1 water : acetonitrile solvent containing 0.3% TFA. The samples were analyzed using MALDI-TOF by diluting them with CHCA matrix at 1:1 ratio.

2.3. α -Syn interactions with compounds

2.3.1. Native mass spectrometry

α -Syn (20 μ M or 10 μ M) was co-incubated with different compounds (rifampicin as standard, β -CD, HQ and its carnosine and cyclodextrin derivatives) at concentration of 100 μ M for molar ratio of 1:5 and/or 1:10 for 10 minutes at room temperature. Immediately the samples were sprayed with needle into Thermo Q-exactive UHMR Native mass spectrometry. The data acquisition on Tune software was for an average of 5 minutes, while MagTran was used for deconvolution.

2.3.2. Aggregation assay

α -Syn (70 μ M) in tris buffer (1 mM) was incubated with different compounds (rifampicin as standard, β -cyclodextrin, HQ and its carnosine and cyclodextrin derivatives) at concentration of 350 μ M in the presence of thioflavin T fluorescence dye on black 96-well plate (Nalge–Nunc, Rochester, NY). The samples were run in duplicates for 4 days and the data were fit according to equation 3 with sigmoidal fit.

$$y = \frac{A_1 - A_2}{1 + e^{(x-x_0)/dx}} + A_2 \quad (\text{Eq. 3})$$

2.3.3. Influence of citicoline on 20S proteasome

Citicoline (100 nM or 1 μ M) were added to α -Syn (10 μ M) digested by 20S proteasome (5 nM) in Tris buffer pH 7.4, 25 mM at 37 $^{\circ}$ C for 1 hr. and 3 hrs. A control reaction in the absence of citicoline was also ran alongside this reaction for a similar time period. Laemmli buffer in combination with heat denaturation were used to stop the reaction, before running the samples on 15% polyacrylamide gel electrophoresis (PAGE) which was subsequently stained by Coomassie Brilliant blue for visualization of bands.

2.4. α -Syn and Amyloid beta

2.4.1. IDE, α -Syn and Amyloid beta

The enzymatic digestion of different concentrations A β ₁₋₂₈ (2 μ M) or A β ₁₋₄₀ (5 μ M) (GenScript) by IDE (5-10 nM) (Giotto biotech s.r.l. Italy) was incubated with different concentrations of α -syn (1-15 μ M) in the presence of phosphate buffer (1 mM) at 37°C. The digestion was halted with 0.5% TFA (Carlo Erba) at different time intervals and subsequently analyzed by nanoLC-HRMS.

2.4.2. Aggregation assay

The aggregation assays of A β and α -syn were carried out by using a turn-on dye ThT sensitive to the amyloid-type fibrils. ThT (40 μ M), A β ₁₋₄₂ (7 μ M) or α -syn (70 μ M) were incubated in water or MOPS buffer (0.5 mM pH 7.4) respectively, containing NaCl (100mM) and 2 glass beads/sample within a black 96-well plate (Nalge–Nunc, Rochester, NY) for 60 hours (A β aggregation) or 5 days (α -syn aggregation) at 37°C in the Varioskan plate reader (Thermo Scientific) under continuous shaking (600rpm). The fluorometric measurements were carried out by monitoring the ThT emission 482 nm and exciting at 440 nm (bandwidth 12nm).

In order to monitor the dose-dependent effect of α -Syn on the A β aggregation, different concentrations of α -Syn were incubated with to A β , being the A β / α -Syn molar ratio equal to 1:0, 1:0.5, 1:1 or 1:2. ThT assay was carried out in triplicates and within a black 384-well plate (Nalge–Nunc, Rochester, NY).

2.5. Proteasome 20S action on A β

2.5.1. 20S mediated A β ₁₋₄₀ hydrolysis

The enzymatic digestion of A β ₁₋₄₀ (2 μ M) (GenScript) was achieved by the initial incubation of proteasome 20S (2 nM) (Giotto biotech s.r.l. Italy) in the presence of Tris buffer pH 8 (1mM) at 37°C for 15 minutes, before the addition of the protein. The reaction mixture was incubated at the same temperature for a total of 60 minutes. The digestion was halted with 0.5% TFA (Carlo Erba) at different time intervals and subsequently analyzed by nanoLC-HRMS.

2.5.2. A β ₁₋₄₀ hydrolysis and Ub role

The enzymatic digestion of A β ₁₋₄₀ (2 μ M) (GenScript) in the presence of different Ub concentrations (0,1,2,4 μ M) was achieved by the initial incubation of proteasome 20S (2 nM) (Giotto biotech s.r.l. Italy) in the presence of Tris buffer pH 8 (1mM) at 37°C for 15 minutes, before the addition of the protein and different Ub concentrations. The reaction mixture was re-incubated at 37°C for a total of 120 minutes. The digestion was halted with 0.5 % TFA (Carlo Erba) at different time intervals and subsequently analyzed by nanoLC-HRMS.

2.5.3. 20S mediated A β ₁₆₋₂₈ hydrolysis

The enzymatic digestion of A β ₁₆₋₂₈ (2 μ M) (GenScript) was achieved by the initial incubation of proteasome 20S (2 nM) (Giotto biotech s.r.l. Italy) in the presence of Tris buffer pH 8 (1 mM) at 37°C for 15 minutes, before the addition of the protein. The reaction mixture was re-incubated at 37°C for a total of 30 minutes. The digestion was halted with 0.5% TFA (Carlo Erba) at different time intervals and subsequently analyzed by nanoLC-HRMS.

2.5.4. The effect of A β ₁₋₄₀ on 20S mediated A β ₁₆₋₂₈ hydrolysis

The enzymatic digestion of A β ₁₆₋₂₈ (2 μ M) (GenScript) in the presence of different A β ₁₋₄₀ concentrations (0,2,4,6 μ M) was achieved by the initial incubation of proteasome 20S (2 nM) (Giotto biotech s.r.l. Italy) in the presence of Tris buffer pH 8 (1mM) at 37°C for 15 minutes, before the addition of both the different A β ₁₋₄₀ concentrations and A β ₁₆₋₂₈. The reaction mixture was incubated at the same temperature for a total of 15 minutes. The digestion was halted with 0.5% TFA (Carlo Erba) and subsequently analyzed by nanoLC-HRMS.

2.5.5. 20S mediated A β ₁₋₂₈ hydrolysis

The enzymatic digestion of A β ₁₋₂₈ (20 μ M) (GenScript) was achieved by the initial incubation of proteasome 20S (5 nM) (Giotto biotech s.r.l. Italy) in the presence of Tris buffer pH 8 (1mM) at 37°C for 15 minutes, before the addition of the protein. The reaction mixture was re-incubated at 37°C for a total of 80 minutes. The digestion was halted with 0.5% TFA (Carlo Erba) at different time intervals followed by 1:10 dilution with water and subsequently analyzed by MALDI-TOF.

2.5.6. The effect of AP on 20S mediated A β ₁₋₂₈ hydrolysis

Aminopyrine (AP) (0-10 μ M) was incubated at 37 °C in Tris-HCl buffer (1 mM pH 8) for 20 minutes, followed by the addition of proteasome (5 nM) and additionally incubation at 37 °C for 15 minutes. A β ₁₋₂₈ (20 μ M) was added and the samples were incubated at 37 °C for different time periods (0-80 minutes). The reaction was stopped with 0.5% TFA and diluted 1:10 with water. N-terminal amidated A β ₁₋₁₆ (0.023 μ M) was dissolved in the matrix solution and it acted as an internal standard. Each sample was spotted three times and four spectra were acquired for each spot, thus obtaining a set of twelve spectra for each sample using MALDI-TOF.

2.6. Insulin degrading enzyme

2.6.1. IDE and nociceptin/orphanin FQ

Insulin (Ins, 2 μ M) and nociceptin (OFQ/N₁₋₁₆, 2 μ M) were hydrolyzed in the presence of Insulin Degrading Enzyme (IDE, 30 nM) in phosphate buffer 1 mM (pH 7.4). Ins and OFQ/N₁₋₁₆ were hydrolyzed both separately and in a mixture. Moreover, a pre-incubation of OFQ/N₁₋₁₆ with IDE for 20 min was also performed before the addition of Ins. In order to quench the reaction, the samples were diluted 1:1 with 1% TFA aqueous solution before proceeding for analysis by nanoLC-HRMS.

2.6.2. Mutant IDE hydrolysis of amyloid beta

The enzymatic digestion of A β ₁₋₄₀ (2 μ M) (GenScript) by IDE (5-10 nM) (Giotto biotech s.r.l. Italy) or by mutant F530A IDE (Giotto biotech s.r.l. Italy) was incubated with 2 μ M Cu²⁺ or Zn²⁺ in the presence of phosphate buffer (1mM) at 37°C. The digestion was halted with 0.5% TFA (Carlo Erba) at different time intervals and subsequently analyzed by nanoLC-HRMS.

2.7. Supplementary experiments

The results of the experiments in this section will be explained in the supplementary section of this thesis. Both are preliminary studies that were not pursued further due to time constrain. These experiments were important for the study of a quick method to detect the oligomers of α -syn in solution (PICUP), and to calculate KD values for α -syn with the enzyme IDE (SPR).

2.7.1. PICUP

Photo-induced cross-linking of unmodified proteins (PICUP) was used to detect the presence of higher α -syn forms in the sample. α -syn (10 μ M) was added to 1:20 molar ratio of ammonium persulfate (APS) and Tris (bipyridine) ruthenium (II) chloride (Ru-bpy) respectively in the presence of 10 mM phosphate buffer (pH 7.4). In the control samples, the reaction was immediately quenched with Dithiothreitol (DTT), however in the test sample the mixture was first irradiated for 1 second with the light source then quenched with DTT. The samples were run in triplicates in MALDI-TOF using sinapinic acid as the matrix.

2.7.2. SPR experiment

The equilibration of the sensor is by an injection of PBS buffer 10 mM (pH 7.4) as flow cell was at 22 ° C. The used sensor is a CMD-3D sensor activated by the reaction of EDC (0.2 M)/NHS (0.05 M) with the carboxyl group of the sensor producing succinimide ester that can interact with amino groups. In order to immobilize IDE on the sensor, the enzyme was dissolved in sodium acetate buffer (10 mM) and run in two injections at concentration of 1.145 μ M at pH 4 and pH 4.2 each for the duration of 20 minutes at 10 μ l / min. The immobilization process was performed using the parallel configuration (in this configuration the autosampler will collect two independent samples on channels 1 and 2 and inject them simultaneously with the selected parameters), while in channel 2 (reference channel) only the running buffer is injected. At the end of the immobilization phase, ethanolamine-HCl 1M (pH 8.5) was injected using the serial configuration (in this configuration the autosampler takes a sample and injects it so that it flows in series through both channels 1 and 2) for 10 minutes at 15 μ l / min to deactivate all active residual sites on the surface. A regeneration step with NaOH (10 mM) with NaCl (2 M) at flow rate 20 μ l / min for 10 minutes, then the buffer is changed from PBS (10 mM) with tween 20 (0.05 %) to Tris (5 mM) without changing Tween 20's concentration. α -Syn is prepared right before injection, the stock solution is at 89.1 μ M in 5 mM Tris buffer pH 7.4. Several solutions of different micromolar concentrations are prepared. It is vital to run a regeneration step in between runs to bring the baseline to starting levels.

Chapter 3

Results and Discussion

In this chapter, the results of numerous experiments will be demonstrated and discussed. The experiments are divided into several sections and they demonstrate the interaction between a protein (α -Syn and/or $A\beta$) and a known factor in protein aggregation: RCS, metal ions, clearance system components (enzymes, 20S proteasome, Ubiquitin), protein-protein interaction and compounds (potential therapy). Initially, a focused study on α -Syn and its interaction with RCS: ACR and MDA in great details using different approaches is described. Next, this protein and its interaction with potential therapeutic compounds is studied. The focus is then shifted towards the interaction between α -Syn and $A\beta$ and their interaction via the influence they impose in their enzymatic degradation via the enzyme IDE. Furthermore, studies on $A\beta$ and clearance system components (ubiquitin and 20S proteasome, IDE) were conducted to highlight the complexity of their interaction, with special focus on IDE and the way its mutation and presence of different metal ions influence its function. These studies tackled the different components of protein aggregation as the goal is to tackle foldopathies from different angles.

3.1. The interplay between α -Syn's carbonylation, aggregation and metal ions

3.1.1. α -Syn carbonylation by ACR

α -Syn was overexpressed in *E.coli* and purified through several chromatographic steps. The purity and identity of the final product was ascertained by means of high-resolution MS spectra (Figure 3.1) where the experimental molecular weight (14459 Da) matches the theoretical mass of the protein.

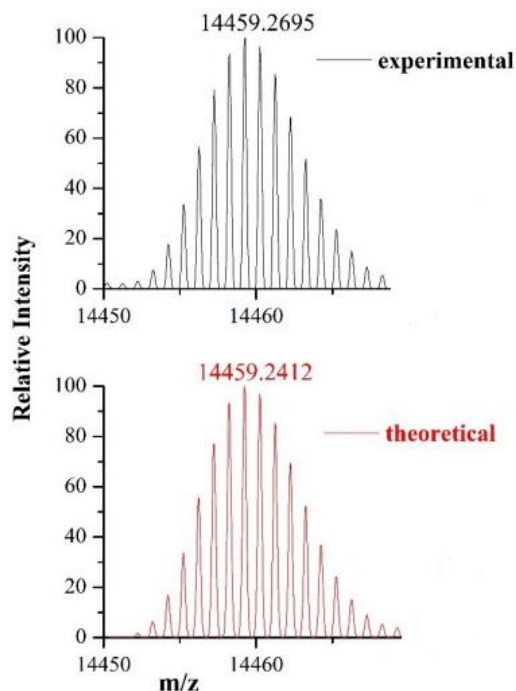


Figure 3.1. The molecular weight of synuclein matches that of theoretical value

Initial studies on the relationship between α -Syn and ACR were carried out in a time- and dose-dependent manner to explore the formation of a mono adduct between ACR and α -Syn. A Michael adduct appears as a +56 Da on LC-MS spectra. When the α -syn/ACR molar ratio was equal to 1:10 (Figure 3.2, left), the mono-derivative is detectable after 1.5 hours. Moreover, the higher the incubation time, the greater the number of adducts. In a dose-dependent experiment (Figure 3.2, right), the best α -syn-ACR molar ratio to monitor the mono modification of ACR on α -syn is 1:10. The type of adducts (Michael and/or Schiff base) between α -syn and ACR as well as the protein sites modified by ACR were probed (Table S1, which shows findings after 4hrs of syn-ACR reaction highlighting Michael

adducts and Schiff base linked to α -syn) by means of a LC-MS-based approach. The combination of a carbonylation assay with trypsin digestion produced several α -syn fragments (some of which are modified) as seen in Table S2 (α -syn digestion by trypsin in the presence of ACR, both carbonylated and non-carbonylated peptides). Interestingly, most of the modified peptides contain a missed tryptic cleavage site. The 46-58 peptide, which is modified at his50 (Figure S1, ms/ms of peptide 46-58 of α -syn showing modification by ACR at his50, while the table highlights the different ms/ms fragments corresponding to the primary sequence), as detected by MS/MS analysis, increases in production as a function of time. It is the sole modified peptide devoid of a missed cleavage site (Figure 3.3). All the peptides without missed cleavage share a similar ionization property, including the unmodified 46-58 peptide, due to their similar intensities except for peptide 1-6. Moreover, the levels of modified α -syn are low as the formation of non-modified peptides aren't affected by the presence of the carbonylation agent.

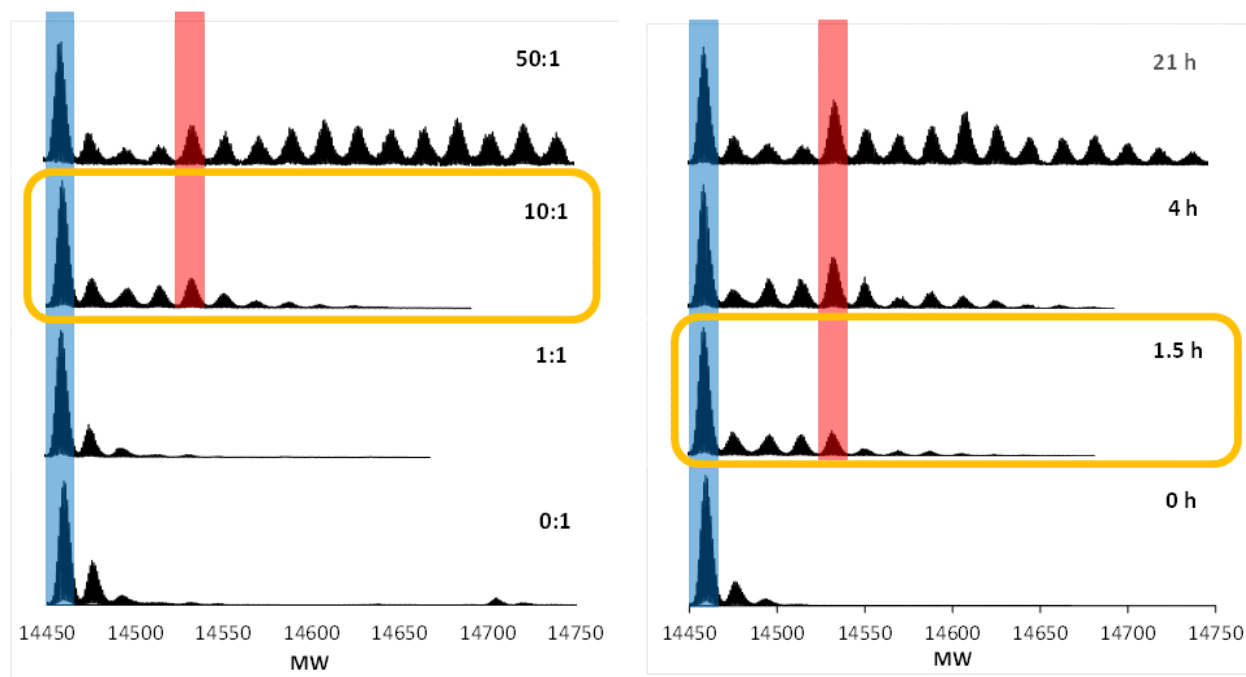


Figure 3.2. Deconvoluted MS spectra of the reaction mixture Left = after 6 h incubation at several α Syn/ACR ratios, Right = α Syn/ACR 1:10 ratio over time: (blue=Syn, Red=Syn-ACR).

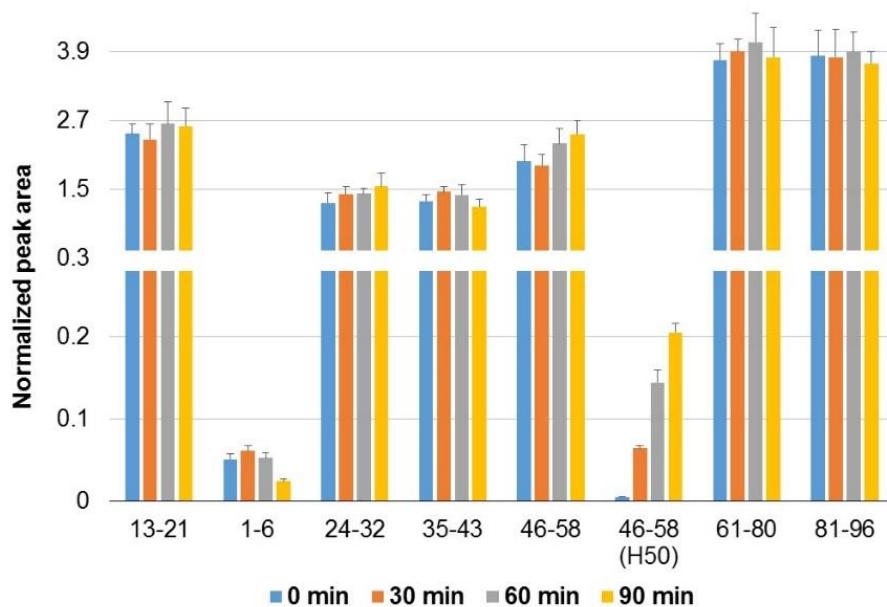


Figure 3.3. Formation of the main α -syn tryptic peptides that do not contain any missed-cleavage. Bars related to each peptide has been reported as a function of the incubation time with ACR. The carbonylated residues are shown in parentheses.

Trypsin targets lysine, but the ACR modifications on lysine prevent the cleavage on that site. Hence, the analysis of modified missed cleavage peptides is necessary to examine ACR modification of lysine residue. Among the fifteen lysine residues in α -syn, ten are modified by ACR (Figure 3.4, right side). However, modification at the highly reactive His site (Figure 3.3) remains more intense in comparison to lysine residues. Only two peptides (59-80 and 81-97) out of the peptides containing missed cleavage are formed without ACR modification (Figure 3.4, left side); however, the levels of these peptides are still minor in comparison to that of peptides without a missed cleavage (Figure 3.3). The MS/MS locates the modified residue even for isobaric fragments (46-60 and 44-58), as reported in Figure S2 (ms/ms of peptide 46-60 of α -syn showing modification by ACR at lys58, while the table highlights the different ms/ms fragments corresponding to the primary sequence) and Figure S3 (ms/ms of peptide 44-58 of α -syn showing modification by ACR at lys45, while the table highlights the different ms/ms fragments corresponding to the primary sequence).

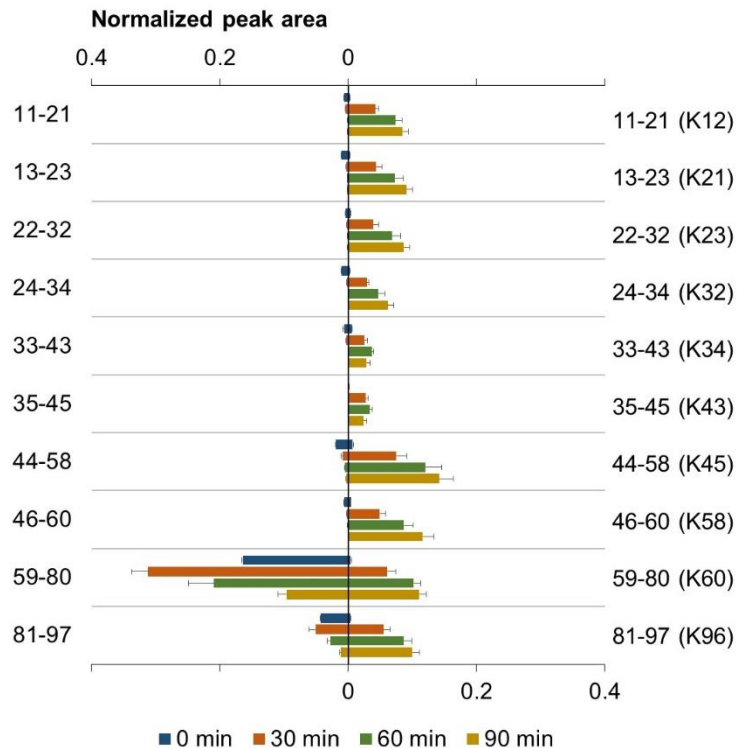


Figure 3.4. Formation of the synuclein tryptic peptide containing a missed-cleavage, modified (right-side bar graph) or not (left-side bar graph) by acrolein. Bars related to each peptide has been reported as a function of the incubation time with acrolein. The carbonylated residues are showed in parentheses.

The effect of copper is also monitored in the Michael adduct forming fragments. Copper, equally to ACR, binds to his50. The competition between Michael adducts formation and coordination with copper is monitored. The increase in copper concentration is inversely proportional to adduct formation with lowest modification levels observed at 1:4 α -syn : copper(II) especially noticed at peptide 46-58 (Figure 3.5). Moreover, a closer look at His50 adduct of peptide 46-58 reveals the relationship between reaction time, adduct formation and copper concentration. From Figure 3.6 we observe the increase in adduct formation in the absence of copper(II) at 90 minutes. However, the increase in copper concentration is competing with ACR on his50 binding which significantly reduces adduct formation. Therefore, longer time=more adduct however, increase in copper(II)=competition and less observed adducts on his50. To verify that the decrease in adduct formation is linked to copper coordination and not a different process, a pH experiment was carried out. Copper(II) coordinated with his50 at neutral pH. At acidic pH, copper(II) no longer coordinates with his50. Therefore, theoretically since copper(II) does

not interact with α -Syn at low pH, adduct formation should not be affected by the increase in copper concentration, which is seen in Figure 3.7 (decrease in α -Syn-ACR modification at neutral pH as copper(II) increases, while similar increases at pH 6 have no effect on the adduct's formation).

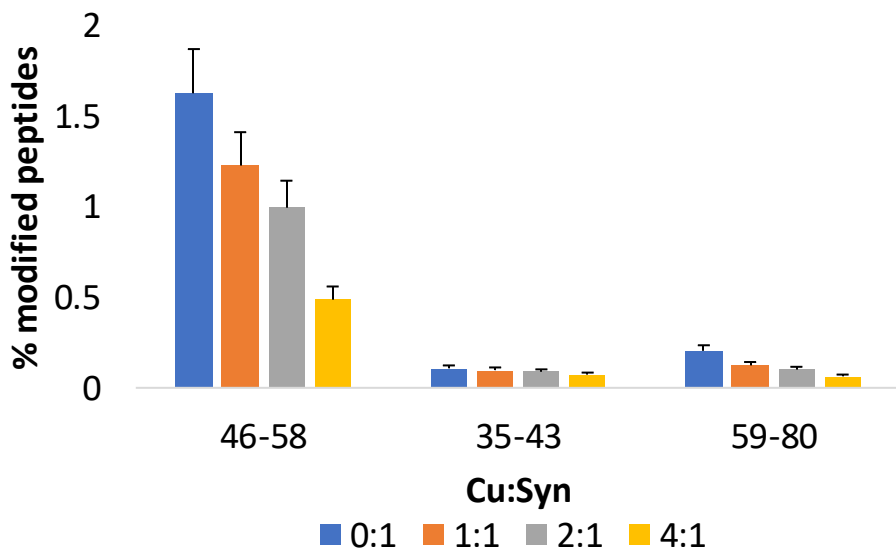


Figure 3.5. Effect of different copper ratio on Michael adducts (MA) fragments. Note that Ma/wt. %= (the LC-MS area of adduct peak /area of unmodified peak)*100.

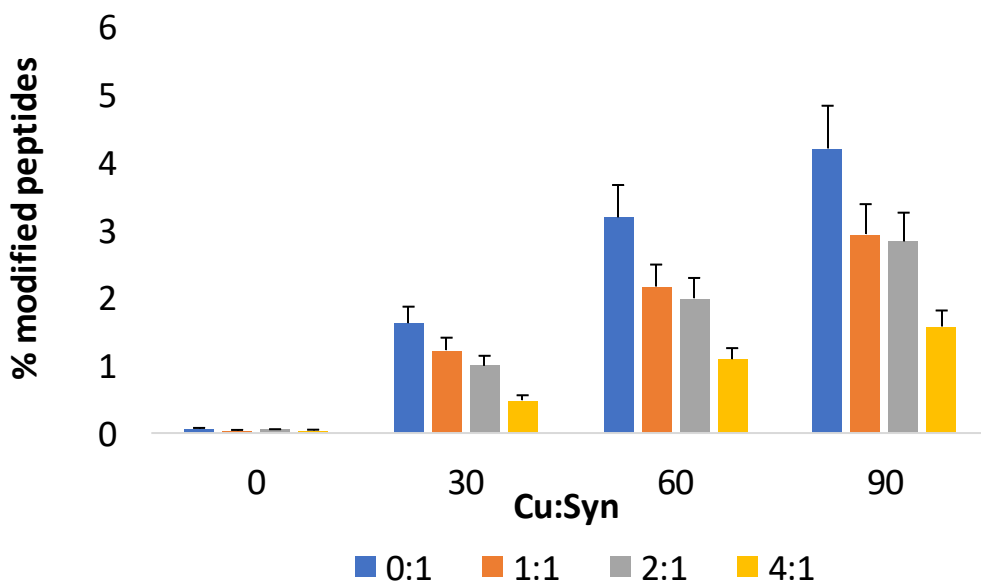


Figure 3.6. The combined effect of [copper] and reaction time on adduct formation (bar plot) of peptide 46-58 at His50, note that Ma/wt. %= (the LC-MS area of adduct peak /area of unmodified peak)*100.

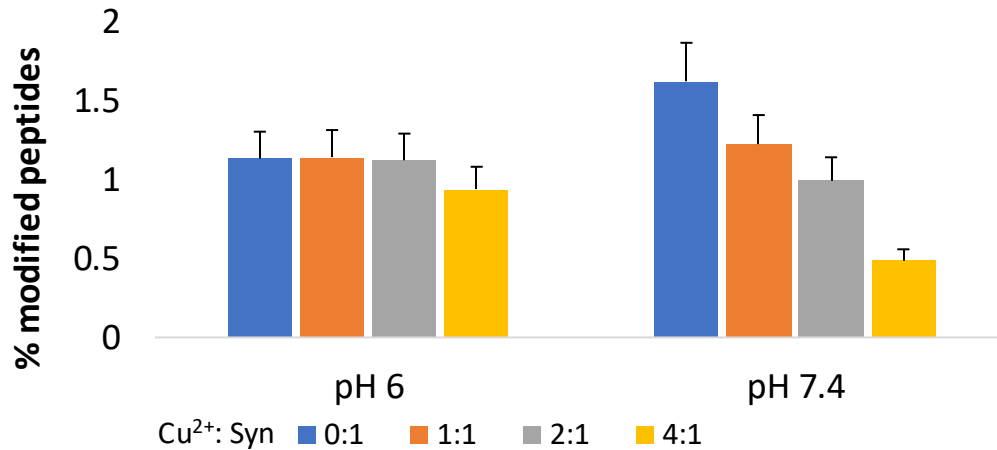


Figure 3.7. The effect of increasing copper concentration on adducts formation of peptide 46-58 at His50 in different pH conditions.

Different concentrations of Cu(II) were used to test its effect on the ACR modification of α -syn. The comparison was carried out between his50 containing peptide and the rest of the peptides which were modified at their lysine residue. The fragment containing his50 (Figure 3.8) is the only fragment affected (reduced) by the increasing levels of Cu^{2+} among the ACR modified peptides (with or without missed cleavage) after 90 min of reaction (Table S3, shows percentage modification of α -syn carbonylated peptides at different times in the presence of different copper(II) ratios). A similar pattern is noticed after 30 and 60 min of reaction (Figure S4, shows a time-dependent increase in his50 modification level, however modification levels decreases as copper(II) increases). This effect is due to the competition between ACR and Cu(II) on His50 binding site.

Therefore:

1. His50 is a unique interaction site for ACR and Cu^{2+} competes on the binding at neutral pH.

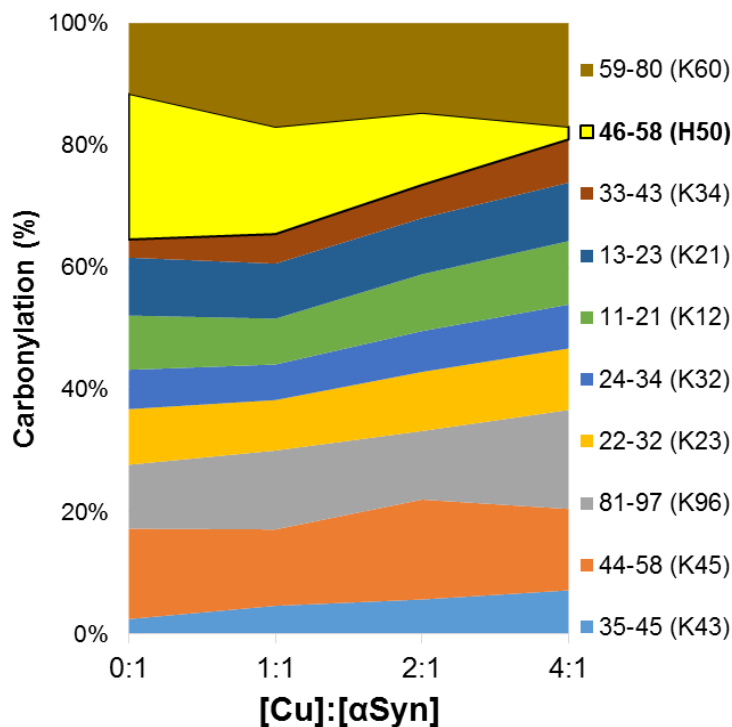


Figure 3.8. Modification percentage of the main ACR-linked tryptic peptides after 90 min reaction, as a function of the Cu^{2+} :Syn molar ratio. The carbonylated residues are shown in parentheses.

3.1.2. DLS and CD measurements

Other measurements involving ACR and α -syn were carried out. Both DLS and CD were recruited to study the interaction between the protein and the reactive species in the presence of Cu^{2+} . The formation of oligomeric species was investigated using DLS, which measures the hydrodynamic radius of the protein forms, directly proportional to their size. Previously conducted experiments^{46,56} involving the monomeric unfolded form of α -syn were in agreement with the Stokes diameter (d_H) found in this experiment (6.3 ± 0.3 nm, red line Figure 3.9 A). However, as the incubation time increases the species shift towards higher d_H values, particularly the presence of higher species with a diameter of 32 nm and 80 nm at $t = 120$ h. However, at 144h the monomer completely shifted towards the aggregates (black line Figure 3.9 A), meaning that *in vitro* at 37°C , α -syn is completely devoid of monomer species in 144h.

The species distribution is different when α -syn/ACR molar ratio is 1:10 (Figure 3.9 B). Higher species are no longer detected, and the main peak observed after 144h of

incubation has an d_H value (7.6 ± 0.2 nm, Figure 3.9 B, Black line) greater than that of monomeric α -syn. Because of the detection limits of the DLS instrument, it is difficult to unambiguously attribute this peak, but it might correspond to a mixture of monomer and dimer species. A second smaller peak at 26 nm corresponding to smaller oligomers (trimers or tetramers) is also formed. The intensity of this peak remains the same during the incubation time, which corresponds to the inhibitory effect of α -syn:ACR adduct formation on the protein's aggregation state.

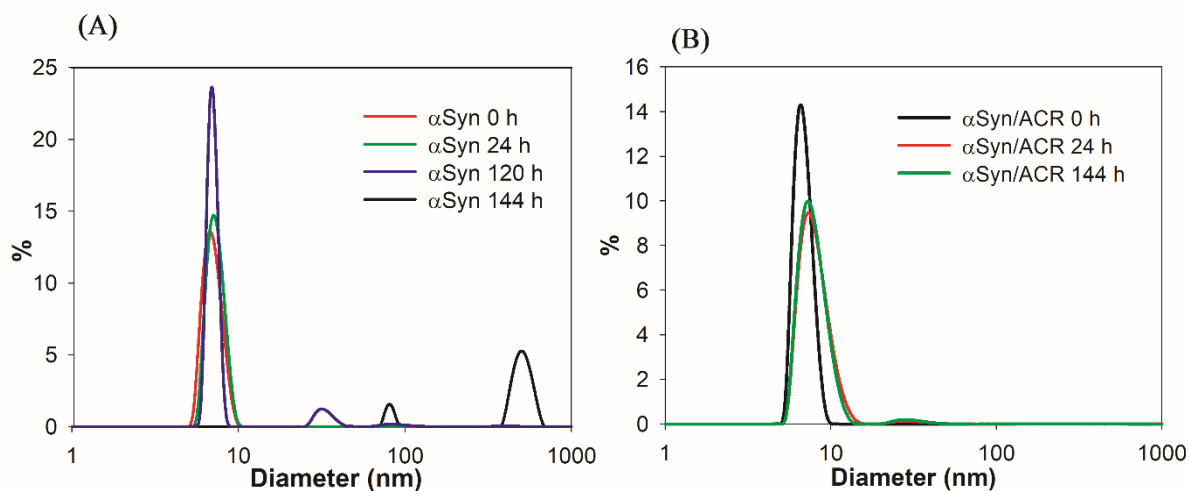


Figure 3.9. The volume distribution of α -syn alone (A) and the mixture α -syn/ACR 1:10 (B) at different times.

Cu^{2+} is also a player in the ACR- α -syn interaction and its roles were tested by using DLS. In the absence of ACR (Figure 3.10, red and black lines) the aggregation pattern of α -syn with Cu^{2+} involves the instantaneous formation of an oligomer with a mean diameter of $44 \text{ nm} \pm 3 \text{ nm}$; the monomeric form ($6.8 \pm 0.2 \text{ nm}$) remains the main species. Upon the addition of ACR, the sole noticeable peak is that related to the monomer and the aggregated forms are not detectable by DLS (Figure 3.10, green and blue lines). Therefore, the co-presence of ACR and Cu^{2+} with α -syn has led to the inability to detect oligomers and/or aggregates in the DLS spectra, while the sole incubation of ACR with α -syn lead to the formation of small oligomers during the incubation time. Hence, ACR might play a potential role in α -syn's aggregation as these spectra show a reduction/inhibition of formation of these higher species during the reaction time.

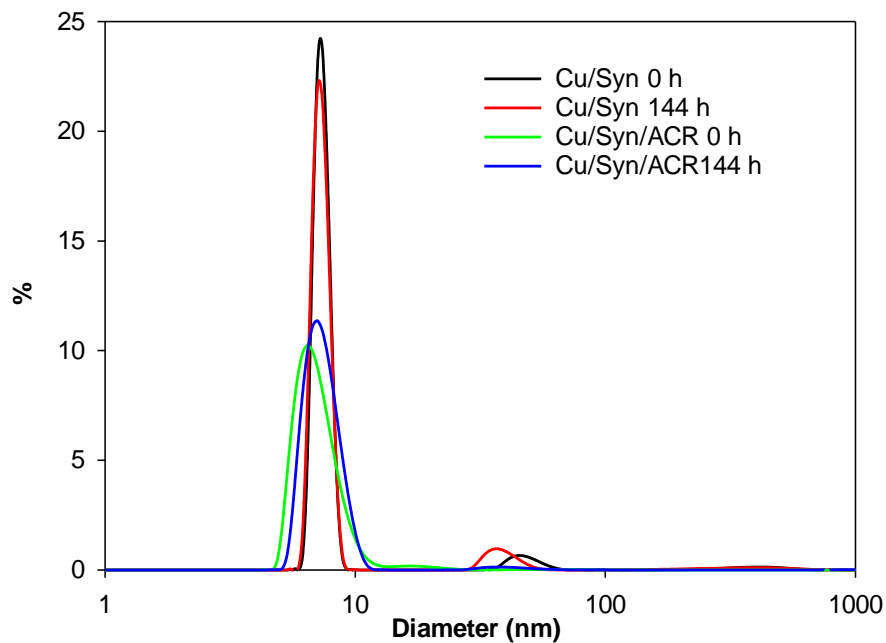


Figure 3.10. The volume size distribution of the mixtures $\text{Cu}^{2+}/\alpha\text{-syn}$ and $\text{Cu}^{2+}/\alpha\text{-syn/ACR}$ at the beginning ($t=0$ h) and at the end ($t=144$ h) of the incubation at 37°C in MOPS (pH 7.4).

Finally, CD measurements of the mixtures $\alpha\text{-syn}/\text{Cu}^{2+}$, $\alpha\text{-syn/ACR}$, and $\alpha\text{-syn/ACR}/\text{Cu}^{2+}$ for total reaction time of 52 hrs., resulted in a local minimum at ~ 198 nm corresponding to a random coil structure of $\alpha\text{-Syn}$ (Figure 3.11). The formation of β -sheet structures was not observed during the incubation time. Overall, ACR inhibited the aggregation process of $\alpha\text{-syn}$ both in the presence and in the absence of Cu^{2+} . Only the formation of $\alpha\text{-syn}$ dimers or other very small oligomers could be observed in the presence of ACR.

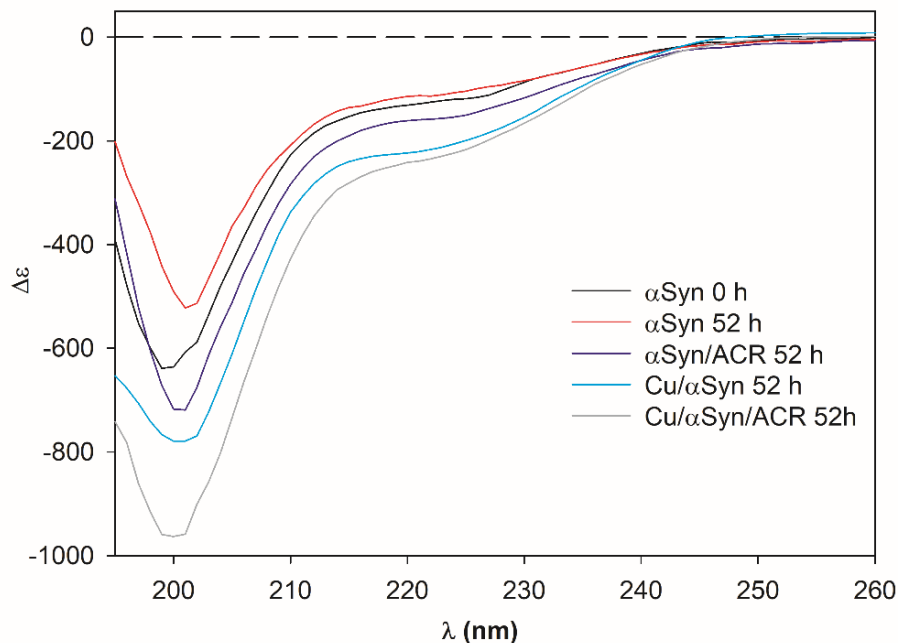


Figure 3.11. CD spectra of α -syn alone and the mixtures α -syn/ACR, Cu^{2+}/α -syn and Cu^{2+}/α -syn/ACR at the beginning ($t=0$ h) and $t=52$ h of the incubation at 37°C in MOPS (pH 7.4).

3.1.3. Aggregation assay syn-ACR

The formation of large protein aggregates, with and without ACR, was monitored by using a fluorometric assay (Figure 3.12). The aggregation assay monitors the formation of aggregated species as a function of the intensity of the fluorescence dye (ThT). In the absence of ACR, the kinetic parameters of the fitted curve (Figure 3.12), i.e. the maximum fluorescence gain ($F_{\text{max}} - F_0$) and the lag time (t_{lag}) were 20.1 ± 0.4 RFU and 43.4 ± 0.8 h, respectively which clearly indicates the presence of aggregates in the sample within the reaction time. The presence of ACR seems to inhibit α -Syn from aggregating within the time period of the experiment as the line (Red) remains flat. These data together with CD, and DLS findings show that the presence of ACR and its carbonylation of His50 in α -syn might be responsible for inhibiting and/or delaying the aggregation process. These reactions were carried out for a limited time period (144hrs for DLS, 52 hrs. for CD and ~ 80 hrs for ThT assay) and since α -syn's aggregation, unlike that of $\text{A}\beta$, is a lengthy procedure. It is possible that this interaction simply delayed the aggregation process and more time is needed to observe the aggregation. However, the observation of a delayed aggregation shows the importance of conducting further future studies on α -syn-ACR.

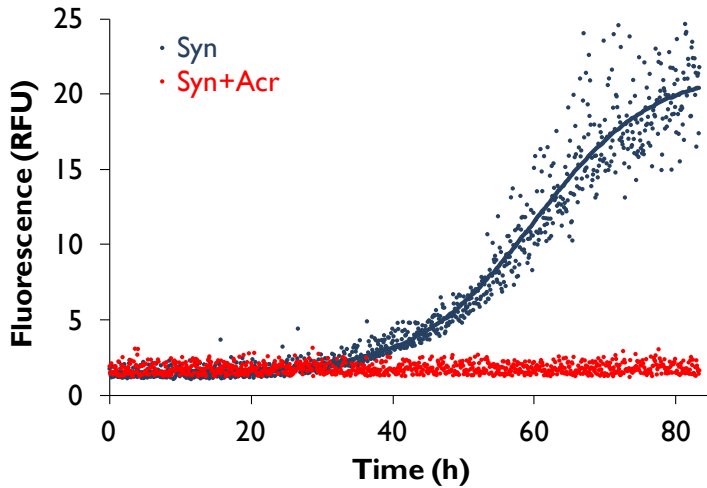


Figure 3.12. ThT aggregation assay of α -Syn-ACR 1:1 molar ratio

The physiological levels of ACR are most probably much lower in comparison to *in vitro* concentrations; however, the low levels lead to damage in a chronic manner. Our study is focused on targeting the early stages of carbonylation process. The mode of interaction between α -syn and ACR in the presence of Cu^{2+} is simplified in a proposed model Figure 3.13 where the presence of ACR modifies α -syn mainly at his50 (unique his in primary sequence), however, the co-presence of increasing concentrations of copper(II) at neutral pH, interferes with this reaction as copper(II) also interacts with his50.

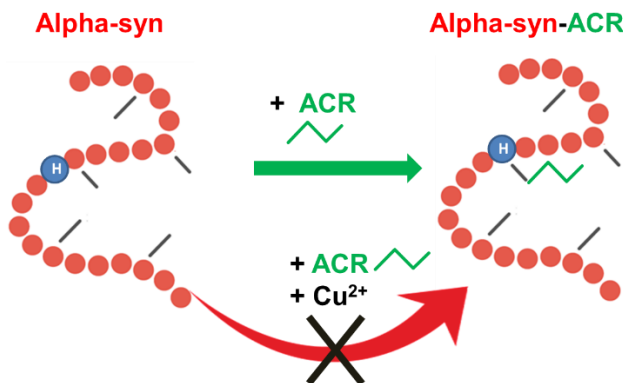


Figure 3.13. The mode of interaction between α -syn, ACR and Cu^{2+} .

3.1.4. P2 peptide and ACR

P2 peptide Ac-EGVVH-NH₂ was synthesized and the peptide mimics the α -syn 45-50 sequence which encompasses his50. The purpose of synthesizing this peptide was to a)

further confirm the interaction between his50 and ACR (Table S4 which shows P2 peptide adduct with ACR via MS and S5 which shows ms/ms of P2-ACR peptide showing modification at his residue) and b) to test the role of Cu^{2+} directly on his50, since Cu^{2+} has three binding sites on α -syn, as mentioned in the introduction. The molecular weight of P2 is 580 Da, an increase of 58 Da on the HRMS spectrum refers to a reduced Michael adduct formation while an increase of 40 Da on the same spectrum would account to a reduced Schiff base formation. The reaction was carried out in the presence of different Cu^{2+} concentrations and Table 1 reports the percentage of the Michael adduct formed to the P2 signal. The production of Michael adduct increases with time, thus confirming that the ACR action is time dependent. Moreover, it is evident that the increasing amounts of Cu^{2+} reduce the adduct formation in all reaction times, which is also graphically represented in Figure 3.14 which shows that pH 7 has a greater effect on the action of copper(II) on the modification level of P2 peptide with ACR in comparison with pH 6 were copper(II) doesn't interact with histidine residue.

Table1. Percentage of ACR adduct formation in the presence of different Cu^{2+} concentrations.

Reaction time	0 min				30 min				60 min			
[Cu^{2+}]: [P2]	0:1	1:1	2:1	4:1	0:1	1:1	2:1	4:1	0:1	1:1	2:1	4:1
% of ACR adduct formation	0.29	0.23	0.13	0.07	4.21	3.44	2.05	1.74	9.69	6.69	5.01	3.51

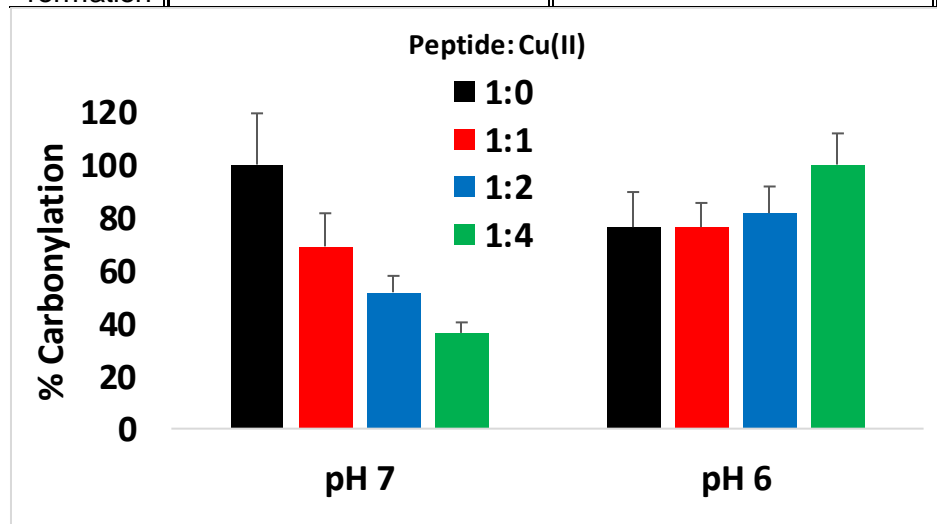


Figure 3.14. The effect of Cu^{2+} on Michael adduct formation on P2 peptide.

ACR modification also occurs by the formation of short-lived and reversible Schiff bases. Nevertheless, Schiff base formation is negligible (Figure S5, percentage modification of P2 peptide by ACR at pH 7.4 in the presence of different copper(II) ratio at different time points). Similar results were observed for the NHE-based carbonylation of α -syn⁵⁷. Schiff base modifications of HNE don't amount to 1%, even if high quantities of HNE are supplied. Whereas, Michael adducts constitute more than 99% of modifications⁵⁷.

All the reactions with ACR were performed at pH 7.4 which ensures the Cu^{2+} interaction with his50. In acidic pH, Cu^{2+} no longer coordinates his50 due to the protonation of the imidazole nitrogen atoms. Therefore, the experiment was also carried out at pH 6 to confirm the competition on his50 as a binding site between ACR and Cu^{2+} . As reported in Figure 3.10, the Michael adduct formation is not affected by Cu^{2+} . Moreover, at the acidic pH the Schiff base values were still negligible (Figure S6, percentage modification of P2 peptide by ACR at pH 6 in the presence of different copper(II) ratio at different time points). Therefore, studies on P2 peptide which mimics α -syn 45-50 containing His50 shows similar results to those observed with α -syn including the competition of ACR and Cu^{2+} on his50 binding site.

3.1.5. MDA and α -Syn

MDA is able to bind α -Syn through two aldehyde groups producing Schiff bases with the nitrogen group of lysine or the imidazole group of histidine. Trypsin digestion targets lysine or arginine, hence, the presence of a missed cleavage site helps the identification of MDA interaction sites. The peptides produced by trypsin digestion of α -Syn were analyzed by using MALDI-TOF (Figure S7 graphic representation of α -Syn tryptic peptides by MALDI were the main unmodified peptides are 46-58 and 81-96 while Table S6 represents the experimental/theoretical masses of the peptides including sodium adducts). The identified peptides are quite similar to those identified by ESI-MS for the same protein (Table S2). The attribution was carried out using the online tool ExPASy FindPept. In the presence of MDA, the modified peptides were identified and as it is shown in Figure 3.15 with peptides 46-58, 59-80 being the most significant ones. The level of unmodified peptides is still higher in comparison to the modified ones however, as noticed from Figure 3.15 the modification level increases with reaction time. In Table

2, which also depicts the modified and unmodified tryptic peptides of α -Syn, the presence of Na^+ and or K^+ is typical for MALDI spectra, and the modified peptides are underlined in the table. Whereas, the error was less than 10 ppm which is a highly accurate correlation between experimental and theoretical peptides. The increase in the m/z value is 56 Da, corresponding to the difference between MDA (72 Da) and a water molecule (18 Da). Hence, it points out towards the formation of a Schiff base. Since trypsin cleaves at C-terminal of lysine, the presence of another lysine (besides the C-terminal residue) within the peptide sequences (59-80, 44-58, 97-102 and 81-97) and his50 in the sequence 46-58 suggests that the interaction of MDA with a basic amino acid inhibits the action of trypsin enzyme on that cleavage site. Interestingly, only four out of the fifteen lysine residues interact with MDA (K45, 60, 96 and 97). Similar to α -Syn interaction with ACR, MDA binds his50 with an affinity higher than that showed with lysine. Since the most significant modification as seen in Figure 3.15 is on peptide 46-58 (which contains His50) and MDA can modify the imidazole group of histidine, it is important to further analyze this peptide to identify the modification site.

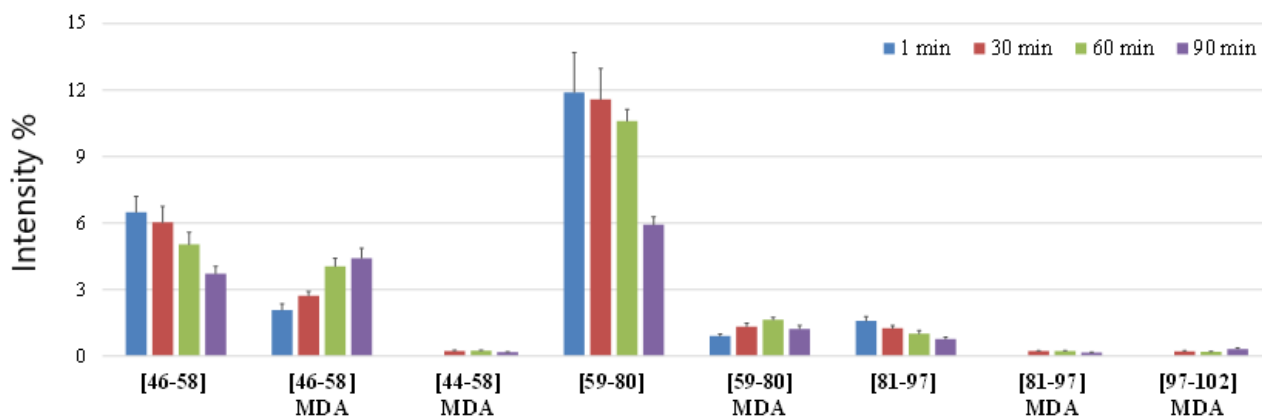


Figure 3.15. MDA modified and non-modified tryptic digestion α -Syn peptides

Table 2. α -Syn-MDA peptides produced by trypsin digestion

Species	Sequence	m/z experimental	m/z theoretical	δ (Da)	Δ (ppm)
[1-6] H ⁺	.MDVFMK.g	770.3587	770.3575	0.0011	1.5
[13-21] H ⁺	k.EGVVAAAEK.t	873.4658	873.4676	-0.0018	-2.1

[13-21] Na ⁺	k.EGVVAAAEK.t	895.4557	895.4496	0.0061	6.8
[35-43] H ⁺	k.EGVLYVGSK.t	951.513	951.5146	-0.0016	-1.7
[46-58] H ⁺	k.EGVVHGVATVAEK.t	1295.6962	1295.6954	0.0008	0.6
[46-58] Na ⁺	k.EGVVHGVATVAEK.t	1317.6898	1317.6773	0.0125	9.5
[46-58] MDA H ⁺	k.EGVV H GVATVAEK.t	1349.7043	1349.706	-0.0016	-1.2
[46-58] MDA , Na ⁺	k.EGVV H GVATVAEK.t	1371.6976	1371.6879	0.0097	7.1
	k.TKEQVTNVGGAVVTGVTAVAQ				
[59-80] H ⁺	K.t	2157.1878	2157.1874	0.0005	0.2
	k.TKEQVTNVGGAVVTGVTAVAQ				
[59-80] Na ⁺	K.t	2179.1745	2179.1693	0.0052	2.4
	k. T K E QVTNVGGAVVTGVTAVAQ				
[59-80] MDA H ⁺	K.t	2211.1955	2211.1979	-0.0025	-1.1
	k. T K E QVTNVGGAVVTGVTAVAQ				
[59-80] MDA Na ⁺	K.t	2233.1819	2233.1799	0.002	0.9
[61-80] H ⁺	k.EQVTNVGGAVVTGVTAVAQK.t	1928.0439	1928.0447	-0.0009	-0.5
[61-80] Na ⁺	k.EQVTNVGGAVVTGVTAVAQK.t	1950.0327	1950.0267	0.006	3.1
[81-96]	k.TVEGAGSIAAATGFVK.k	1478.7851	1478.7849	0.0002	0.1
[81-96] Na ⁺	k.TVEGAGSIAAATGFVK.k	1500.7762	1500.7669	0.0093	6.2
[44-58] MDA H ⁺	k. T K E GVVHGVATVAEK.t	1578.8344	1578.8486	-0.0142	-9.0
[81-97] H ⁺	k.TVEGAGSIAAATGFVKK.d	1606.8805	1606.8799	0.0006	0.4
[81-97] Na ⁺	k.TVEGAGSIAAATGFVKK.d	1628.8718	1628.8618	0.0099	6.1
[81-97] MDA H ⁺	k.TVEGAGSIAAATGFV K .d	1660.8901	1660.8905	-0.0004	-0.2
[97-102] MDA H ⁺	k. K DQLGK.n	742.4108	742.4094	0.0014	1.9

Upon further inspection of the peptide fragments by MS/MS acquisition, the covalent modification site is identified as MS/MS allows for the detection of the primary sequences of each peptide. In Table 4 and Figure 3.16, the MS/MS identification of peptide 46-58 modified at his50 is shown, b and y fragments correspond to amino acid sequence from the N- and C-terminal respectively. An increase in the molecular weight of any of these fragments corresponding to the molecular weight of MDA would mean that one of the

amino acids in that sequence is modified, which is His50 in this case as seen in Table 4 as only fragments containing His50 are modified. In order to study the interaction between MDA and α -Syn quantitatively, the intensities were calculated as a percentage of TIC, as shown in Figure 3.16. Both modified and unmodified peptides were compared as a function of the reaction time. The trend shows the decrease in unmodified peptides (46-58, 59-80 and 81-97), whereas the intensity of the related modified peptides was increasing. Moreover, the his50 containing modified fragment is the most intense one at the end of the reaction time, thus confirming the importance of this his50 in the reaction with RCS.

Table 3. The identification of MS/MS fragments of 46-58 peptide corresponding to his50 modification.

Annotation	Meas. m/z	Calc. m/z	δ (Da)
y5 [9-13]	547.317	547.309	0.008
y6 [8-13]	618.397	618.346	0.051
y7 [7-13]	717.383	717.414	-0.032
y8 [6-13]	774.454	774.436	0.019
b5 [1-5] MDA	576.292	576.278	0.015
b6 [1-6] MDA	633.293	633.299	-0.006
b7 [1-7] MDA	732.359	732.368	-0.009
b8 [1-8] MDA	803.406	803.405	0.001
b9 [1-9] MDA	904.455	904.452	0.003
b10 [1-10] MDA	1003.480	1003.521	-0.041
b11 [1-11] MDA	1074.540	1074.558	-0.018
b12 [1-12] MDA	1203.599	1203.600	-0.001

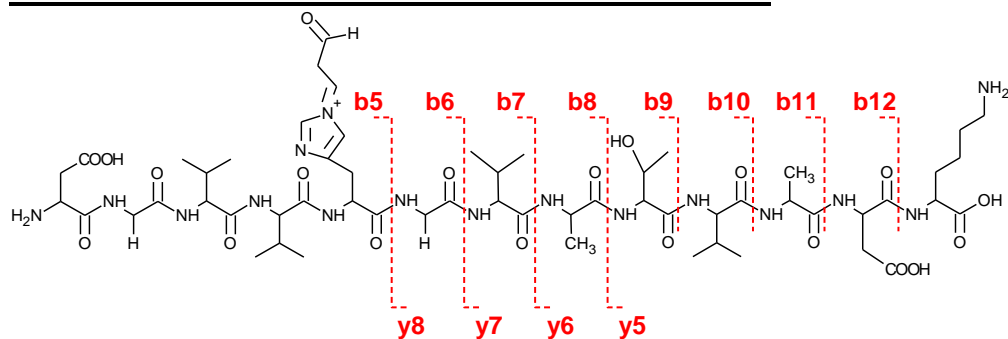


Figure 3.16. Representation of MS/MS of 46-58 peptide showing his50 modification

In conclusion, to study the effect of RCS on α -Syn, ACR interaction with α -Syn was studied using LC/MS where the interaction site was determined to be his50 and a competition in this site with copper(II) was established and confirmed when these experiments were repeated with a synthetic peptide (P2) corresponding to an α -Syn short peptide containing his50. CD experiments showed that the interaction of α -Syn with ACR in the presence and/or absence of copper(II) leads to a secondary structure of random coils and no aggregation inducing β -sheets, similarly ThT aggregation assay resulted in the absence of aggregation within the time limit of the experiment when α -Syn interacts with ACR. DLS experiments showed that aggregated species are replaced with reduced levels of oligomers in the presence of ACR alone and in the co-presence of copper(II). Studies using MALDI showed the interaction of α -Syn with another RCS called MDA at his50 too. Therefore, his50 is an important site for future studies on α -Syn and the interactions of RCS with this site have a direct effect on the protein's aggregation ability.

3.2. α -Syn interaction with compounds

3.2.1. Native mass spectrometry

Mass spectrometry is making a stand in structural studies of protein especially native mass spectrometry, as the entire protein sequence can be studied without any enzyme treatment. α -Syn is analyzed in ammonium acetate, which is a volatile buffer required for the ionization of native mass spectrometry samples. The signal stability indicates that the ionic strength of this particular buffer had little or no effect on α -Syn stability in solution (Figure 3.17, where native mass spectrum of the protein and its charge distribution can be seen). Other buffers such as MOPS and Tris, commonly used for α -Syn assays, interfere in the analysis of samples directly introduced to the ionization source. The sample was also analyzed on the negative mode (Figure S8), however the number of signals were less, so we proceeded with carrying out the experiments on the positive mode. α -Syn generally has better signal in the positive mode due to the abundance of protonation-prone (basic) amino acids in the sequence. The analysis of α -Syn with this technique revealed a charge state distributions (CSDs) as can be seen in Figure 3.17. The charge states of α -Syn are spread out from 7+ to 18+, which is a typical profile for an IDP since it samples multiple conformations in solution. Moreover, an ordered protein would display a lesser range of variation in the charge state. In this sample, with standard buffer pH 6.8,

the structure of the protein is in a less compacted state as the relative abundance of high charge state (15+) is prevalent. CSDs are indicative of conformation, compacted structures have less charges whereas an increase in mass is linked to an increase in charge depending on the conformation. Hence, a good correlation between the use of native MS and protein structure can be established⁵⁸.

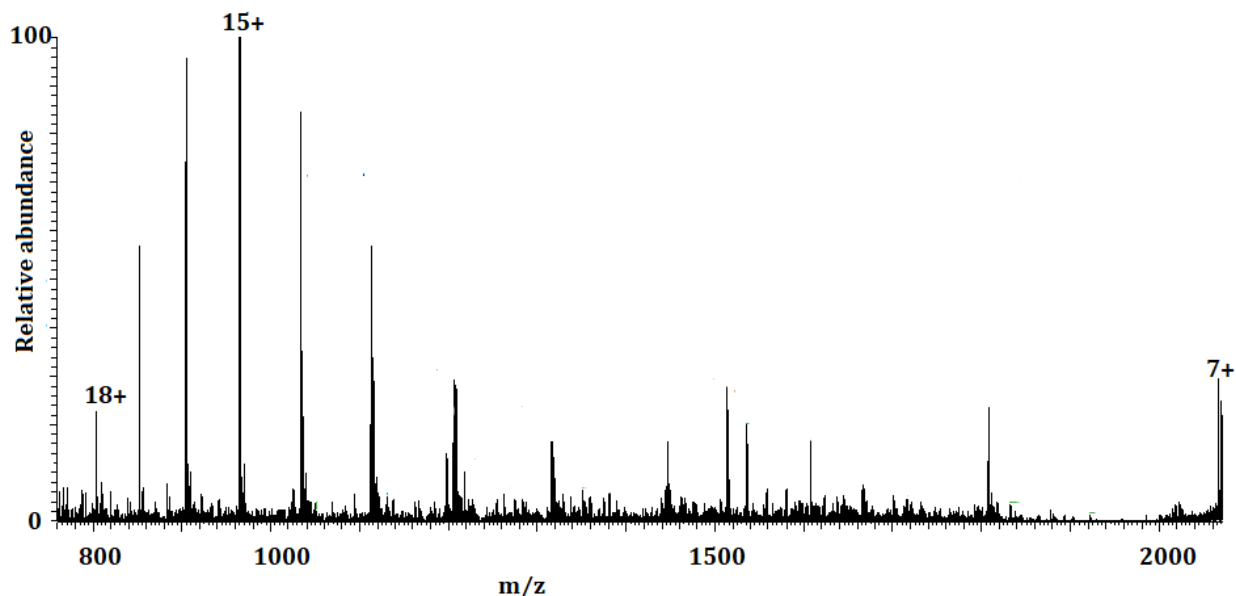


Figure 3.17. α -Syn profile in native mass spectrometry

In order to monitor the effect of the pH on the conformation, the protein was introduced to multiple pH conditions ranging from acidic to neutral to basic: (pH 3, 4.5, 6.5, 7.4, 8.5). The changes in the CSDs are an indicative of the effect the environment has on α -Syn's structure. In the acidic environment shown in Figure S9 (pH 3), Figure 3.18 (pH 4.5) and Figure S10 (pH 6.5), the compacted structure, the lower charge states, is prevalent. The charge state 7+ representing the compact structure is dominating at pH 3, and although the non-compacted structures are also present their relative abundance is only ~40% (represented by 14+) of that of compacted 7+ state. However, as the pH increases, there is an equilibrium between the compact (7+) and the non-compact (16+) structures as seen in both pH 4.5 and pH 6.5 in Figure 3.18 and Figure S10 respectively.

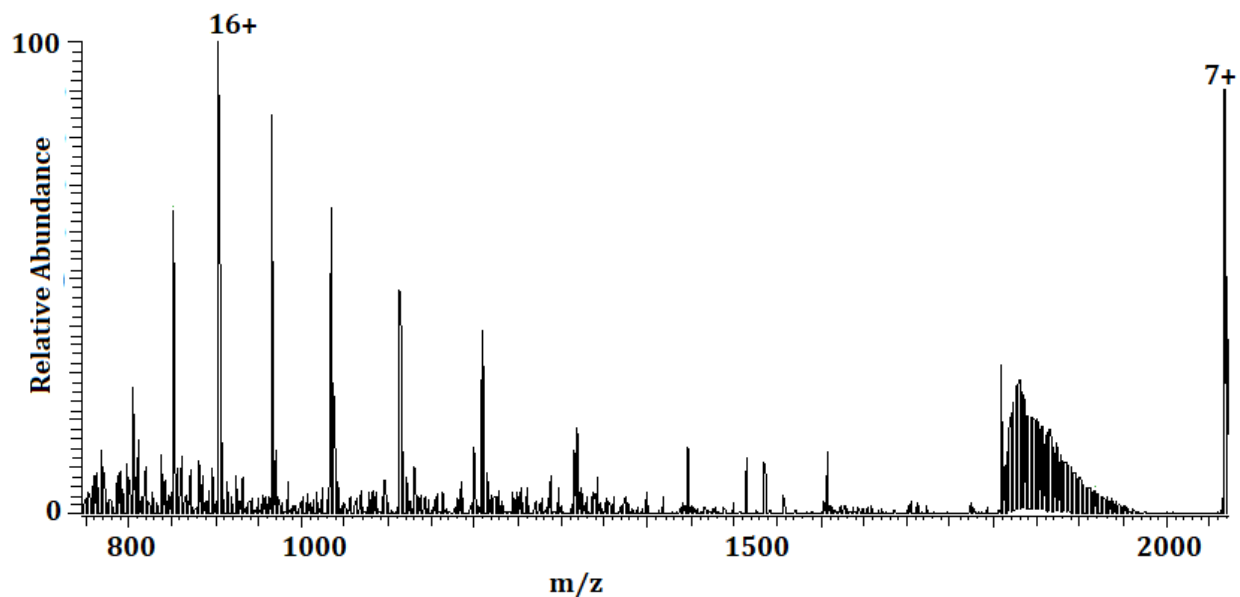


Figure 3.18. α -syn profile in native mass spectrometry pH 4.5.

In physiological conditions (Figure S11, pH 7.4) and basic environment (Figure 3.19, pH 8.5) the non-compact structure is the prevalent one. In Figure S11, the non-compact (15+) structure is dominating while the compact (7+) structure is at ~70% relative abundance compared to dominant charge. A further increase of the pH into basic (pH 8.5) as seen in Figure 3.19 reveals a further decrease in the relative abundance of the compact structure (7+) to ~40% compared to the maximum charge, while the compact (7+) charge remains dominant. These experiments at different pH suggest that pH plays a role in altering the already dynamic structure of α -Syn. Moreover, α -Syn takes different conformations in solution ranging from a dominant compact structure at acidic pH to a dominant non-compact structure at basic pH, which are readily investigated by native MS. These findings are consistent with the general consensus that IDPs could take different forms in solution and some of these forms can be stabilized at extreme pH conditions which aid in structural studies¹.

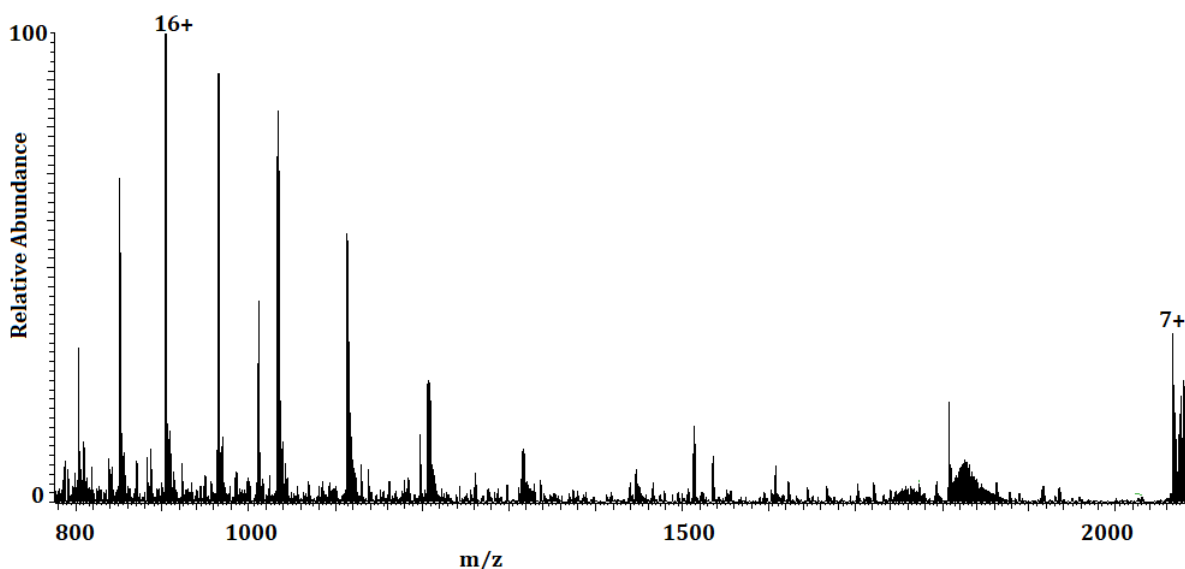


Figure 3.19. α -syn profile in native mass spectrometry pH 8.5.

Several compounds were tested against α -Syn to establish the possibility of interaction and therapeutic benefit. Most of the compounds were hydroxyquinoline (HQ) derivatives; which included the compound itself, a carnosine derivative (CarHQ) and a cyclodextrin derivatives (CDHQ and ABCDHQ). Additionally, Rifampicin is also utilized as a control as it is already known to inhibit the aggregation of α -Syn⁴⁸. Initially, the compounds were analyzed on native MS in the absence of α -Syn to check their stability in ammonium acetate. All compounds produced a reasonable spectrum as seen in the supplementary figures (Figures S12 (Rifampicin \approx 823 Da), S13 CarHQ \approx 397 Da, S14 CDHQ \approx 1305 Da, S15 ABCDHQ \approx 1475 Da) corresponding to their molecular weights, HQ spectra was not recorded as its m/z range is not within the limits of the instrument. The predicted contact between α -syn and each of these compounds is presented in Table S7 based on calculations of m/z value of α -Syn in addition to that of the specified compound, it aids in speeding up the identification process of α -Syn-compound. The calculations are based on the most frequently observed charge states in α -Syn's native MS spectrum.

All of the HQ derivatives were added in a concentration 5 times that of α -Syn. Rifampicin adduct was detected and marked with the red circles as seen (Figure 3.20, upper graph),

the value is similar to that calculated in Table S7. The deconvolved spectrum, which shows the molecular weights instead of the m/z value, confirms the molecular weight of the protein adduct as it equals the addition of α -Syn's molecular weight (14459 Da) with that of Rifampicin (Figure S12), moreover, Figure 3.20, lower graph, the larger image is a zoom-in on α -Syn-Rifampicin. As seen from both spectra, the relative abundance is low for α -Syn-Rifampicin, however it is still a known effective compound in preventing the aggregation of α -Syn⁴⁸. Hence, it is advisable to not dismiss the potential effect of any of these compounds without further testing.

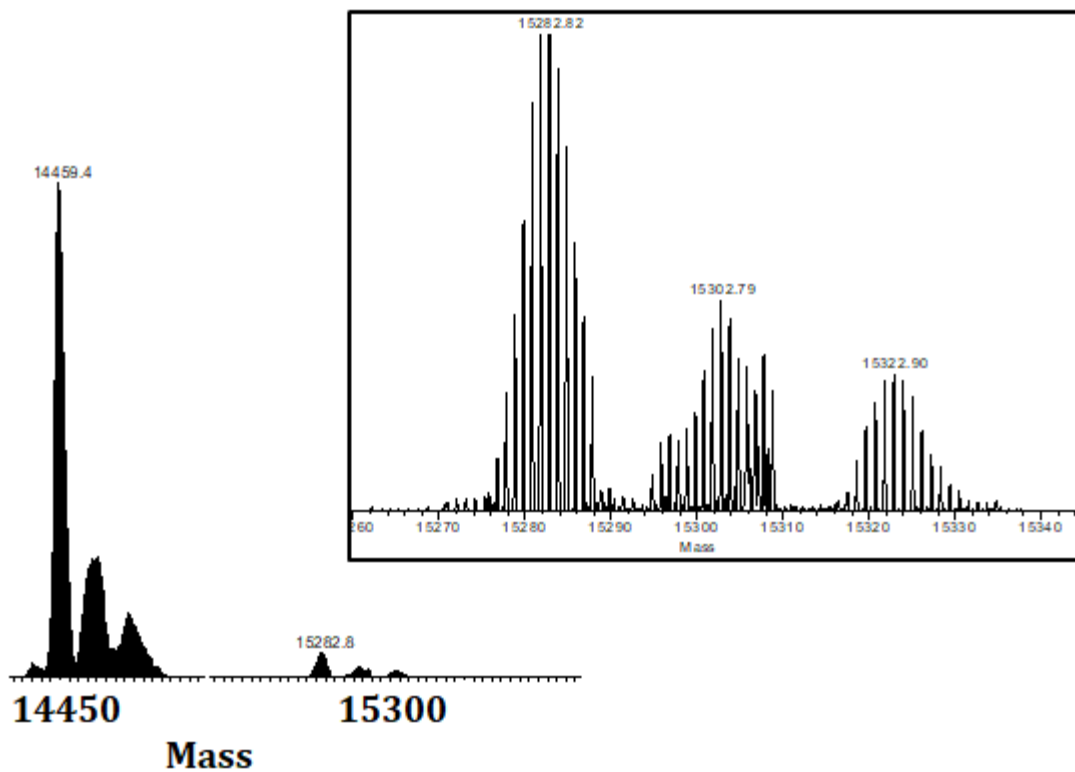
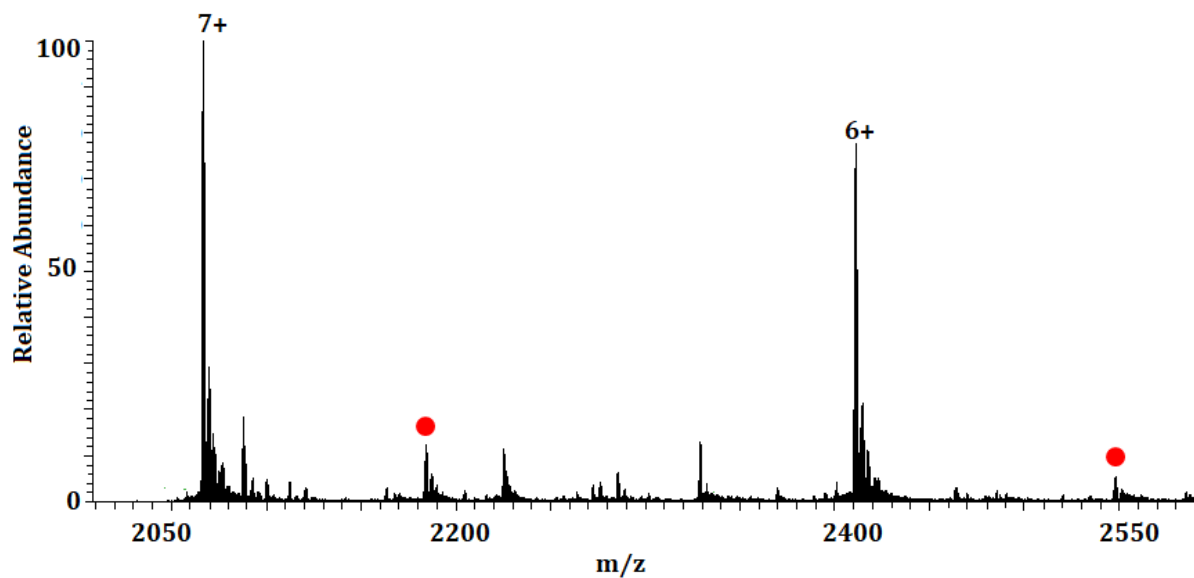


Figure 3.20. The interaction between α -Syn : rifampicin 1:5, (upper) original spectrum, (lower) deconvoluted spectrum.

The interplay between α -Syn and CarHQ is demonstrated in Figure 3.21. The upper graph which indicates the original spectrum shows a similar pattern to α -Syn-Rifampicin were the α -Syn-CarHQ signal is located at higher m/z values corresponding to those calculated in Table S7. The deconvolution (lower graph, the larger image is a zoom-in on α -Syn-CarHQ) translates to the molecular weight of α -Syn-CarHQ, molecular weight of CarHQ is displayed in Figure S13.

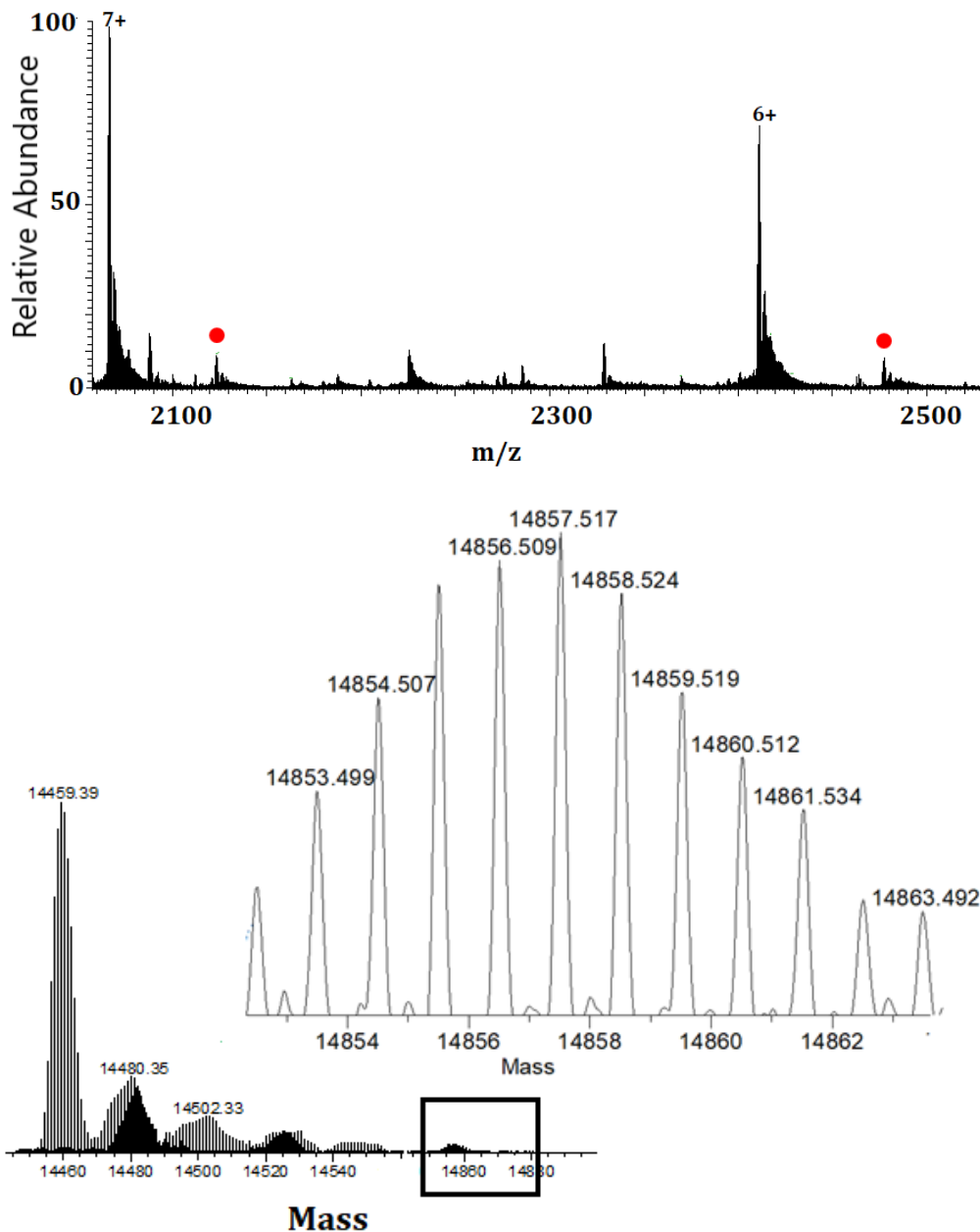


Figure 3.21. The interaction between α -Syn : CarHQ 1:5, (upper) original spectrum, (lower) deconvoluted spectrum.

Interestingly in Figure 3.22 (upper), CDHQ shows a very low interaction signal with α -syn at 1:5 α -Syn: CDHQ molar ratio which is quite difficult to deconvolute. When the ratio increases to 1:10 α -Syn/CDHQ, a better signal is obtained (Figure 3.22 middle), corresponding to calculated values in Table S7, the signal translates to a better deconvolution spectrum (Figure 3.22, lower) matching the molecular weight of CDHQ- α -Syn (molecular weight of CDHQ is displayed in Figure S14). The increase in the compound ratio as opposed to α -Syn is not a guarantee for a better native MS signal, since some spectra were difficult to record for some of the α -Syn-compounds at 1:10 molar ratio. Hence, several factors play a role in both the interaction and in giving rise to the final MS spectrum. The higher ratio, in this case, translated to a better signal at both the original and the deconvoluted spectra. It is possible that a CD derivatization of HQ might somewhat interfere with the native MS signal, since ABCD HQ interaction with α -Syn was also difficult to record in native MS. Perhaps a different derivatization and/or conditions might lead to a better signal in lower concentrations and further studies are needed to optimize these conditions.

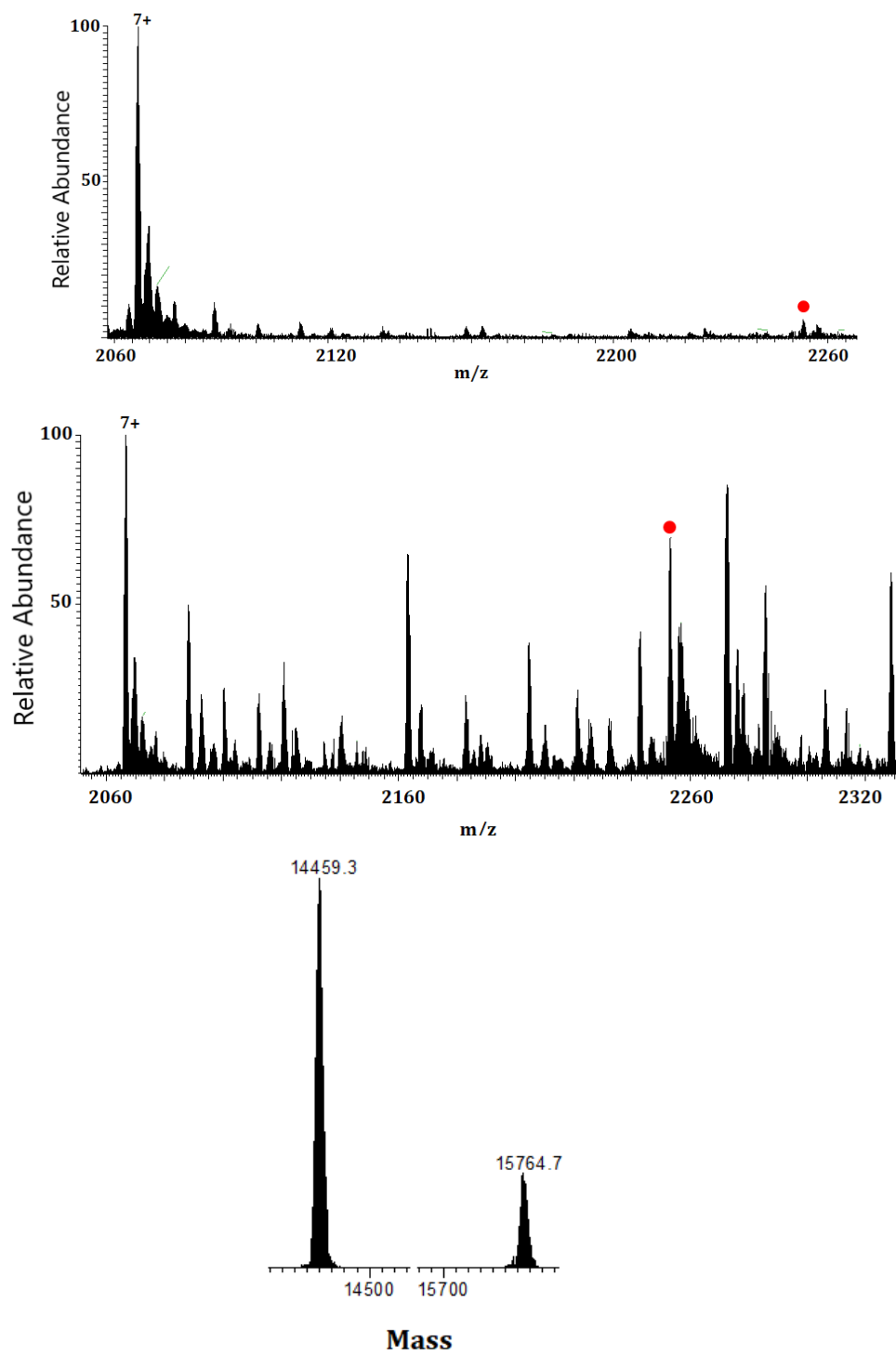


Figure 3.22. The interaction between α -syn/CDHQ (upper) original spectrum 1:5 molar ratio, (middle) original spectrum 1:10 molar ratio, (lower) deconvoluted spectrum 1:10 molar ratio.

An important benefit of HQ derivatization/conjugation with other compounds can be highlighted in the experiment between α -Syn-HQ 1:5 molar ratio where it was difficult to visualize the interplay on Native MS spectrum. Moreover, the deconvoluted spectrum showed an interaction with a small relative abundance in comparison to free α -Syn. Interestingly, the molecular mass of the contact corresponds to 2 HQ molecules (Table S7 shows the molecular weight of compounds and calculated m/z values for the interaction with 1 compound) interacting with 1 α -Syn which is worth further investigating (Figure 3.23). Likewise, it was difficult to record and/or deconvolute a spectrum for ABCDHQ, however we will proceed with it for future experiments as an HQ compound.

The native MS instrument is configured to focus on both low and high m/z one region at a time and through these investigations it was evident that for α -Syn less crowded and easily recognized signals are at higher m/z. The general observation is that it is easier to detect the adducts at higher m/z which corresponds to less charged states (compacted structures). The interplay between HQ and its derivatives with α -Syn can be detected via Native MS. Although the relative abundance of these contacts is relatively low in comparison to that of free α -Syn, it is still possible for some, if not all, these compounds to play a role in the inhibition of the aggregation of α -Syn, just like Rifampicin. This possibility will be explored next with a fluorescence dye assay.

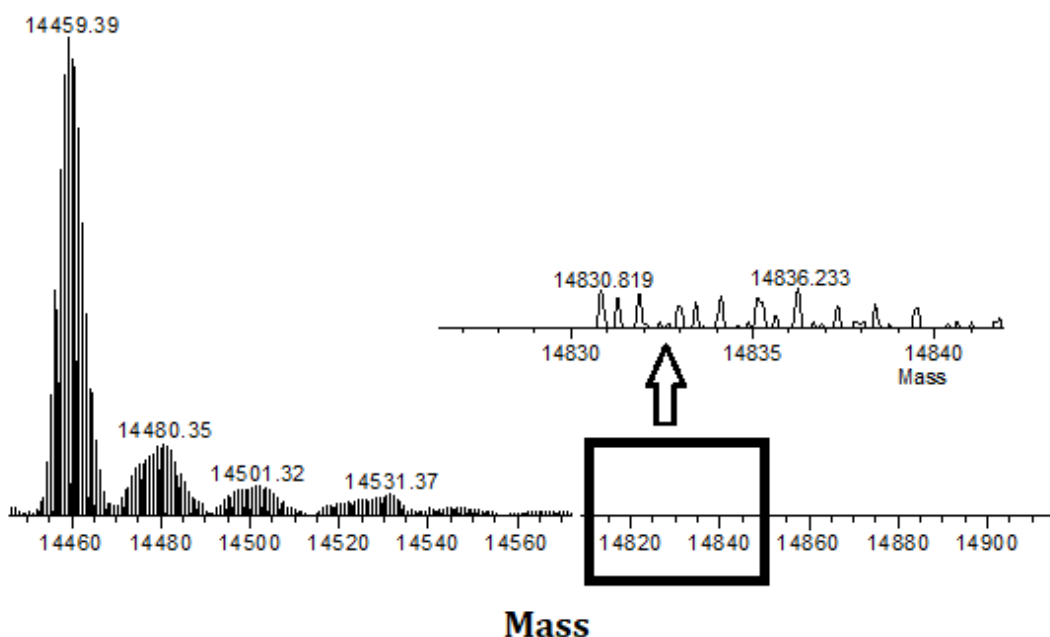


Figure 3.23. The interaction between α -syn : HQ 1:5 molar ratio, deconvoluted spectrum.

3.2.2. Aggregation assay

In order to understand the effect of the tested compounds on the aggregation of the protein, a fluorometric aggregation assay was carried out in the presence of each of these compounds in a molar ratio similar to that used for the native MS studies (1:5). As reported in Figure 3.24, ABCDHQ (light green), have the highest antiaggregant potential to halt the progression of α -syn aggregation. CDHQ (blue) and Rifampicin (red) have a similar antiaggregant potential as ABCDHQ, but it was much difficult to fit the data. The kinetic parameters for the sigmoidal fit of the Syn aggregation data in the absence and in the presence of the compounds are shown in Table 4. These parameters are extracted from the single best run/fit of each experiment category. In Table 4, the fit was clearly not good for CDHQ as it resulted in a negative lag time value, however, rifampicin has a maximum fluorescence gain of 3 ± 0.04 and t-lag value of 30 ± 1 both consistent with its role as an antiaggregant.

On the other hand, CarHQ (pink) seems to have an activating effect on the protein's aggregation. The comparison between CarHQ and α -Syn in the absence of compounds shows that the maximum fluorescence gain of the former is 144 ± 7 which is much higher than the latter's 91 ± 3 , while the lag time (CarHQ 15 ± 3 , α -Syn 19 ± 2) is almost similar. These results solidify CarHQ role as an aggregation activator which speeds up the aggregation process while producing more aggregates in comparison to the protein alone. Finally, ABCDHQ has an antiaggregant potential as its fluorescence gain maximum is 18 ± 1 and lag time 32 ± 3 , the values indicate that this compound has the most potential in delaying the aggregation of α -Syn due to its high t-lag value and low fluorescence. Further testing of some of these compounds (especially ABCDHQ) and their anti-aggregate ability could have an impact on therapeutic studies of this protein.

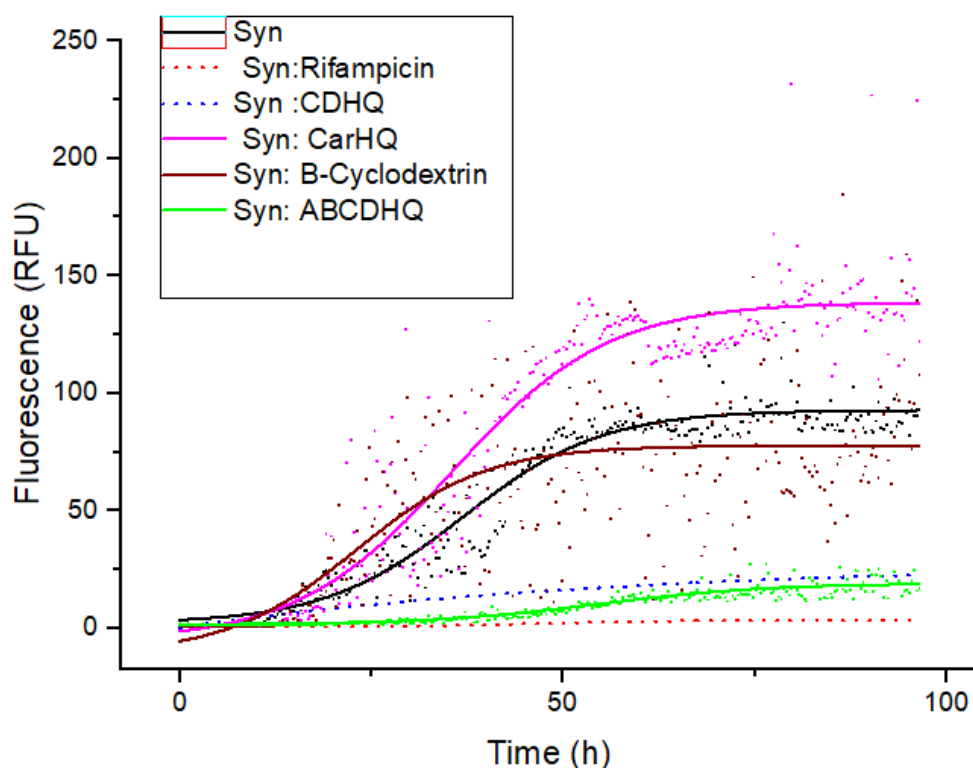


Figure 3.24. Aggregation assay of α -syn in the presence of different compounds.

Table 4. ThT aggregation assay sigmoidal fit to obtain maximum fluorescence gain and lag time.

	Maximum fluorescence gain	t-lag
α -Syn	91 \pm 3	19 \pm 2
ABCDHQ	18 \pm 1	32 \pm 3
β -cyclodextrin	89 \pm 14	6 \pm 7
CarHQ	144 \pm 7	15 \pm 3
CDHQ	159 \pm 18.5	(-) $38\pm$ 13
Rifampicin	3 \pm 0.04	30 \pm 1

The goal of these studies was to discover a potential therapeutic compound for PD. Native mass spectrometry was employed in the study of α -Syn and establish a protocol for transferring it to an appropriate buffer (ammonium acetate) before studying its different properties. More studies were carried out in the presence of different HQ compounds to detect the native mass spectrometry spectra. Additional studies with aggregation assay

showed that 2 of these compounds (ABCDHQ and CDHQ) have potential in preventing the aggregation of α -Syn hence it is important to proceed with these compounds for additional studies.

3.2.3. Citicoline and 20S proteasome

α -syn, known to be degraded by the proteasome system, was incubated with 20S as well as different concentrations of citicoline (100 nM and 1 μ M) for 1 hr. and 3 hrs. A control experiment in the absence of citicoline was also run. The SDS-PAGE analysis of the reaction mixture is shown in Figure 3.25. In the absence of 20S, the levels of α -syn are quite similar in the different time points (Figure 3.25, upper left side). Upon the addition of 20S, it is clear that there is a time-dependent α -syn decrease as it is being degraded by 20S. The reduction is further noticed upon the addition of 100 nM of citicoline (Figure 3.25 third row): after 3 hrs. almost 40% of α -syn is removed. However, the addition of 1 μ M citicoline has no effect on the degrading activity of 20S towards α -syn. Meaning that although citicoline is a good candidate for aiding in protein clearance via proteasome mechanism, the levels of this compound also play a crucial role in determining the extent of proteasome activation. In addition, when a proteasome inhibitor (epoxomicin) is added to the reaction mixture, α -syn (Figure 3.25 right side) degradation via 20S was hindered. Hence citicoline plays an activation role towards 20S activity in a specific concentration window, which is a useful property that can be utilized in conditions where proteasome activity is lowered due to certain diseases and/or biochemical conditions. Therefore, citicoline plays a concentration-dependent activating and an inhibiting role in the activity of 20S proteasome. It points out towards the possibility of two binding sites of citicoline on 20S proteasome and the proteasome switching between an open (substrate access) and a closed (substrate not allowed) conformations. Moreover, the activating activity of citicoline towards 20S action on α -syn could point towards its role in PD therapeutics.

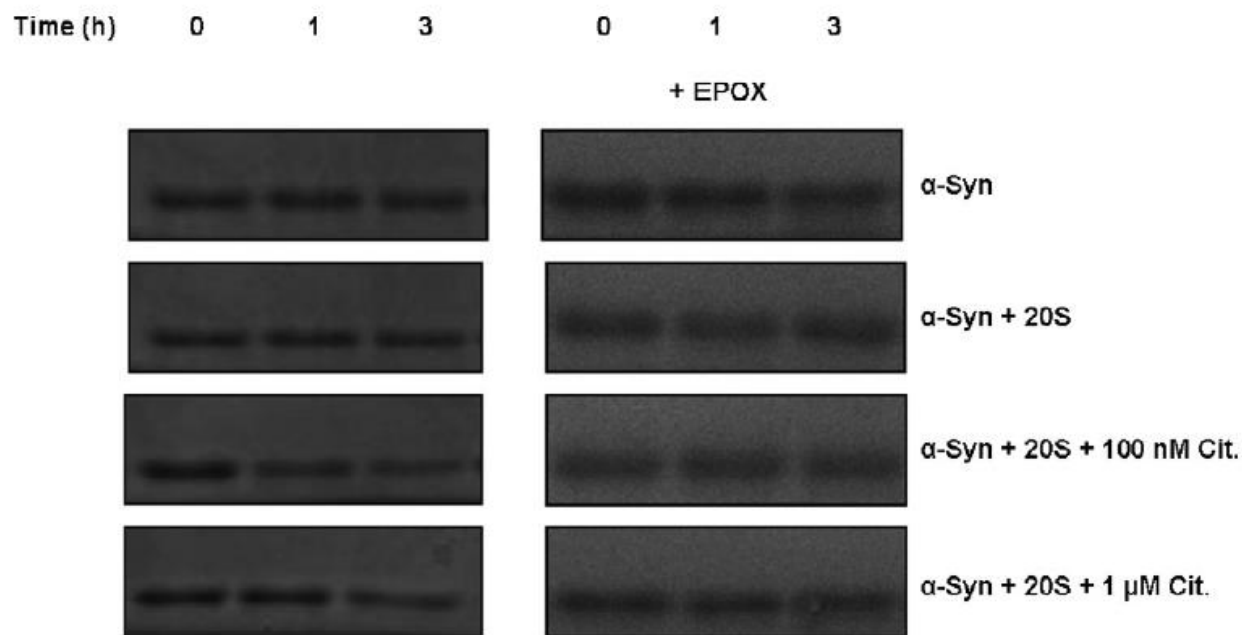


Figure 3.25. SDS-PAGE of α -syn degradation via 20S proteasome in the absence (left) and presence (right) of inhibitor.

3.3. α -Syn and amyloid beta

The interaction of different proteins in neurodegeneration is not an unheard-of phenomenon. α -Syn and $A\beta$ for example were studied in order to foresight the effect of their cooperation on the disease progression. In order to get insight into the structural details of the interaction between α -Syn and $A\beta$, several experiments of proteolysis, aggregation and interaction assays have been carried out and described in the following paragraphs.

3.3.1. IDE, α -Syn and amyloid beta

Different concentrations of α -syn were incubated with both $A\beta_{1-40}$ and $A\beta_{1-28}$ to explore the effect of α -syn on the IDE-mediate hydrolysis of the amyloid peptides. As previously reported⁵⁹ several fragments of $A\beta_{1-42}$ produced by IDE can be properly detected using Mass Spectrometry. The detected hydrolytic peptide fragments are highlighted in Figure 3.26. The action of IDE on $A\beta$ is mainly focused to the first 28 amino acids.

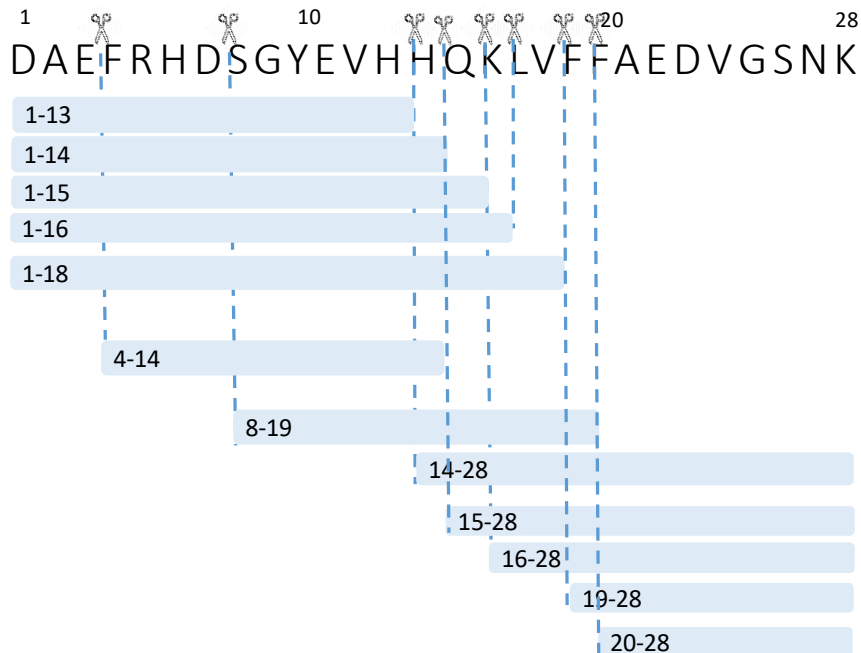


Figure 3.26. A β_{1-28} (5 μ M) fragments by IDE in the presence of α -Syn (0-5 μ M).

Figure 3.27 clearly shows the time-dependent formation of the hydrolytic peptides due to the IDE action on A β_{1-28} . The vicinal his and phe residues (positions 13-14 and 19-20) are the main cleavages sites, as previously reported⁵⁹. In the absence of α -Syn (Figure 3.27, upper graph), peptides 20-28 and 15-28 are the main formed peptides. Upon the addition of A β_{1-28} / α -Syn 1:0.5 molar ratio (Figure 3.27, middle graph), the trend is similar to that in the absence of α -Syn, however peptides 20-28 and 15-28 are released more in comparison to their levels in the absence of α -Syn. Moreover, comparing similar incubation times points out to the increase of formation of these peptides in the presence of α -Syn which is much noticeable upon the addition of A β_{1-28} / α -Syn 1:1 molar ratio (Figure 3.27, lower graph).

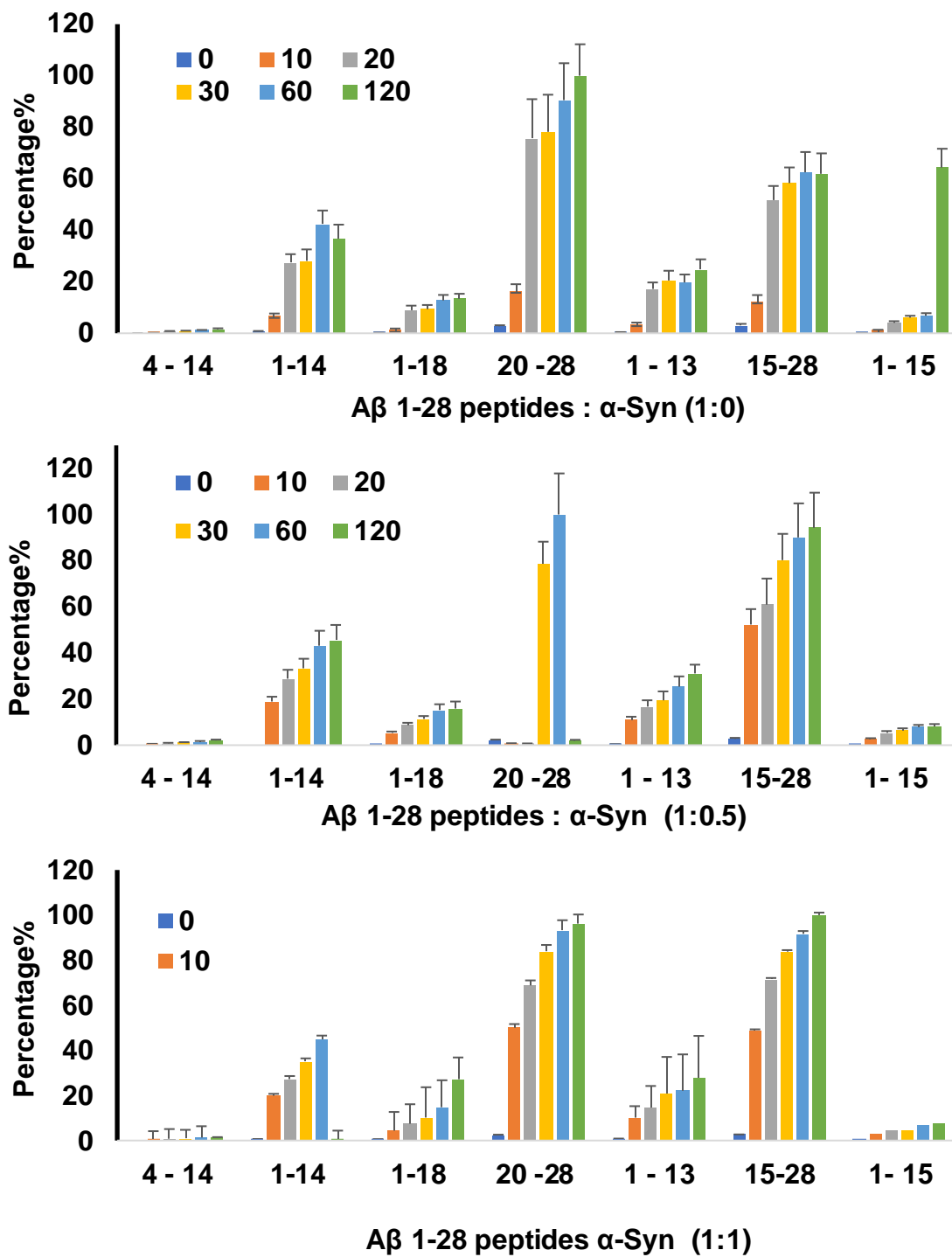


Figure 3.27. Summary of LC-MS results of $A\beta_{1-28}$ ($5 \mu\text{M}$) fragments by IDE at different time intervals (0-120 minutes) in the presence of different α -syn concentrations. Upper graph [α -syn] = 0, middle graph [α -syn] = $2.5 \mu\text{M}$, lower graph [α -syn] = $5 \mu\text{M}$.

In order to test the effect of α -Syn concentration on IDE function, a gradual increase of α -Syn's concentration was experimented with. (Figure 3.28, upper graph), peptides 20-28 and 15-28 are the main formed peptides at $A\beta_{1-28}/\alpha$ -Syn 1:1. Upon the addition of $A\beta_{1-28}/\alpha$ -Syn 1:2 molar ratio (Figure 3.28, middle graph) and/or $A\beta_{1-28}/\alpha$ -Syn 1:3 (Figure 3.28, lower graph), the trend is similar to that of $A\beta_{1-28}/\alpha$ -Syn 1:1. Moreover, the increase in peptide formation is not significantly different regardless of $[\alpha$ -Syn] increase. It is possible that IDE is allosterically affected by some substrates and a concentration beyond 1:1 has no effect if the site is already saturated.

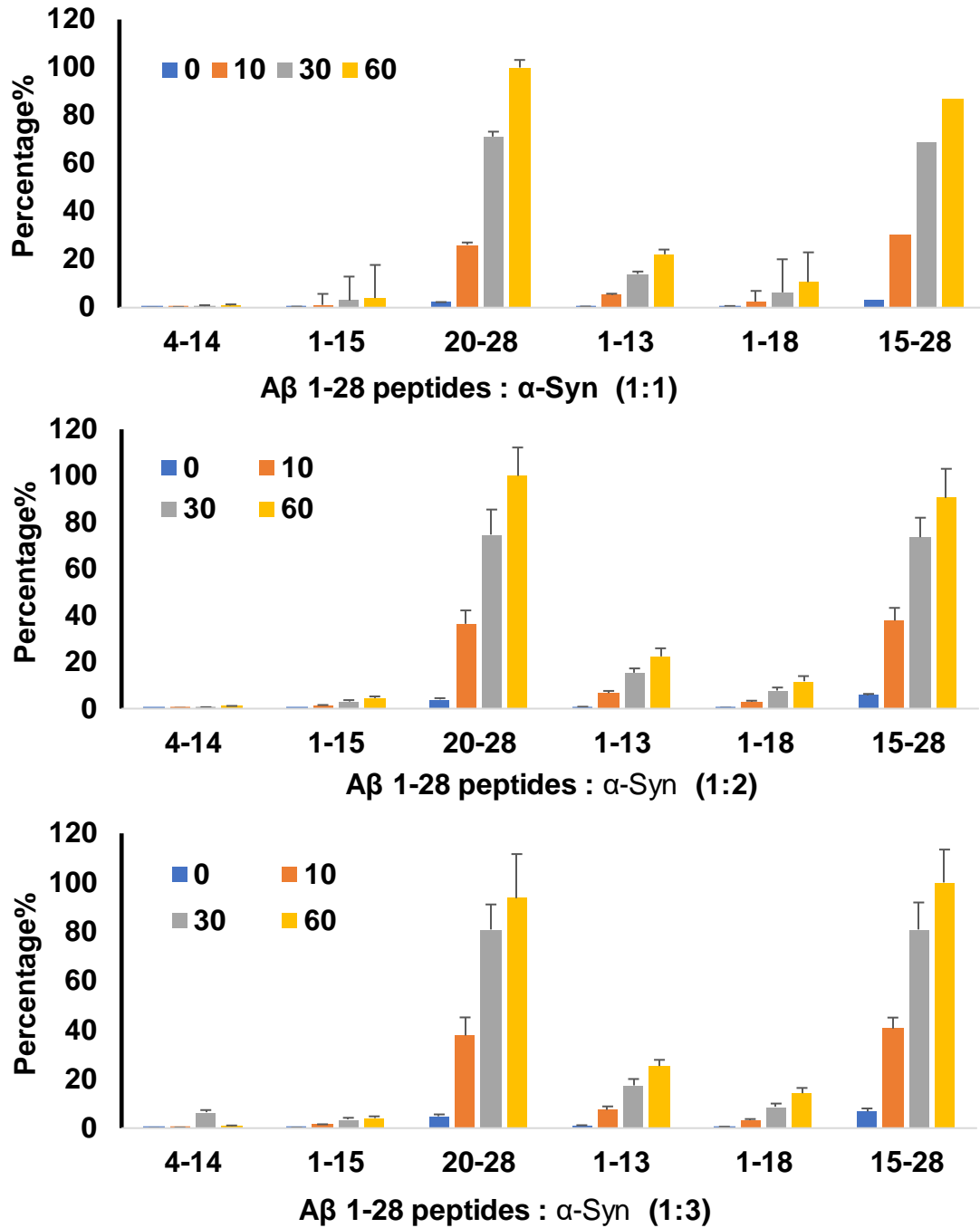


Figure 3.28. Summary of LC-MS results of A β ₁₋₂₈ (5 μ M) fragments by IDE at different time intervals (0-60 minutes) in the presence of different α -syn concentrations Upper graph [α -syn] = 5 μ M, middle graph [α -syn] = 10 μ M, lower graph [α -syn] = 15 μ M.

In the case of $A\beta_{1-40}$ degradation by IDE, the significant peptides (1-13, 1-14, 1-19) are different than those formed by $A\beta_{1-28}$ degradation. In the absence of α -Syn (Figure 3.29) peptides (1-19, 1-14) reach peak formation at 80-minute reaction time. The trend is similar in the presence of $A\beta_{1-40}/\alpha$ -Syn at different molar ratios (1:0.5, 1:1, 1:3), however the presence of α -Syn speeds up the formation of these peptides hence the percentage formation of peptide 1-19 at 20 minutes reaction increases as $[\alpha$ -Syn] increases. A possible explanation of these observations could be due to the exosite has been found that the IDE-C subunit has an exosite (positively charged) which can bind some peptides³¹. The binding increases the IDE activity. α -syn C-terminal is rich of negative charges, hence is able to bind the exosite³¹. Sub-stoichiometric amounts of α -syn with respect to the amyloid content may promote the α -syn-induced IDE activation. On the other hand, higher α -syn concentrations could also favor the Syn- $A\beta$ non-covalent interaction that, in turn, may inhibit further α -syn from binding effectively to IDE's exosite site leading to a plateau effect. In conclusion, α -syn concentration determines its effect on IDE's function.

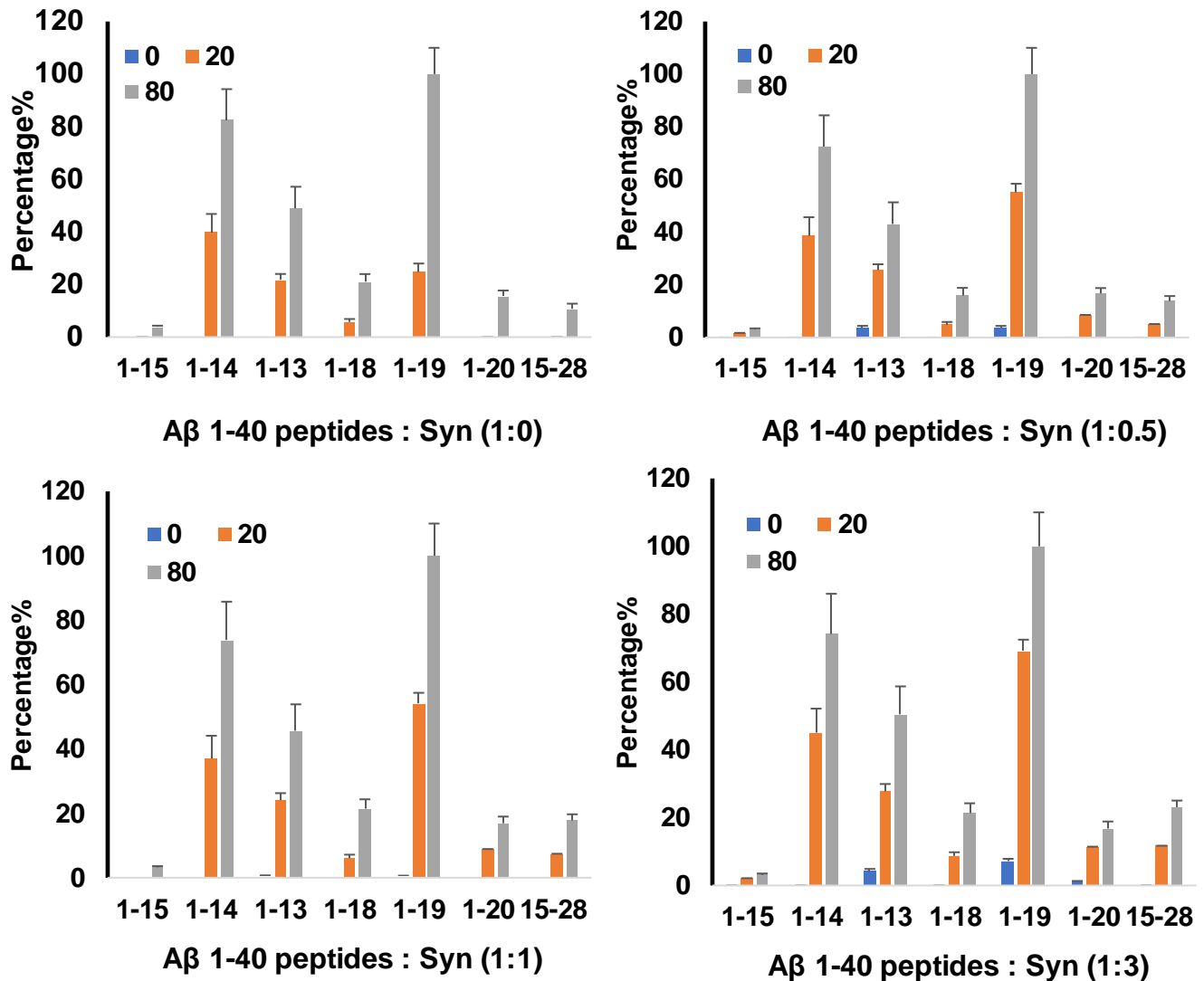


Figure 3.29. Summary of LC-MS results of $A\beta_{1-40}$ (2 μ M) fragments by IDE at different time intervals (0-80 minutes) in the presence of different α -syn concentrations (0-6 μ M).

3.3.2. Aggregation assay

Aggregation is the main issue for foldopathies. Studying the aggregation process of a mixture containing both α -Syn and $A\beta_{1-42}$ would be quite difficult because both the proteins are prone to aggregate. However, the time scale of their own aggregation pathway in vitro is very different. $A\beta_{1-42}$ forms amyloid fibrils within few hours, whereas α -Syn starts to aggregate after 20-30 hours. For this reason, the effect of α -Syn on the $A\beta_{1-}$

42 amyloid aggregation was monitored by using ThT assay (Figure 3.30). α -Syn was added in different concentrations to $A\beta_{1-42}$. It is clear that the higher concentration of α -Syn, the longer the lag phase. This set of experiments further proof the interaction of both proteins *in vitro*.

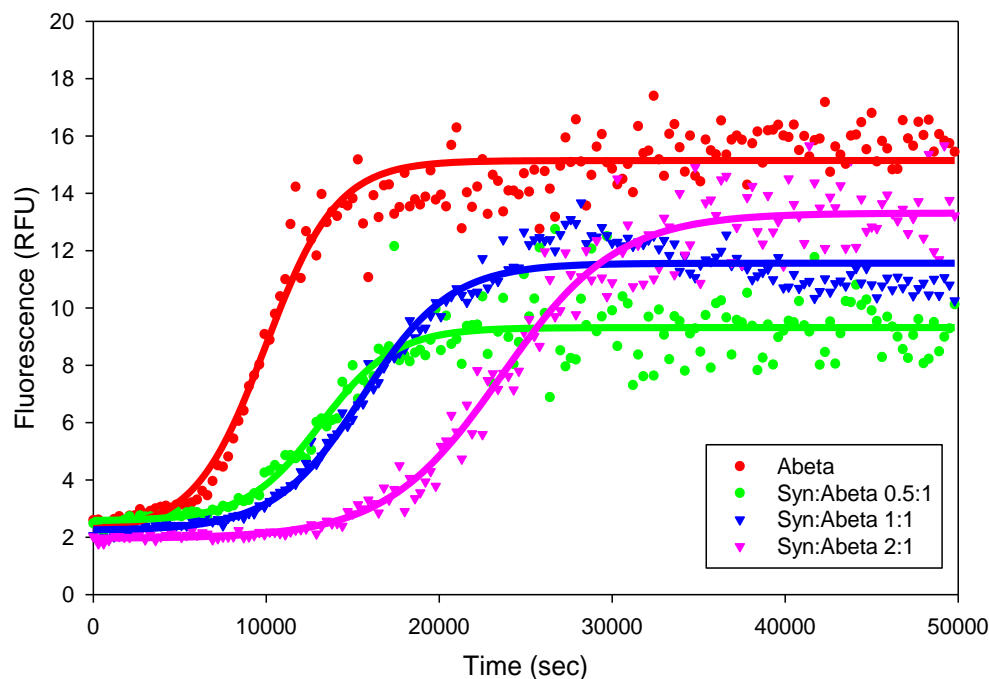


Figure 3.30. The effect of different α -Syn concentrations on $A\beta_{1-42}$ aggregation

3.4. Proteasome 20S action on $A\beta$: effect of Ub and AP

3.4.1. 20S mediated $A\beta_{1-40}$ hydrolysis

The interplay between $A\beta$, proteasome 20S and Ub was experimentally examined. Initially, a simple degradation pattern of $A\beta_{1-40}$ by proteasome 20S in 60 minutes timeframe was established using mass spectrometry techniques. The chromatographic and MS features of all the peptides formed upon the degradation of $A\beta_{1-40}$ are reported in Table S9. The time-dependent formation of most abundant peptides was represented in Figure 3.31 and Table S9 as a percentage of the maximum peak area (peptide 1-20 at 60 minutes). The peaks formed as a result of the proteasome-mediated degradation of $A\beta_{1-40}$ are 1-17, 35-45, 1-20 and 21-34, peptide 1-20 having the highest production levels (highlighted in bold in Table S9).

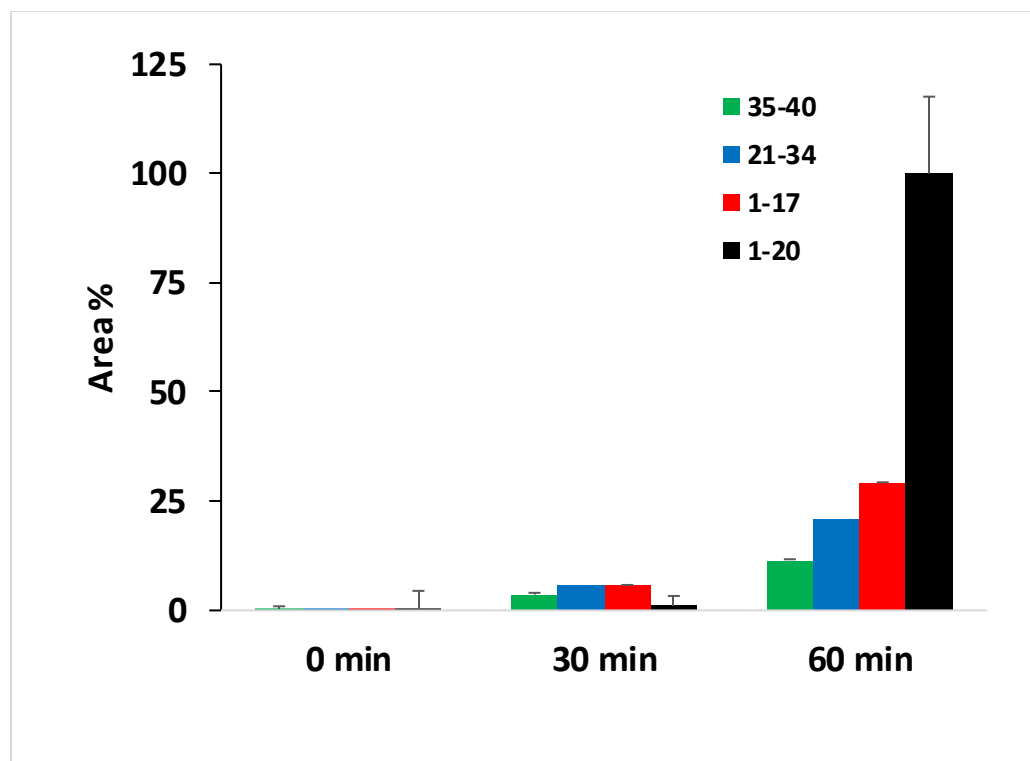


Figure 3.31. The most abundant $A\beta_{1-40}$ peptides formed by proteasome 20S degradation, the table represents the percentage of each peak area divided by the maximum peak (peptide 1-20 after 60 minutes).

3.4.2. $A\beta_{1-40}$ hydrolysis and Ub role

Next the dose-dependent effect of Ub on the $A\beta_{1-40}$ hydrolysis by proteasome 20S was investigated. Figure 3.32 clearly shows that when Ub: $A\beta_{1-40}$ molar ratio increases, the $A\beta$ degradation and subsequent fragment formation is promoted in a dose-dependent manner after 2 h. These data are consistent with those obtained after 20 min and 60 min (Figure S17, S18 and S19, which show the reaction after 0,20 and 60 minutes were peptides 1-20 and 1-17 were the main peptides and the increase in Ub concentration had a positive effect on their release). Moreover, Figure 3.33 shows the gradual increase of the peptide 1-20 as a function of incubation time and Ub concentration. The activation activity of Ub towards $A\beta$ degradation may be due to the enhanced solubility of the substrate and/or the inhibition to form oligomer species.

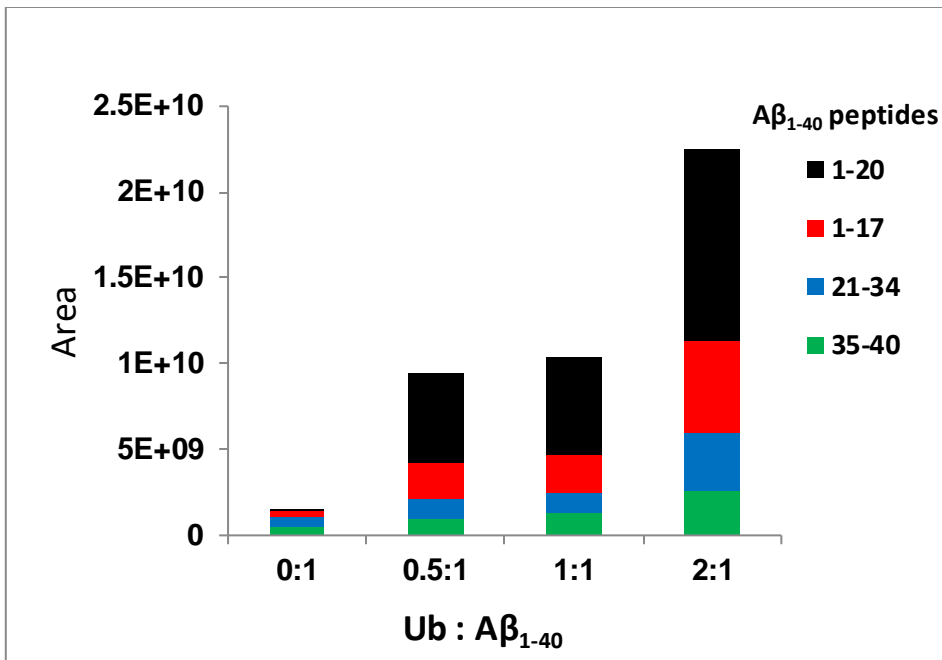


Figure 3.32. The effect of different Ub concentrations on the formation of Aβ₁₋₄₀ fragments via a proteasomal degradation.

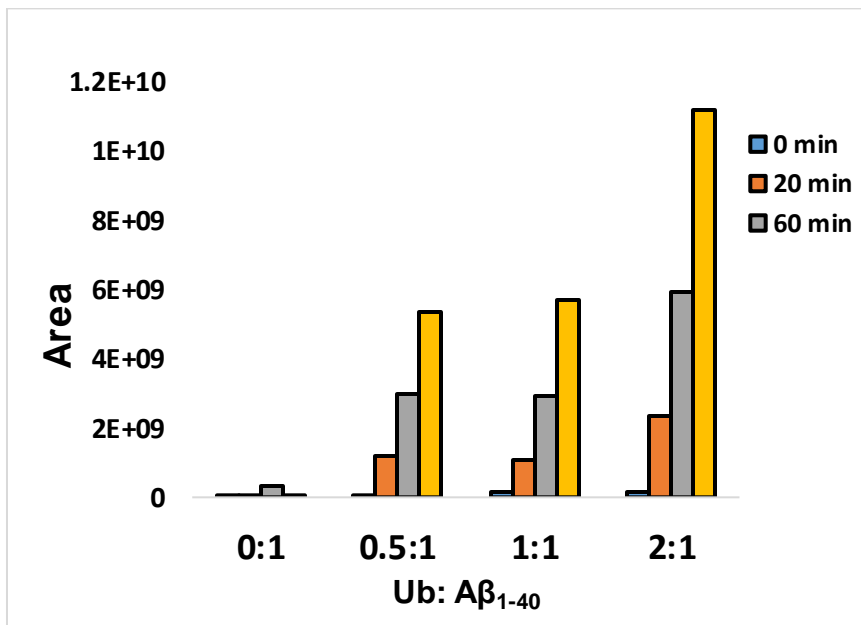


Figure 3.33. The formation of 1-20 peptide as a function of time and Ub concentration.

3.4.3. The effect of A β ₁₋₄₀ on 20S mediated A β ₁₆₋₂₈ hydrolysis

A smaller A β peptide, A β ₁₆₋₂₈ was studied to establish its degradation pattern with proteasome 20S. The peptide upon interaction with the proteasome was degraded within 30 minutes. The degradation pattern of A β ₁₆₋₂₈ can be followed in Figure 3.34. Moreover, in Figure S20, the raw data for A β ₁₆₋₂₈ peak in LC-MS can be found. The m/z value corresponding to A β ₁₆₋₂₈ is 498.94 at z=3, the area corresponding to this peak can be assigned and followed as a function of different factors (time, concentration, etc.).

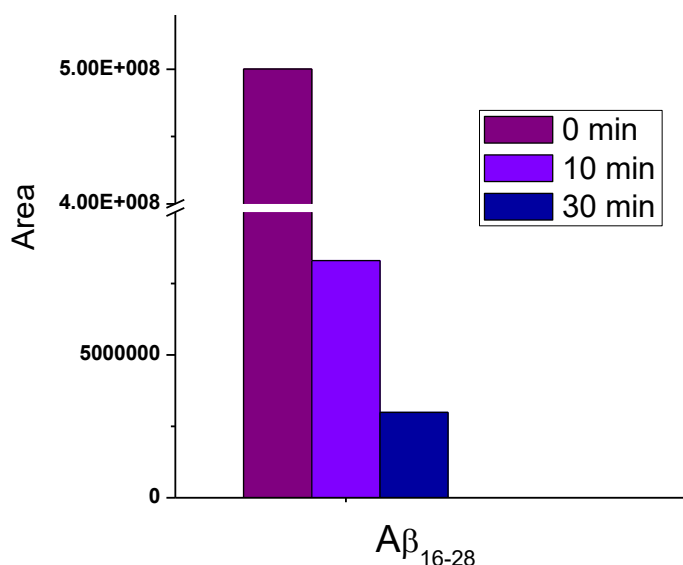


Figure 3.34. A β ₁₆₋₂₈ degradation by proteasome 20S.

A β ₁₋₄₀ has been tested as a substrate of proteasome 20s. However, it has also been reported that the amyloid peptide also modulates the proteasomal activity⁶⁰ b. In order to discriminate between the modulating and the hydrolysis activity, we used A β ₁₆₋₂₈ as a substrate in the presence of A β ₁₋₄₀ because the degradation of the former (Figure 3.34) is faster than that of the latter (Figure 3.31). The reaction was carried out for 15 minutes to avoid significant degradation of A β ₁₋₄₀. As reported in Figure 3.35, the amount of substrate A β ₁₆₋₂₈ increases as the concentration of A β ₁₋₄₀ increases. Therefore, A β ₁₋₄₀ has an

inhibitory effect on the action of 20S towards the clearance of substrate $A\beta_{16-28}$ as it prevents its degradation.

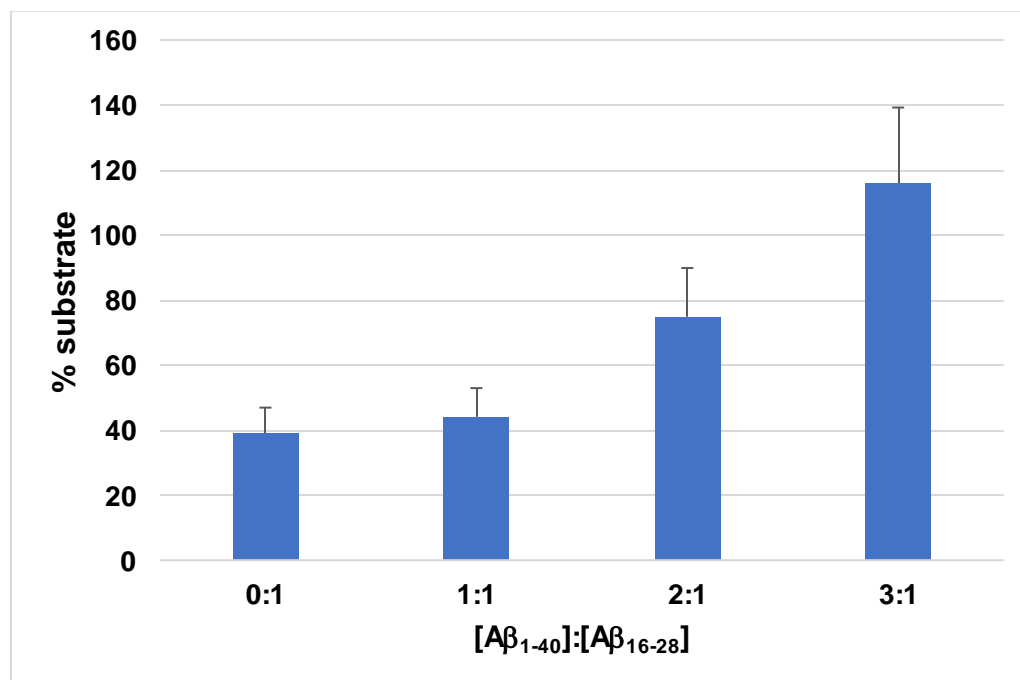


Figure 3.35. The effect of $A\beta_{1-40}$ on the proteasomal degradation of $A\beta_{16-28}$.

3.4.4. 20S mediated $A\beta_{1-28}$ hydrolysis

Several analgesic compounds were tested to examine their effect on the proteasomal degradation of $A\beta$. Aminopyrine (AP) showed the most potential hence utilized for other experiments. The use of aminopyrine is for an effort to find new therapeutic potentials for drugs already in the market. In order to investigate how AP modulates the proteasome activity, an MS-based assay of the $A\beta$ enzymatic digestion has been carried out. Thus, all the peptide fragments formed by the 20S-catalysed digestion of a soluble fragment of the peptide ($A\beta_{1-28}$) were detected (Figure 3.36); their relative amounts were compared as a function of the AP concentration (Figure 3.37). The involvement of several cleavage sites makes this MS-based approach useful to also assess the site-specific effect (if any) of an effector on the enzyme-mediated $A\beta$ hydrolysis⁶¹. Therefore, this assay detect the proteasome activity as a whole⁶² and the modulation of the trypsin-, chymotrypsin- and

caspase-like activities exerted by an effector could be clearly distinguished, based on the cleavage sites involved.

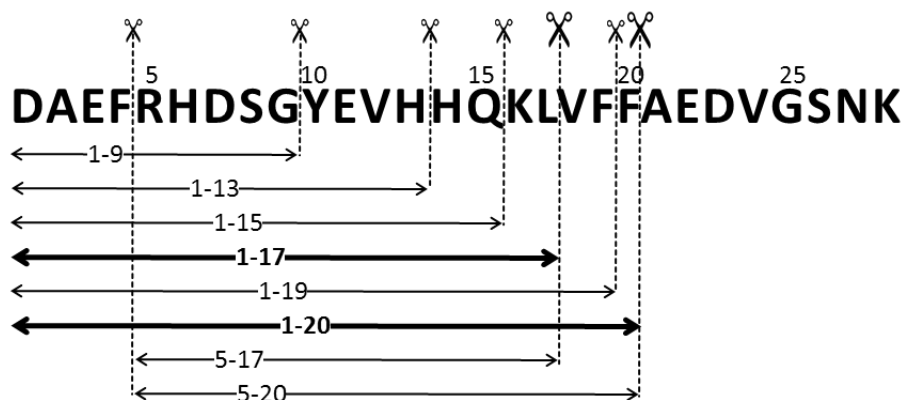


Figure 3.36. Schematic of the main (bigger scissors) and secondary (smaller scissors) cleavage sites of the proteasome-mediated hydrolysis $A\beta_{1-28}$ at 37 °C within 40 min reaction.

3.4.5. The effect of AP on 20S mediated $A\beta_{1-28}$ hydrolysis

The 20S-mediated hydrolysis of $A\beta_{1-28}$ at 37 °C produces at least eight peptide fragments within 40 minutes reaction (Figure 3.36). Their formation has been already reported in the literature referring to the 20S proteasome activity towards $A\beta$ peptide⁶³. The main hydrolytic peptides ($A\beta_{1-17}$ and $A\beta_{1-20}$) have Leu and Phe as C-terminal residues, indicating that they are products of the chymotrypsin-like activity of 20S on the $A\beta$ degradation. N-truncated forms of the fragments ($A\beta_{1-17}$ and $A\beta_{1-20}$) were also obtained through the same type of proteasome activity. Secondary cleavage sites are also involved, even though to a lesser extent.

The hydrolytic pattern of $A\beta_{1-28}$ has been compared to those detected in the presence of AP after 40 min (Figure 3.37) and 60 min (Figure S21, were data show the dual effect of AP on the main peptides 1-17, 1-20 and 1-15 specially the increase in their levels at [AP] =10 μ M). As for the main hydrolytic peptide ($A\beta_{1-17}$), the normalized intensity of the related peak in the MS spectrum significantly reduces with AP 1 μ M and it is more than halved when the concentration of AP is 5 μ M. The higher concentration of AP used (10 μ M)

clearly reverse the trend: the amount of A β ₁₋₁₇ roughly increases four-fold compared to the control value (in the absence of AP). Such a behavior is also observed with the second primary peptide fragment (A β ₁₋₂₀) as well as by a secondary product (A β ₁₋₁₅).

Based on these data, AP has a dose-dependent effect on the 20S proteasome activity towards the A β hydrolysis. When its concentration progressively increases to 5 μ M, a dose-proportional inhibition activity is observed. On the contrary, AP acts as a proteasome activator when its concentration reaches 10 μ M. Such a dose-dependent dual activity could be reasonably due to a multi-modal, dose-dependent interaction of AP with the catalytic subunits of 20S proteasome.

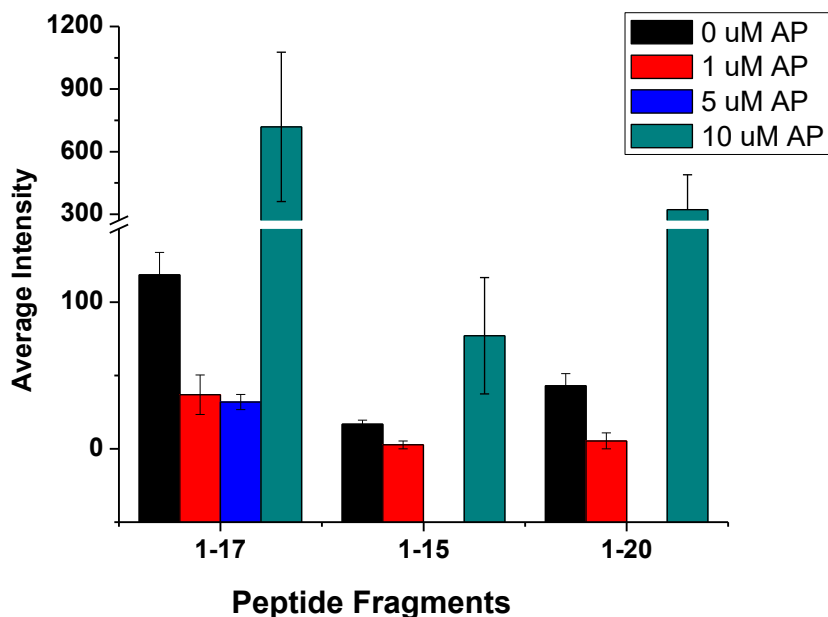


Figure 3.37. Formation of three representative hydrolytic peptides function of the aminopyrine (AP) concentration at 40 min.

The results obtained in these experiments with the proteasome 20S and A β were as follow:

- The different proteasomal hydrolysis pattern between different soluble A β peptides was identified
- Ub stimulates the hydrolysis of A β ₁₋₄₀ by 20S proteasome as a function of concentration

- A β ₁₋₄₀ has a dose dependent inhibitory effect on the proteasomal degradation of A β ₁₆₋₂₈
- AP has a dual function on proteasome 20S action on A β ₁₋₂₈: an inhibitory effect at low concentration (5 μ M) and an activating effect at higher concentration (10 μ M), The use of aminopyrine is for an effort to find new therapeutic potentials for drugs already in the market.

3.5. Insulin degrading enzyme and its studies

3.5.1. Insulin degrading enzyme and nociceptin/orphanin FQ

AD and DM are linked since both Ins and A β can be degraded by the same clearance enzyme (IDE). Hence, studies on IDE are vital to understand the clearance system of A β . Since Ins is a simpler model for studies, it was recruited for IDE studies in the presence of a peptide (OFQ/N₁₋₁₆) associated with brain disorders such as AD.

Ins is hydrolyzed by IDE producing several fragments, these fragments were compared to those produced by IDE degradation of bovine Ins⁶⁴ and the molecular weight was estimated based on amino acid differences (Table S10). This estimation aided in the identification of Ins peptide since Ins consists of two chains which are easier to distinguish on MS with prior knowledge about the fragmentation pattern. Next, a further spectrometry analysis assigned each peak to its corresponding peptide chains as seen in Figure 3.38 and Table S11 (shows the Ins peptides produced from IDE degradation detected by LC-MS). In the experimental conditions used, A1-13_B1-9 and A14-21_B10-30 are the main products. The content of the full-length substrate is more than halved after 30 min incubation and it almost disappears after 90 min. When OFQ/N₁₋₁₆ is co-incubated with Ins (1:1 molar ratio) (Figure 3.39), the kinetic profiles of both the Ins degradation and the formation of the digested peptides do not significantly differ from those detected without OFQ/N₁₋₁₆.

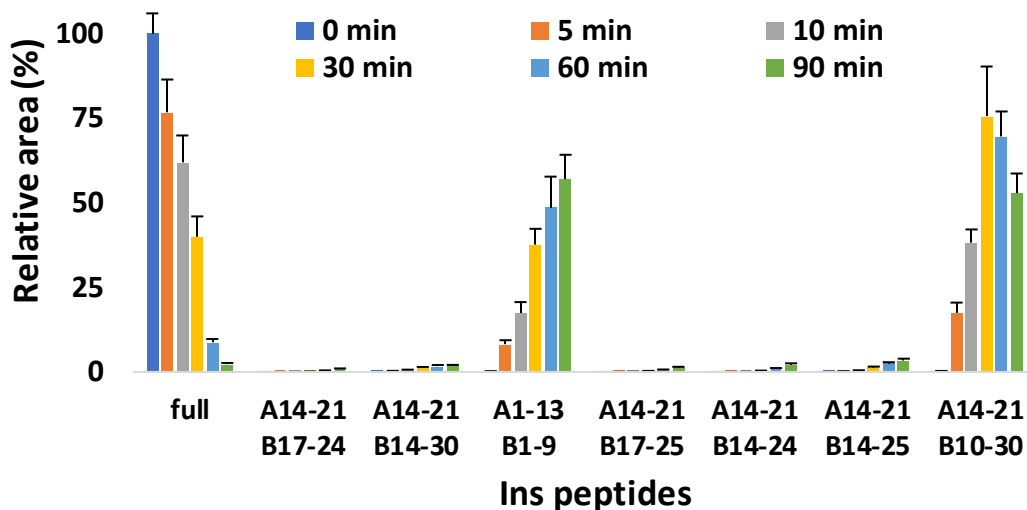


Figure 3.38. Hydrolytic pattern of the time-course insulin (Ins) degradation catalyzed by IDE. The content of the full-length substrate (full) and the main hydrolytic peptides were detected at 37 °C for 90 min.

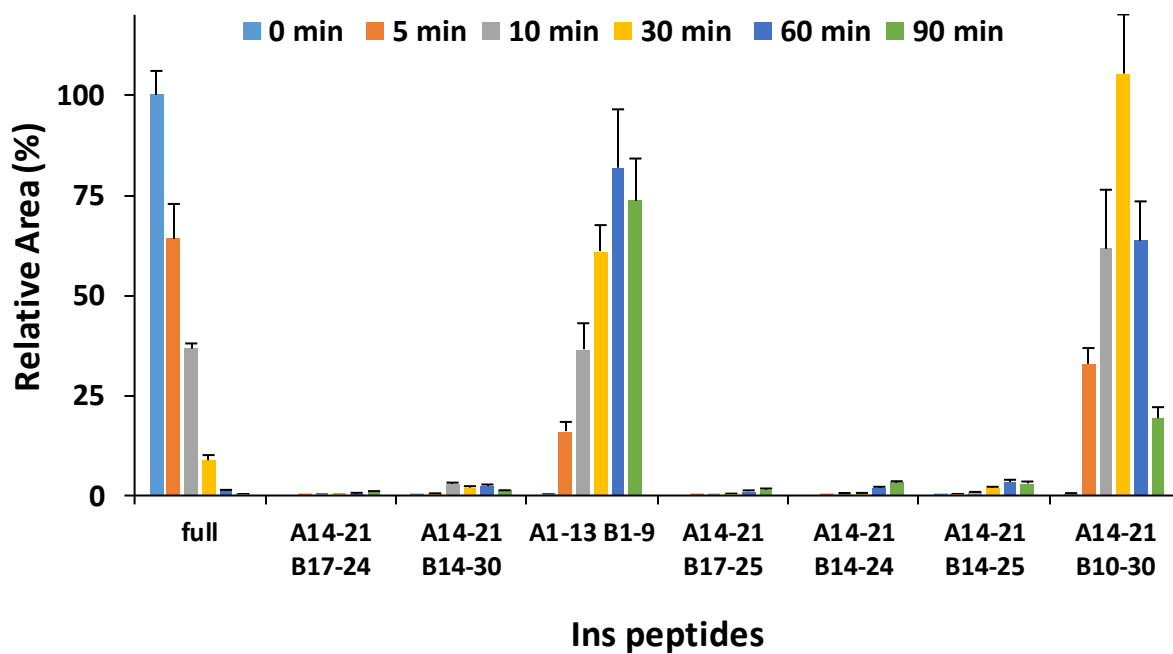


Figure 3.39. Hydrolytic pattern of the time-course insulin (Ins) degradation catalyzed by IDE. The content of the full-length substrate (full) and the main hydrolytic peptides was detected in the presence of OFQ/N1-₁₆, at 37 °C for 90 min.

As for the IDE-mediated OFQ/N₁₋₁₆ degradation, Figure S22 shows data collected for 20 and 40 minutes incubation times with IDE, the main peptides were 1-8,1-11 and 1-7 however, the main peptide 1-16 is not fully degraded hence proceed with total incubation time of 90 minutes. Table S12 shows the peptides obtained and visualized by LC-MS after 90 minutes and these data were organized in Figure 3.40, the substrate (1-16) is almost completely degraded within 10 min; the first and main product (1-11) reaches its peak amount after 30 min; 1-8 and 1-10 are also formed by the 1-16 processing, but also by 1-11. When OFQ/N₁₋₁₆ and Ins (1:1 molar ratio) are co-incubated with IDE (Figure 3.41), 1-16 is 80% of the original value after 30 min reaction. 1-11 is still the main product, but the formation of the peptide is inhibited with respect to the condition in the absence of Ins. The formation of 1-8 is reduced as well; on the contrary, the content of 1-10 slightly increases.

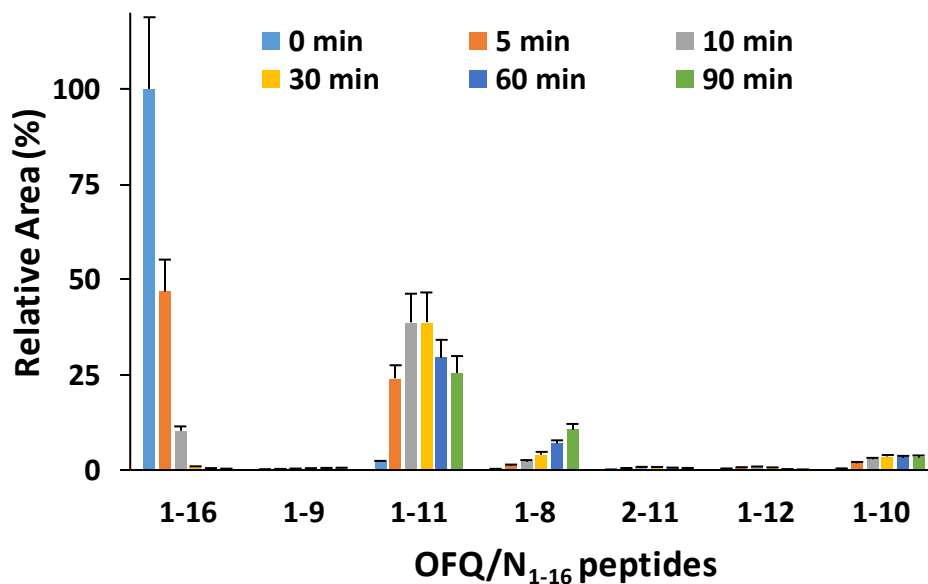


Figure 3.40. Hydrolytic pattern of the time-course nociceptin OFQ/N₁₋₁₆ degradation catalyzed by IDE. The content of the full-length substrate (1-16) and the main hydrolytic peptides was detected in the absence of Ins, at 37 °C for 90 min.

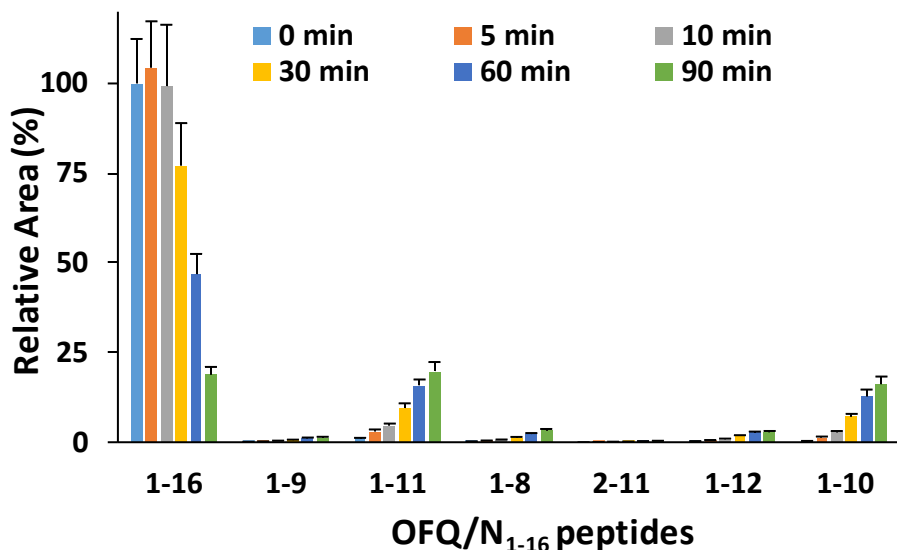


Figure 3.41. Hydrolytic pattern of the time-course nociceptin OFQ/N₁₋₁₆ degradation catalyzed by IDE. The content of the full-length substrate (1-16) and the main hydrolytic peptides was detected in the presence of Ins, at 37 °C for 90 min.

These data clearly point out that Ins and OFQ/N₁₋₁₆ compete for one to each other for the interaction with IDE, thus affecting their own hydrolytic patterns. The digestion of OFQ/N₁₋₁₆ is significantly affected by the presence of Ins. On the contrary, the kinetic profile of the Ins hydrolysis does not clearly change in the presence of OFQ/N₁₋₁₆.

In order to assess the effect (if any) of the OFQ/N₁₋₁₆ hydrolytic fragments of the IDE-catalyzed Ins hydrolysis, OFQ/N₁₋₁₆ was pre-incubated at 37°C with IDE. After 20 min, Ins was added to the reaction mixture. At this point, the content of OFQ/N₁₋₁₆ five-fold decreases over the starting value (Figure 3.42), whereas the amounts of neither the substrate (1-16) nor the main hydrolytic peptides (1-11, 1-10 and 1-8) significantly change after the addition of Ins. This clearly means that the IDE-mediated digestion of the residual amount of OFQ/N₁₋₁₆ after the pre-incubation step is inhibited by Ins even more than that reported for the co-incubation of the substrates.

Focusing on the Ins digestion, the hydrolytic pattern was analyzed when IDE was pre-incubated alone or with OFQ/N₁₋₁₆ for 20 min at 37 °C. In the first case (Figure 3.43), the

amount of full-length substrate gradually decreases, and the content of digested peptides increases (A1-13 B1-9, A14-21 B10-30). If OFQ/N₁₋₁₆ is pre-incubated with IDE (Figure 3.44), the hydrolysis and the formation rates of the substrates and the main products, respectively, significantly decreases, for example the total degradation of full length Ins after 90 minutes decreased from 70% in the absence of OFQ/N₁₋₁₆ pre-incubation (Figure 3.43) to 55% in the presence of OFQ/N₁₋₁₆ pre-incubation (Figure 3.44). Differently from the scenario outlined after the co-incubation of Ins and OFQ/N₁₋₁₆ with IDE, OFQ/N₁₋₁₆ pre-incubated with IDE clearly slow down the Ins hydrolysis. The main hydrolytic peptides of OFQ/N₁₋₁₆ and the residual amount of the latter might exert the inhibitor activity towards the IDE-mediated Ins degradation.

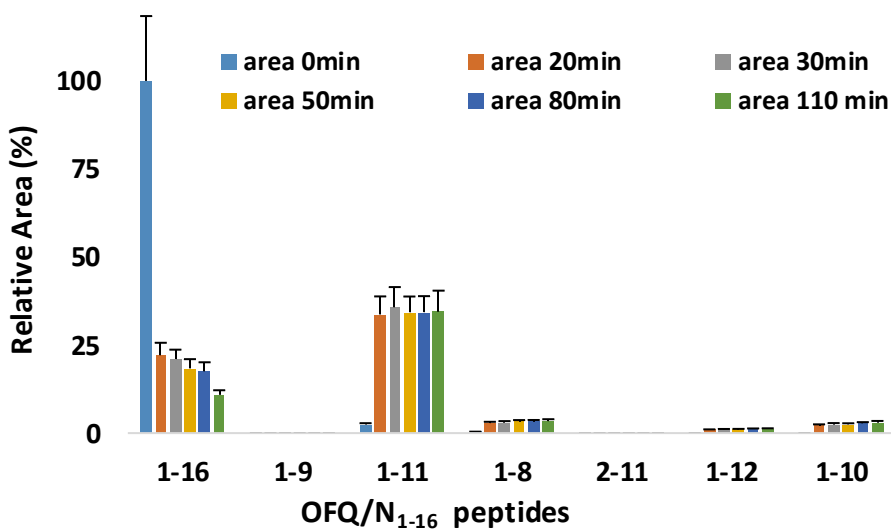


Figure 3.42. Hydrolytic pattern of the time-course nociceptin (OFQ/N₁₋₁₆) degradation catalyzed by IDE at 37 °C. OFQ/N₁₋₁₆ was incubated with IDE for 20 min at 37 °C before the addition of Ins.

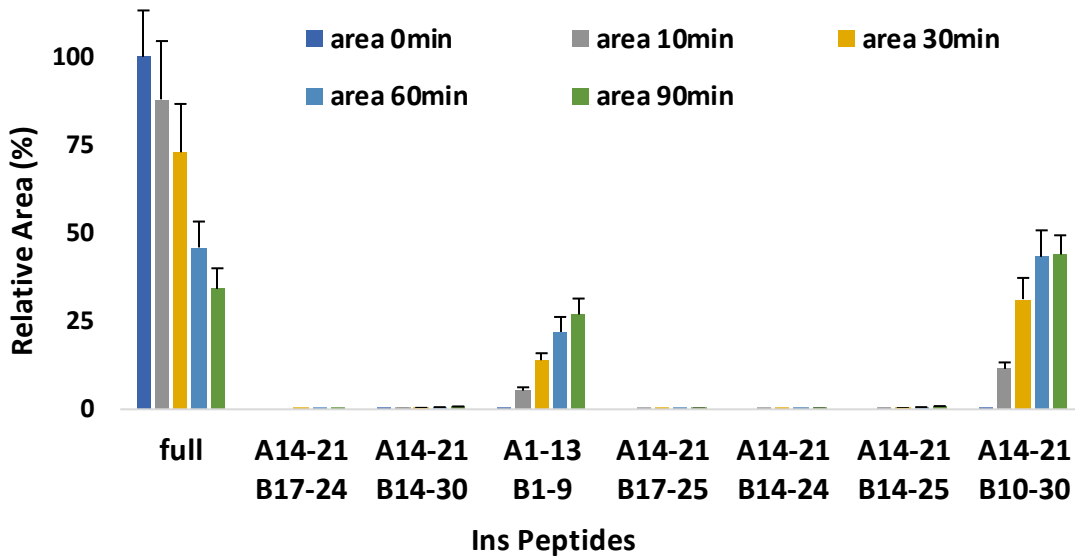


Figure 3.43. The kinetic profile of the Ins degradation was analyzed when IDE was pre-incubated alone at 37 °C for 20 min.

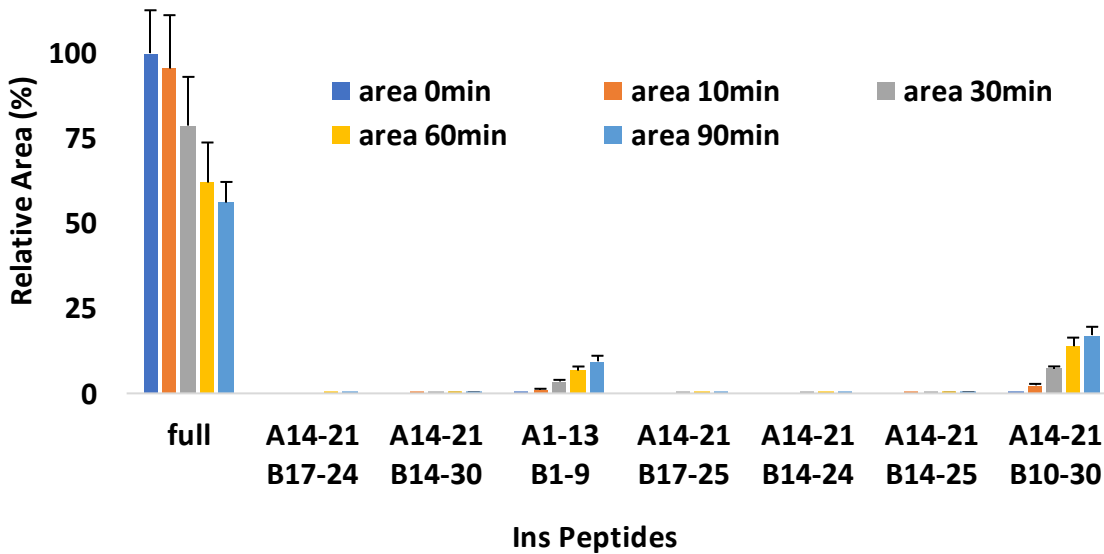


Figure 3.44. The kinetic profile of the Ins degradation was analyzed when IDE was pre-incubated with OFQ/N₁₋₁₆ (C) at 37 °C for 20 min.

The results obtained in these experiments with the Ins and OFQ/N₁₋₁₆ in the presence of IDE were as follow:

- Ins is the main substrate for IDE and its hydrolytic pattern is not disturbed by the co-presence of OFQ/N₁₋₁₆ however, the pre-incubation of OFQ/N₁₋₁₆ slows down the hydrolysis of Ins
- OFQ/N₁₋₁₆ degradation by IDE is disturbed by the competition of Ins on the enzyme
- The communication between the pain modulation peptide OFQ/N₁₋₁₆ and Ins in the presence of the clearance system IDE could point out to growing interest in the association between AD and DM.

3.5.2. Insulin degrading enzyme mutation and the role of metal ion

Previous studies⁶⁵ on the effect of metal ions on the action of IDE enzyme showed the inhibitory effect of copper and the neutral effect of zinc on IDE hydrolysis of A β . The enzyme IDE has several mutations, among which is F530A mutation. The amino acid phenylalanine (F530), located in the linker region of IDE, upon mutation to alanine increases IDE's activity by 20 folds⁶⁶. Incubation of a 1:1 A β /metal ion (copper and/or zinc) molar ratio with IDE (wild type or mutant F530A) is carried out with the main A β peptides being 1-13, 1-14, 1-19 as evident in Figure 3.45. The experiment goal is to monitor whether the effect of metal ions on F530A IDE-mediated hydrolysis of A β is similar to that of wild type IDE. The metal ions have the same effect on F530 IDE and are not affected by its increased activity (Figure 3.45). Therefore, copper and zinc play similar roles in IDE's function, inhibitory and neutral respectively, whether it's a wild type or F530A mutated, however the effect of Zn²⁺ in the results of the mutated form experiment (Figure 3.45 Right, bottom figure) is slightly reduced in comparison to that of non-mutated IDE .

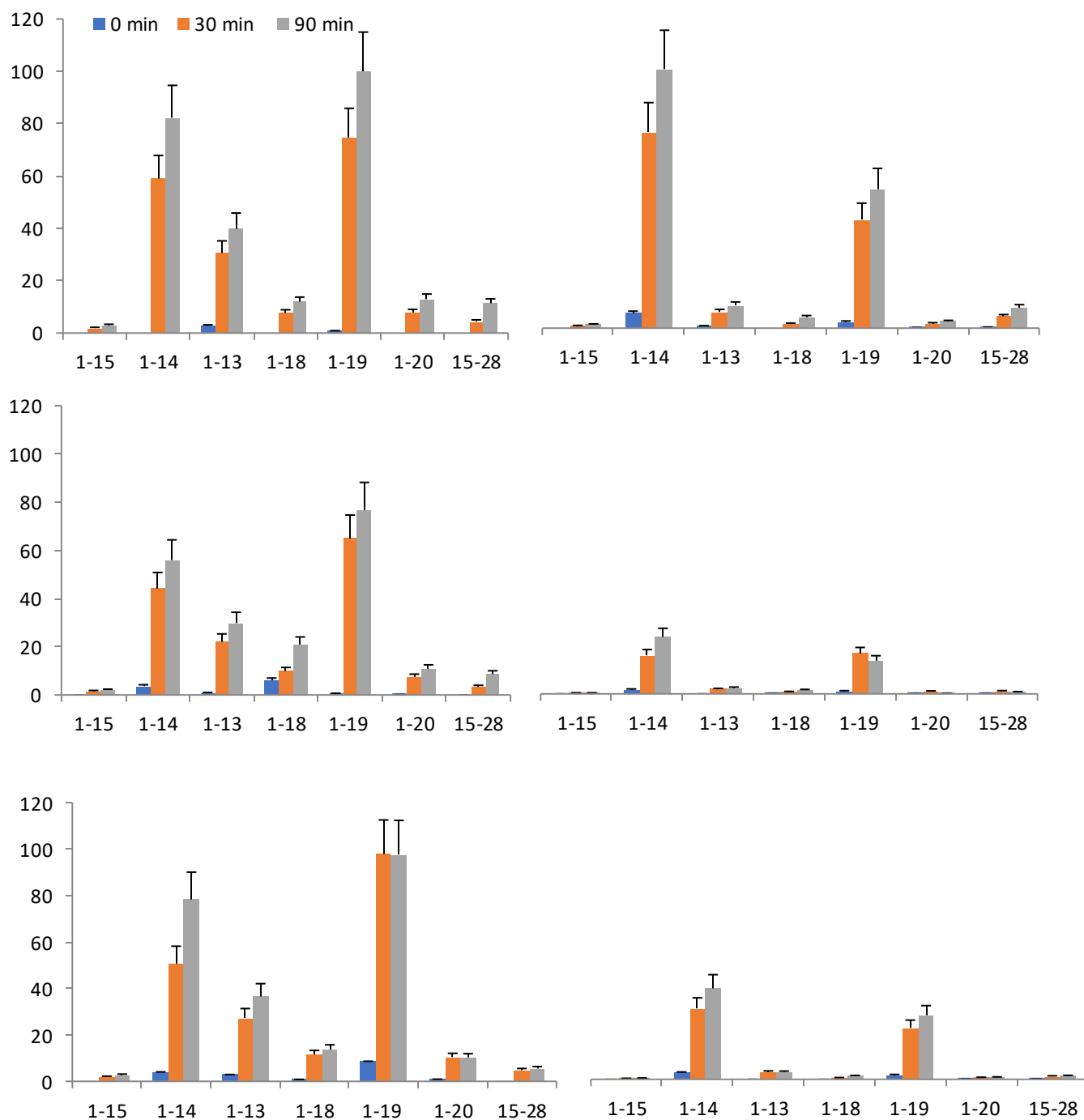


Figure 3.45. Summary of LC-MS results of Aβ₁₋₄₀ (2μM) fragments by 5 nM IDE (Left side) or 10 nM IDE mutant F530A (Right side) at different time intervals (0-90 minutes), without metal ions (upper figures), in the presence of (2μM) Copper (middle figures) and in the presence of (2μM) Zinc (lower figures).

Summary of the main results

Topic	Experimental partners	Methods	Main results
RCS and Metal ions	α -Syn, ACR, Cu^{2+} α -syn, MDA	LC-MS, MALDI, fluorescence assay, CD, DLS, peptide synthesis	His 50 of Syn is the main carbonylation site for ACR and MDA. Cu^{2+} interferes with ACR interaction on the same site
Compounds for therapy (HQ derivatives)	α -Syn, compounds	Native mass spectrometry, fluorescence assay	The interaction between full-length α -Syn and the compounds is ascertained in native conditions. Some derivatives of HQ show antiaggregant effects on α -Syn.
Protein-protein interaction by limited proteolysis	$\text{A}\beta$, α -syn, IDE	LC-MS	IDE-mediated $\text{A}\beta$ digestion is affected by α -syn in a dose dependent manner
Clearance system (20S)	$\text{A}\beta$, 20S, Ubiquitin $\text{A}\beta$, 20S, aminopyrine	LC-MS	Ub stimulates the hydrolysis of $\text{A}\beta_{1-40}$ by 20S proteasome as a function of concentration. AP has a dual function on proteasome 20S action on $\text{A}\beta$
Clearance system (IDE)	Nociceptin, Insulin, IDE $\text{A}\beta$, wt. and F530A IDE, Cu^{2+} , Zn^{2+}	LC-MS	Nociceptin degradation by IDE is inhibited by insulin, and vice versa. Copper and Zinc play a role in the wild-type and mutated IDE activity

Concluding remarks

Unveiling the molecular basis of neurodegenerative disorders represent an urgent task to be addressed because of the huge number of people interested in these severe diseases. Many of them are part of the large area of foldopathies due to the fact that the protein unfolding/misfolding represents an important aspect of the onset and/or consequence of the diseases. The complexity of this class of disorders arises from the involvement of numerous proteins, each linked to a different disease creating a complex web of factors to be considered when conducting studies. Hence, identifying some “common grounds” to minimize the complexity of the study is a logical approach for foldopathies

Scientific research in this field is truly complex, requires a long time and financial resources due to the involvement of diverse factors. Notwithstanding the peculiar characteristics of any disorder, many molecular factors are common to most of the neurodegenerative diseases. These include protein aggregation, oxidative stress, post-translational modifications (metal ions and oxidative reactive species) and cross-seeding among amyloidogenic proteins. Studying the facets of these disorders and their own mutual correlation represents the core aim of this research project.

The proteins alpha synuclein and amyloid beta were the focus of this research. The optimization of protein purification protocol to produce the protein α -synuclein was the initial step. The protein was studied in the presence of copper(II) and Acrolein using mass spectrometry for the determination of the interaction site which was Histidine 50 which was also confirmed by studies with synthesized short peptide P2 which also interacted with acrolein at histidine residue. More studies with circular dichroism showed a random coil secondary structure in the presence of acrolein regardless of the presence of copper(II) while the aggregation inducing structure (β -sheet) was not observed which adds to the knowledge gained from ThT assay which shows that the presence of acrolein delays/inhibits the aggregation of α -Synuclein. Moreover, dynamic light scattering studies showed a shift from aggregated to oligomeric species in the presence of acrolein with and/or without copper(II) which adds to cyclodextrin and aggregation assay results that acrolein plays a role in the aggregation of α -Synuclein. Malondialdehyde was also studied using MALDI and it showed its interaction with Histidine 50. Next, the interaction of this

protein with hydroxyquinoline derivatives, for their therapeutic properties, was carried out using native mass spectrometry, fluorescence aggregation assay and other techniques which lead to the conclusion that Cyclodextrin hydroxyquinoline derivatives have therapeutic potential worth perusing for Parkinson's disease. Additionally, alpha synuclein oligomers were studied as well as synuclein interaction with amyloid beta in the presence of insulin degrading enzyme which showed that increase in alpha synuclein levels lead to faster formation (less experiment time) of amyloid beta peptides. Furthermore, the effect of clearance system on amyloid beta hydrolysis was studied which showed that 20S proteasome hydrolysis of amyloid beta is increased by increased concentration of ubiquitin (another clearance system component), while the anti-inflammatory aminopyrine has a dual function on amyloid beta hydrolysis: inhibiting until 5uM aminopyrine while 10uM aminopyrine increases peptide production. The use of aminopyrine is for an effort to find new therapeutic potentials for drugs already in the market. This enzyme and its mutant were also recruited in order to understand the role played by copper(II) and zinc(II) in the degradation process of the enzyme. Both metal ions hindered the hydrolytic function of the mutant enzyme. Finally, the action of insulin degrading enzyme on insulin and the neuropeptide Nociceptin was studied which showed a preference for insulin hydrolysis. Many of these experiments were conducted using LC-MS and/or MALDI which was a new area of research studied in-depth during this project.

In the past three years, different experimental approaches were enlisted in the study of the protein α -Synuclein in depth, its interactions and possibilities for therapy. Time limit is indeed cruel in the face of tackling a large developing area of science, but hopefully the work conducted in this thesis might have added some insight in the future of therapy for neurodegenerative diseases.

Acknowledgment












This PhD was funded thanks to financial support from the European Union funding (H2020-Marie Sklodowska Curie Actions; grant agreement INCIPIT n. 665403) and the National Research Council (CNR).

Million Thanks to my supervisors Dr. Francesco Bellia and Prof. Graziella Vecchio for the continuous support and the advice they gave me for my research and for my future career. Moreover, for the time they invested in me and the useful discussions we had, the word thank you is not remotely enough to give justice to all of your efforts. I am glad I did my PhD in this environment; I am glad I was here for the last three years.

I am indebted to Prof. Ron Heeren and Dr. Berta Cillero Pastor for hosting me for four months in M4I in Masstricht where I learned a lot and I gained new experiences, and I can't even begin to thank Anjusha Mathew for giving me all of her time and showing me how to navigate the world of native mass spectrometry, good luck in your PhD journey. And to all the collaborators in this project, many thanks, I hope our research benefit others.

CNR was my home for three years and there I met the most amazing people on earth who helped me get over the feeling of loneliness while teaching me Italian as a bonus, I truly became part of a huge family in Sicily and it is all thanks to your kindness. One of the highlights of this degree is that I navigated it with Sara, I am proud to be your friend and I hope our friendship continues for a long time, thank you for making office life fun and bringing lots of Tomarchio cupcakes.

To the best parents in the whole world (dad I'm happy you are recovering), to my family and my friends, I am grateful for the continues support. To all the teachers and supervisors, I had so far, I really hope I have made you proud. Finally, to my sister Fatma who is my support, I believe I called you every single day in the past three years, thank you for picking up these calls.

 <p>Graziella Vecchio (ACR data support, review)</p> <p>Valentina Oliveri (CD & DLS experiments)</p> <p>Francesca Guarino (recombinant cells)</p> <p>Giuseppe Grasso (Nociceptin experiment idea, MDA, SPR)</p>	 <p>Enrico Falcone (P2 peptide synthesis, support in ACR data analysis)</p> <p>Peter Faller (P2 peptide synthesis)</p>  <p>Michel Goedert (plasmid (pRK172 for α-synuclein synthesis))</p>	 <p>AGH AGH UNIVERSITY OF SCIENCE AND TECHNOLOGY</p> <p>Jerzy Silberring (Nociceptin experiment idea)</p>  <p>Massimo Coletta Grazia Raffaella Tundo Diego Sbardella (Citicoline experiments)</p>
 <p>Francesco Bellia (Data analysis, review)</p> <p>Giuseppe Pappalardo</p> <p>Giuseppe Di Natale</p>	 <p>Jennifer C. Lee (plasmid pRK172 for α-synuclein synthesis)</p> <p>Ryan McGlinchey (Input in α-synuclein purification)</p>	  <p>Anjusha Mathew Berta Cillero Pastor Ron Heeren</p> <p>(Native Mass spectrometry, short-term mobility)</p>

List of abbreviations

ACR: Acrolein

AD: Alzheimer's disease

AD-LBV: Lewy Body Variant with Alzheimer's Disease

AFM: Atomic force microscopy

ALP: Autophagy-lysosomal pathway

AP: Aminopyrine

APP: Amyloid Precursor Protein

APS: Ammonium persulfate

A β : amyloid Beta

Car: Carnosine

CD: Circular dichroism

CD: Cyclodextrin

CHCA: α -Cyano-4-hydroxycinnamic acid

CNS: Central nervous system

CP: Core particle

d_H: Stokes diameter

DLS: Dynamic light scattering

DM: Diabetes mellitus

DTT: Dithiothreitol

DUBs: Deubiquitinating enzymes

ESI-MS: Electron spray ionization- mass spectrometry

FA: Formic acid

FPLC: Fast protein liquid chromatography

GC: Gas chromatography

HNE: 4-hydroxy2-nonenal

HQ: Hydroxyquinoline

IAPP: Islet amyloid polypeptide

IDE: Insulin degrading enzyme

IDP: Intrinsically disordered proteins

IDRs: Intrinsically disordered regions

Ins: Insulin

LB: Lewy Body

LC: Liquid chromatography

MALDI-TOF: Matrix-assisted laser desorption/ionization-Time of flight

MDA: Malondialdehyde

MMPs: Matrix metalloproteinases

MOPS: (3-(N-morpholino)propanesulfonic acid)

MS/MS: Tandem mass spectrometry

MS: Mass spectrometry

MudPIT: Multidimensional protein identification

MW: Molecular weight

N/OFQ: Nociceptin/orphanin FQ

NAC: Non-amyloid β Component

NEP: Nephilysin

PD: Parkinson's disease

PDD: Parkinson's disease with dementia

PICUP: Photo induced cross-linking unmodified proteins

PMD: Protein Misfolding Disorders

PTMs: Post translational modifications

RCS: Reactive carbonyl species

ROS: Reactive oxygen species

RP: Regularity particle

RP: Reverse phase

Ru-bpy: Tris (bipyridine) ruthenium (II) chloride

SCX: Strong cation exchange chromatography

SEC: Size Exclusion Chromatography

SN: Substantia nigra

T2DM: type two diabetes mellitus

TEM: Transmission electron microscopy

TFA: Trifluoroacetic acid

TH: Tyrosine hydroxylase

ThT: Thioflavin T

Ub: Ubiquitin

UPS: Ubiquitin-Proteasome system

XIC: Extracted ion chromatogram

α -syn: Alpha Synuclein

References

- (1) Habchi, J.; Tompa, P.; Longhi, S.; Uversky, V. N. Introducing Protein Intrinsic Disorder. *Chem Rev* **2014**, *114* (13), 6561–6588. <https://doi.org/10.1021/cr400514h>.
- (2) Atrian-Blasco, E.; Gonzalez, P.; Santoro, A.; Alies, B.; Faller, P.; Hureau, C. Cu and Zn Coordination to Amyloid Peptides: From Fascinating Chemistry to Debated Pathological Relevance. *Coord Chem Rev* **2018**, *375*, 38–55. <https://doi.org/10.1016/j.ccr.2018.04.007>.
- (3) Chen, G.-F.; Xu, T.-H.; Yan, Y.; Zhou, Y.-R.; Jiang, Y.; Melcher, K.; Xu, H. E. Amyloid Beta: Structure, Biology and Structure-Based Therapeutic Development. *Acta Pharmacol Sin* **2017**, *38* (9), 1205–1235. <https://doi.org/10.1038/aps.2017.28>.
- (4) Conway, K. A.; Rochet, J. C.; Bieganski, R. M.; Lansbury, P. T. J. Kinetic Stabilization of the Alpha-Synuclein Protofibril by a Dopamine-Alpha-Synuclein Adduct. *Science* **2001**, *294* (5545), 1346–1349. <https://doi.org/10.1126/science.1063522>.
- (5) Lashuel, H. A.; Overk, C. R.; Oueslati, A.; Masliah, E. The Many Faces of Alpha-Synuclein: From Structure and Toxicity to Therapeutic Target. *Nat Rev Neurosci* **2013**, *14* (1), 38–48. <https://doi.org/10.1038/nrn3406>.
- (6) Dehay, B.; Bourdenx, M.; Gorry, P.; Przedborski, S.; Vila, M.; Hunot, S.; Singleton, A.; Olanow, C. W.; Merchant, K. M.; Bezdard, E.; Petsko, G. A.; Meissner, W. G. Targeting Alpha-Synuclein for Treatment of Parkinson's Disease: Mechanistic and Therapeutic Considerations. *Lancet Neurol* **2015**, *14* (8), 855–866. [https://doi.org/10.1016/S1474-4422\(15\)00006-X](https://doi.org/10.1016/S1474-4422(15)00006-X).
- (7) Shamoto-Nagai, M.; Maruyama, W.; Hashizume, Y.; Yoshida, M.; Osawa, T.; Riederer, P.; Naoi, M. In Parkinsonian Substantia Nigra, Alpha-Synuclein Is Modified by Acrolein, a Lipid-Peroxidation Product, and Accumulates in the Dopamine Neurons with Inhibition of Proteasome Activity. *J Neural Transm (Vienna)* **2007**, *114* (12), 1559–1567. <https://doi.org/10.1007/s00702-007-0789-2>.
- (8) Okochi, M.; Walter, J.; Koyama, A.; Nakajo, S.; Baba, M.; Iwatsubo, T.; Meijer, L.; Kahle, P. J.; Haass, C. Constitutive Phosphorylation of the Parkinson's Disease Associate d Alpha-Synuclein. *J Biol Chem* **2000**, *275* (1), 390–397. <https://doi.org/10.1074/jbc.275.1.390>.
- (9) Souza, J. M.; Giasson, B. I.; Chen, Q.; Lee, V. M.; Ischiropoulos, H. Dityrosine Cross-Linking Promotes Formation of Stable Alpha -Synuclein Polymers. Implication of Nitritative and Oxidative Stress in the Pathogenesis of Neurodegenerative Synucleinopathies. *J Biol Chem* **2000**, *275* (24), 18344–18349. <https://doi.org/10.1074/jbc.M000206200>.
- (10) Periquet, M.; Fulga, T.; Myllykangas, L.; Schlossmacher, M. G.; Feany, M. B. Aggregated Alpha-Synuclein Mediates Dopaminergic Neurotoxicity in Vivo. *J Neurosci* **2007**, *27* (12), 3338–3346. <https://doi.org/10.1523/JNEUROSCI.0285-07.2007>.
- (11) De Ricco, R.; Valensin, D.; Dell'Acqua, S.; Casella, L.; Dorlet, P.; Faller, P.; Hureau, C. Remote His50 Acts as a Coordination Switch in the High-Affinity N-Terminal Centered Copper(II) Site of Alpha-Synuclein. *Inorg Chem* **2015**, *54* (10), 4744–4751. <https://doi.org/10.1021/acs.inorgchem.5b00120>.
- (12) González, N.; Arcos-López, T.; König, A.; Quintanar, L.; Menacho Márquez, M.; Outeiro, T. F.; Fernández, C. O. Effects of Alpha-Synuclein Post-Translational Modifications on Metal Binding. *Journal of Neurochemistry* **2019**, *150* (5), 507–521. <https://doi.org/10.1111/jnc.14721>.
- (13) Acosta, G.; Race, N.; Herr, S.; Fernandez, J.; Tang, J.; Rogers, E.; Shi, R. Acrolein-Mediated Alpha-Synuclein Pathology Involvement in the Early Post-Injury Pathogenesis of Mild Blast-Induced Parkinsonian Neurodegeneration. *Mol Cell Neurosci* **2019**, *98*, 140–154. <https://doi.org/10.1016/j.mcn.2019.06.004>.

- (14) Vistoli, G.; De Maddis, D.; Cipak, A.; Zarkovic, N.; Carini, M.; Aldini, G. Advanced Glycoxidation and Lipoxidation End Products (AGEs and ALEs): An Overview of Their Mechanisms of Formation. *Free Radic Res* **2013**, *47 Suppl 1*, 3–27. <https://doi.org/10.3109/10715762.2013.815348>.
- (15) Xiang, W.; Menges, S.; Schlachetzki, J. C.; Meixner, H.; Hoffmann, A.-C.; Schlötzer-Schrehardt, U.; Becker, C.-M.; Winkler, J.; Klucken, J. Posttranslational Modification and Mutation of Histidine 50 Trigger Alpha Synuclein Aggregation and Toxicity. *Mol Neurodegener* **2015**, *10*. <https://doi.org/10.1186/s13024-015-0004-0>.
- (16) Ambaw, A.; Zheng, L.; Tambe, M. A.; Strathearn, K. E.; Acosta, G.; Hubers, S. A.; Liu, F.; Herr, S. A.; Tang, J.; Truong, A.; Walls, E.; Pond, A.; Rochet, J.-C.; Shi, R. Acrolein-Mediated Neuronal Cell Death and Alpha-Synuclein Aggregation: Implications for Parkinson's Disease. *Mol Cell Neurosci* **2018**, *88*, 70–82. <https://doi.org/10.1016/j.mcn.2018.01.006>.
- (17) Wang, Y.-T.; Lin, H.-C.; Zhao, W.-Z.; Huang, H.-J.; Lo, Y.-L.; Wang, H.-T.; Lin, A. M.-Y. Acrolein Acts as a Neurotoxin in the Nigrostriatal Dopaminergic System of Rat: Involvement of Alpha-Synuclein Aggregation and Programmed Cell Death. *Sci Rep* **2017**, *7*, 45741. <https://doi.org/10.1038/srep45741>.
- (18) Lanza, V.; Bellia, F.; Rizzarelli, E. An Inorganic Overview of Natural A β Fragments: Copper(II) and Zinc(II)-Mediated Pathways. *Coordination Chemistry Reviews* **2018**, *369*, 1–14. <https://doi.org/10.1016/j.ccr.2018.04.004>.
- (19) Malgieri, G.; Grasso, G. The Clearance of Misfolded Proteins in Neurodegenerative Diseases by Zinc Metalloproteases: An Inorganic Perspective. *Coordination Chemistry Reviews* **2014**, *260*, 139–155. <https://doi.org/10.1016/j.ccr.2013.10.008>.
- (20) Serpell, L. C. Alzheimer's Amyloid Fibrils: Structure and Assembly. *Biochim Biophys Acta* **2000**, *1502* (1), 16–30.
- (21) Dikic, I. Proteasomal and Autophagic Degradation Systems. *Annu Rev Biochem* **2017**, *86*, 193–224. <https://doi.org/10.1146/annurev-biochem-061516-044908>.
- (22) Bustamante, H. A.; Gonzalez, A. E.; Cerda-Troncoso, C.; Shaughnessy, R.; Otth, C.; Soza, A.; Burgos, P. V. Interplay Between the Autophagy-Lysosomal Pathway and the Ubiquitin-Proteasome System: A Target for Therapeutic Development in Alzheimer's Disease. *Front Cell Neurosci* **2018**, *12*, 126. <https://doi.org/10.3389/fncel.2018.00126>.
- (23) Kumar Deshmukh, F.; Yaffe, D.; Olshina, M. A.; Ben-Nissan, G.; Sharon, M. The Contribution of the 20S Proteasome to Proteostasis. *Biomolecules* **2019**, *9* (5). <https://doi.org/10.3390/biom9050190>.
- (24) Atrian-Blasco, E.; Conte-Daban, A.; Hureau, C. Mutual Interference of Cu and Zn Ions in Alzheimer's Disease: Perspectives at the Molecular Level. *Dalton Trans* **2017**, *46* (38), 12750–12759. <https://doi.org/10.1039/c7dt01344b>.
- (25) Morales, R.; Moreno-Gonzalez, I.; Soto, C. Cross-Seeding of Misfolded Proteins: Implications for Etiology and Pathogenesis of Protein Misfolding Diseases. *PLoS Pathog* **2013**, *9* (9), e1003537. <https://doi.org/10.1371/journal.ppat.1003537>.
- (26) Iwai, A.; Yoshimoto, M.; Maslah, E.; Saitoh, T. Non-A Beta Component of Alzheimer's Disease Amyloid (NAC) Is Amyloidogenic. *Biochemistry* **1995**, *34* (32), 10139–10145.
- (27) Han, H.; Weinreb, P. H.; Lansbury, P. T. J. The Core Alzheimer's Peptide NAC Forms Amyloid Fibrils Which Seed and Are Seeded by Beta-Amyloid: Is NAC a Common Trigger or Target in Neurodegenerative Disease? *Chem Biol* **1995**, *2* (3), 163–169.
- (28) Jensen, P. H.; Hojrup, P.; Hager, H.; Nielsen, M. S.; Jacobsen, L.; Olesen, O. F.; Gliemann, J.; Jakes, R. Binding of Abeta to Alpha- and Beta-Synucleins: Identification of Segments in Alpha-Synuclein/NAC Precursor That Bind Abeta and NAC. *Biochem J* **1997**, *323* (Pt 2), 539–546.
- (29) Yoshimoto, M.; Iwai, A.; Kang, D.; Otero, D. A.; Xia, Y.; Saitoh, T. NACP, the Precursor Protein of the Non-Amyloid Beta/A4 Protein (A Beta) Component of Alzheimer Disease Amyloid, Binds A

- Beta and Stimulates A Beta Aggregation. *Proc Natl Acad Sci U S A* **1995**, *92* (20), 9141–9145. <https://doi.org/10.1073/pnas.92.20.9141>.
- (30) Marsh, S. E.; Blurton-Jones, M. Examining the Mechanisms That Link Beta-Amyloid and Alpha-Synuclein Pathologies. *Alzheimers Res Ther* **2012**, *4* (2), 11. <https://doi.org/10.1186/alzrt109>.
- (31) Sharma, S. K.; Chorell, E.; Wittung-Stafshede, P. Insulin-Degrading Enzyme Is Activated by the C-Terminus of Alpha-Synuclein. *Biochem Biophys Res Commun* **2015**, *466* (2), 192–195. <https://doi.org/10.1016/j.bbrc.2015.09.002>.
- (32) Delgado-Morales, R.; Esteller, M. Opening up the DNA Methylome of Dementia. *Mol Psychiatry* **2017**, *22* (4), 485–496. <https://doi.org/10.1038/mp.2016.242>.
- (33) Kawamura, T.; Umemura, T.; Hotta, N. Cognitive Impairment in Diabetic Patients: Can Diabetic Control Prevent Cognitive Decline? *J Diabetes Investig* **2012**, *3* (5), 413–423. <https://doi.org/10.1111/j.2040-1124.2012.00234.x>.
- (34) Lin, L. Commonality between Diabetes and Alzheimer's Disease and a New Strategy for the Therapy. *Clin Med Pathol* **2008**, *1*, 83–91.
- (35) Lee, H. J.; Seo, H. I.; Cha, H. Y.; Yang, Y. J.; Kwon, S. H.; Yang, S. J. Diabetes and Alzheimer's Disease: Mechanisms and Nutritional Aspects. *Clin Nutr Res* **2018**, *7* (4), 229–240. <https://doi.org/10.7762/cnr.2018.7.4.229>.
- (36) Sharma, S. K.; Chorell, E.; Steneberg, P.; Vernersson-Lindahl, E.; Edlund, H.; Wittung-Stafshede, P. Insulin-Degrading Enzyme Prevents α -Synuclein Fibril Formation in a Nonproteolytical Manner. *Sci Rep* **2015**, *5*. <https://doi.org/10.1038/srep12531>.
- (37) Tang, W.-J. Targeting Insulin-Degrading Enzyme to Treat Type 2 Diabetes Mellitus. *Trends Endocrinol Metab* **2016**, *27* (1), 24–34. <https://doi.org/10.1016/j.tem.2015.11.003>.
- (38) Song, M. K.; Bischoff, D. S.; Song, A. M.; Uyemura, K.; Yamaguchi, D. T. Metabolic Relationship between Diabetes and Alzheimer's Disease Affected by Cyclo(His-Pro) plus Zinc Treatment. *BBA Clinical* **2017**, *7*, 41–54. <https://doi.org/10.1016/j.bbacli.2016.09.003>.
- (39) Meunier, J. C.; Mollereau, C.; Toll, L.; Suaudeau, C.; Moisand, C.; Alvinerie, P.; Butour, J. L.; Guillemot, J. C.; Ferrara, P.; Monsarrat, B. Isolation and Structure of the Endogenous Agonist of Opioid Receptor-like ORL1 Receptor. *Nature* **1995**, *377* (6549), 532–535. <https://doi.org/10.1038/377532a0>.
- (40) Reinscheid, R. K.; Nothacker, H. P.; Bourson, A.; Ardati, A.; Henningsen, R. A.; Bunzow, J. R.; Grandy, D. K.; Langen, H.; Monsma, F. J. J.; Civelli, O. Orphanin FQ: A Neuropeptide That Activates an Opioidlike G Protein-Coupled Receptor. *Science* **1995**, *270* (5237), 792–794. <https://doi.org/10.1126/science.270.5237.792>.
- (41) Adeghate, E.; Saeed, Z.; D'Souza, C.; Tariq, S.; Kalasz, H.; Tekes, K.; Adeghate, E. A. Effect of Nociceptin on Insulin Release in Normal and Diabetic Rat Pancreas. *Cell Tissue Res* **2018**, *374* (3), 517–529. <https://doi.org/10.1007/s00441-018-2903-1>.
- (42) Beveridge, R.; Chappuis, Q.; Macphee, C.; Barran, P. Mass Spectrometry Methods for Intrinsically Disordered Proteins. *Analyst* **2013**, *138* (1), 32–42. <https://doi.org/10.1039/C2AN35665A>.
- (43) Amunugama, R.; Jones, R.; Ford, M.; Allen, D. Bottom-Up Mass Spectrometry-Based Proteomics as an Investigative Analytical Tool for Discovery and Quantification of Proteins in Biological Samples. *Adv Wound Care (New Rochelle)* **2013**, *2* (9), 549–557. <https://doi.org/10.1089/wound.2012.0384>.
- (44) Leney, A. C.; Heck, A. J. R. Native Mass Spectrometry: What Is in the Name? *J Am Soc Mass Spectrom* **2017**, *28* (1), 5–13. <https://doi.org/10.1021/jasms.8b05378>.
- (45) LeVine, H. 3rd; Ding, Q.; Walker, J. A.; Voss, R. S.; Augelli-Szafran, C. E. Cloquinol and Other Hydroxyquinoline Derivatives Inhibit A β (1-42) Oligomer Assembly. *Neurosci Lett* **2009**, *465* (1), 99–103. <https://doi.org/10.1016/j.neulet.2009.08.002>.

- (46) Oliveri, V.; Sgarlata, C.; Vecchio, G. Cyclodextrins 3-Functionalized with 8-Hydroxyquinolines: Copper-Binding Ability and Inhibition of Synuclein Aggregation. *Chem Asian J* **2016**, *11* (17), 2436–2442. <https://doi.org/10.1002/asia.201600824>.
- (47) Oliveri, V.; Bellia, F.; Grasso, G. I.; Pietropaolo, A.; Vecchio, G. Trehalose-8-Hydroxyquinoline Conjugates as Antioxidant Modulators of A β Aggregation. *RSC Adv.* **2016**, *6* (53), 47229–47236. <https://doi.org/10.1039/C6RA04204J>.
- (48) Li, J.; Zhu, M.; Rajamani, S.; Uversky, V. N.; Fink, A. L. Rifampicin Inhibits Alpha-Synuclein Fibrillation and Disaggregates Fibrils. *Chem Biol* **2004**, *11* (11), 1513–1521. <https://doi.org/10.1016/j.chembiol.2004.08.025>.
- (49) Oliveri, V.; Vecchio, G. 8-Hydroxyquinolines in Medicinal Chemistry: A Structural Perspective. *European Journal of Medicinal Chemistry* **2016**, *120*, 252–274. <https://doi.org/10.1016/j.ejmech.2016.05.007>.
- (50) Zhang, H.; Dong, X.; Sun, Y. Carnosine-LVFFARK-NH₂ Conjugate: A Moderate Chelator but Potent Inhibitor of Cu(2+)-Mediated Amyloid Beta-Protein Aggregation. *ACS Chem Neurosci* **2018**, *9* (11), 2689–2700. <https://doi.org/10.1021/acchemneuro.8b00133>.
- (51) Zhang, Z.; Marshall, A. G. A Universal Algorithm for Fast and Automated Charge State Deconvolution of Electrospray Mass-to-Charge Ratio Spectra. *J Am Soc Mass Spectrom* **1998**, *9* (3), 225–233. [https://doi.org/10.1016/S1044-0305\(97\)00284-5](https://doi.org/10.1016/S1044-0305(97)00284-5).
- (52) Cox, J.; Mann, M. MaxQuant Enables High Peptide Identification Rates, Individualized p.p.b. - Range Mass Accuracies and Proteome-Wide Protein Quantification. *Nat Biotechnol* **2008**, *26* (12), 1367–1372. <https://doi.org/10.1038/nbt.1511>.
- (53) Strohmalm, M.; Hassman, M.; Kosata, B.; Kodicek, M. MMass Data Miner: An Open Source Alternative for Mass Spectrometric Data Analysis. *Rapid Commun Mass Spectrom* **2008**, *22* (6), 905–908. <https://doi.org/10.1002/rcm.3444>.
- (54) Pfefferkorn, C. M.; Lee, J. C. 5-Fluoro-D,L-Tryptophan as a Dual NMR and Fluorescent Probe of Alpha-Synuclein. *Methods Mol Biol* **2012**, *895*, 197–209. https://doi.org/10.1007/978-1-61779-927-3_14.
- (55) Falcone, E.; Ahmed, I. M. M.; Oliveri, V.; Bellia, F.; Vilenò, B.; El Khoury, Y.; Hellwig, P.; Faller, P.; Vecchio, G. Acrolein and Copper as Competitive Effectors of α -Synuclein. *Chemistry* **2020**, *26* (8), 1871–1879. <https://doi.org/10.1002/chem.201904885>.
- (56) Yamin, G.; Uversky, V. N.; Fink, A. L. Nitration Inhibits Fibrillation of Human Alpha-Synuclein in Vitro by Formation of Soluble Oligomers. *FEBS Lett* **2003**, *542* (1–3), 147–152. [https://doi.org/10.1016/s0014-5793\(03\)00367-3](https://doi.org/10.1016/s0014-5793(03)00367-3).
- (57) Rauniyar, N.; Prokai, L. Detection and Identification of 4-Hydroxy-2-Nonenal Schiff-Base Adducts along with Products of Michael Addition Using Data-Dependent Neutral Loss-Driven MS3 Acquisition: Method Evaluation through an in Vitro Study on Cytochrome c Oxidase Modifications. *Proteomics* **2009**, *9* (22), 5188–5193. <https://doi.org/10.1002/pmic.200900116>.
- (58) Santambrogio, C.; Natalello, A.; Brocca, S.; Ponzini, E.; Grandori, R. Conformational Characterization and Classification of Intrinsically Disordered Proteins by Native Mass Spectrometry and Charge-State Distribution Analysis. *Proteomics* **2019**, *19* (6), e1800060. <https://doi.org/10.1002/pmic.201800060>.
- (59) Rogeberg, M.; Furlund, C. B.; Moe, M. K.; Fladby, T. Identification of Peptide Products from Enzymatic Degradation of Amyloid Beta. *Biochimie* **2014**, *105*, 216–220. <https://doi.org/10.1016/j.biochi.2014.06.023>.
- (60) Tseng, B. P.; Green, K. N.; Chan, J. L.; Blurton-Jones, M.; LaFerla, F. M. A β Inhibits the Proteasome and Enhances Amyloid and Tau Accumulation. *Neurobiol Aging* **2008**, *29* (11), 1607–1618. <https://doi.org/10.1016/j.neurobiolaging.2007.04.014>.

- (61) Oliveri, V.; Zimbone, S.; Giuffrida, M. L.; Bellia, F.; Tomasello, M. F.; Vecchio, G. Porphyrin Cyclodextrin Conjugates Modulate Amyloid Beta Peptide Aggregation and Cytotoxicity. *Chemistry* **2018**, *24* (24), 6349–6353. <https://doi.org/10.1002/chem.201800807>.
- (62) Bellia, F.; Lanza, V.; Garcia-Vinuales, S.; Ahmed, I. M. M.; Pietropaolo, A.; Iacobucci, C.; Malgieri, G.; D'Abrosca, G.; Fattorusso, R.; Nicoletti, V. G.; Sbardella, D.; Tundo, G. R.; Coletta, M.; Pirone, L.; Pedone, E.; Calcagno, D.; Grasso, G.; Milardi, D. Ubiquitin Binds the Amyloid Beta Peptide and Interferes with Its Clearance Pathways. *Chem Sci* **2019**, *10* (9), 2732–2742. <https://doi.org/10.1039/c8sc03394c>.
- (63) Zhao, X.; Yang, J. Amyloid-Beta Peptide Is a Substrate of the Human 20S Proteasome. *ACS Chem Neurosci* **2010**, *1* (10), 655–660. <https://doi.org/10.1021/cn100067e>.
- (64) Grasso, G.; Rizzarelli, E.; Spoto, G. AP/MALDI-MS Complete Characterization of the Proteolytic Fragments Produced by the Interaction of Insulin Degrading Enzyme with Bovine Insulin. *J Mass Spectrom* **2007**, *42* (12), 1590–1598. <https://doi.org/10.1002/jms.1348>.
- (65) Grasso, G.; Pietropaolo, A.; Spoto, G.; Pappalardo, G.; Tundo, G. R.; Ciaccio, C.; Coletta, M.; Rizzarelli, E. Copper(I) and Copper(II) Inhibit Aβ Peptides Proteolysis by Insulin-Degrading Enzyme Differently: Implications for Metallostasis Alteration in Alzheimer's Disease. *Chemistry* **2011**, *17* (9), 2752–2762. <https://doi.org/10.1002/chem.201002809>.
- (66) McCord, L. A.; Liang, W. G.; Dowdell, E.; Kalas, V.; Hoey, R. J.; Koide, A.; Koide, S.; Tang, W.-J. Conformational States and Recognition of Amyloidogenic Peptides of Human Insulin-Degrading Enzyme. *Proc Natl Acad Sci U S A* **2013**, *110* (34), 13827–13832. <https://doi.org/10.1073/pnas.1304575110>.
- (67) Vollers, S. S.; Teplow, D. B.; Bitan, G. Determination of Peptide Oligomerization State Using Rapid Photochemical Crosslinking. *Methods Mol Biol* **2005**, *299*, 11–18. <https://doi.org/10.1385/1-59259-874-9:011>.

Scientific activities

1. Activities

- F. Bellia, E. Falcone, I. M.M. Ahmed, V. Oliveri, G. Vecchio. Reactive carbonyl species and copper(II) as competitive effectors of α -Synuclein. 47th National congress of the inorganic chemistry division of the Italian chemical society, Bari (Italy), 9-12 September 2019.
- I.M.M. Ahmed, E. Falcone, V. Oliveri, G. Vecchio, F. Bellia. The effect of reactive carbonyl compounds on alpha-synuclein structure and aggregation. Synuclein Meeting, Porto (Portugal), 1-4 September 2019 (Poster presentation).
- G. Grasso, F. Bellia, V. Lanza, I.M.M. Ahmed, S. Garcia-Vinuales, M. Arizzi, D. Calcagno, D. Milardi. Site directed mutagenesis of insulin-degrading enzyme allows singling out the molecular basis of peptidase versus E1-like activity: the role of metal ions. 7th International Symposium on Metallomics, Warsaw (Poland), 30 June -3 July 2019.
- I.M.M. Ahmed, E. Falcone, V. Oliveri, G. Vecchio, F. Bellia. The interplay between post-translational modifications (PTMs) on alpha synuclein (α -Syn). IDP f(un) IDP week, Padova (Italy), 3-7 June 2019 (Talk presenter).
- I.M.M. Ahmed, E. Falcone, V. Oliveri, G. Vecchio, F. Bellia. His50 of alpha-synuclein plays a central role in its interaction with acrolein in the presence of copper (II). EMBO practical course Quantitative proteomics: Strategies and tools to probe biology, Heidelberg (Germany), 5-10 May 2019 (Poster presentation).
- F. Bellia, E. Falcone, I.M.M. Ahmed, V. Oliveri, G. Vecchio. Effects of Copper on the α -Synuclein carbonylation XIII Workshop on PharmacoBioMetallics (Biomet 19), Arezzo (Italy), 22 - 23 February 2019.
- F. Bellia, V. Lanza, S. García-Viñuales, I.M.M. Ahmed, A. Pietropaolo, C. Iacobucci, G. Malgieri, G. D'Abrosca, R. Fattorusso, V. G. Nicoletti, D. Sbardella, G.R. Tundo, M. Coletta, D. Calcagno, G. Grasso, D. Milardi. A β binds Ubiquitin and inhibits polyubiquitination: alternative mechanisms for amyloid toxicity. International Symposium on Pathomechanisms of Amyloid Diseases. Miami, Florida (USA), 20-21 December 2018.
- I.M.M. Ahmed, G. Vecchio, F. Bellia Cross-talk between alpha-synuclein and amyloid-beta: new in vitro studies (National Congress of the Division of Chemistry of Biological Systems, (Caserta) Italy, September 2018 (Poster presentation).
- F. Bellia, V. Oliveri, E. Falcone, I.M.M. Ahmed, G. Vecchio. Acrolein modification of α -Synuclein: structural details, copper(II) interference and effects on the protein oligomerization. National Congress of the Division of Chemistry of Biological Systems, (Caserta) Italy, 26-28 September 2018.
- V. Oliveri, E. Falcone, I.M.M. Ahmed, F. bellia, G. Vecchio. α -synuclein and copper: effects of lipid peroxidation products. National congress of inorganic chemistry, (Bologna) Italy, 10-13 September 2018.
- E. Falcone, I.M.M. Ahmed, F. bellia, V. Oliveri, G. Vecchio. Interplay of α -synuclein, acrolein and copper. Copper Bioinorganic Chemistry Symposium, (Marseille) France, 21-24 May 2018.

2. Publications

- I.M.M. Ahmed, A. Mathew, V. Oliveri, F. Bellia, G. Vecchio, R.M.A. Heeren, B. Cillero Pastor. Potential anti-aggregant candidates for Parkinson's disease: A collaboration between Native mass spectrometry and aggregation assay (Manuscript in preparation).
- F. Bellia, G.I. Grasso, I.M.M. Ahmed, V. Oliveri, G. Vecchio. Carnoquinolines Target Copper Dyshomeostasis, Aberrant Protein-Protein Interactions, and Oxidative Stress. Chem. Eur. J (2020).
- D. Sbardella, A. Coletta, G. RaffaellaTundo, I.M.M.Ahmed, F. Bellia, F. Oddone, G. Manni, M.Coletta. Structural and functional evidence for citicoline binding and modulation of 20S proteasome activity: Novel insights into its pro-proteostatic effect. Biochem. Pharmacol (2020), 177:113977.
- E. Falcone, I.M.M. Ahmed, V. Oliveri, F. Bellia, B. Vileno, Y. El Khoury, P. Hellwig, P. Faller, G.Vecchio. Acrolein and Copper as Competitive Effectors of α - Synuclein. Chem. Eur. J.(2020), 26(8):1871-1879.
- M. Santoro; V.Lanza; F. Bellia; D. Sbardella; G. R. Tundo; A. Cannizzo; G. Grasso; M. Arizzi; V.G. Nicoletti; S. Alcaro; G. Costa; A. Pietropaolo; G. Malgieri; G. D'Abrosca; R. Fattorusso; S. Garcia-Vinuales; I. M. M. Ahmed; M. Coletta; D. Milardi. Pyrazolones activate proteasome by gating mechanisms and protect neuronal cells from A β amyloid toxicity. ChemMedChem (2020), 15(3):302-316.
- G.A. Zingale, F. Bellia , I.M.M. Ahmed, P. Mielczarek , J. Silberring, G. Grasso. IDE Degrades Nociceptin/Orphanin FQ through an Insulin Regulated Mechanism. Int J Mol ci.(2019), 20(18).
- F.Bellia, V. Lanza, S. Garcia-Vinuales, I.M.M. Ahmed, A. Pietropaolo, C. Iacobucci, G. Malgieri , G. D'Abrosca, R. Fattorusso, V.G. Nicoletti, D. Sbardella, G.R. Tundo, M. Coletta, L. Pirone, E. Pedone, D. Calcagno, G. Grasso, D. Milardi. Ubiquitin binds the amyloid β peptide and interferes with its clearance pathways. Chem Sci. (2019), 10(9):2732-2742.
- F. Bellia , V. Lanza , I.M.M. Ahmed, S. Garcia-Vinuales, E. Veiss , M. Arizzi, D. Calcagno, D. Milardi , G. Grasso. Site directed mutagenesis of insulin-degrading enzyme allows singling out the molecular basis of peptidase versus E1-like activity: the role of metal ions. Metallomics, (2018),11(2):278-281.

3. Training courses

- International Trends (Webinar) by Andrea Renda, CNR – Naples, 7 July 2020.
- Clinical Trials by Maria Rosaria Piccirillo, CNR – Naples, 7 November 2019.
- Entrepreneurship and start-up creation by Annunziata D'Elia, CNR - Naples, 21-22 October 2019.
- Postdocopportunities in Germany, Webinar, 26 June 2019.
- The importance of communication with specific sensitive category (patients and their families) and with general public. Elena Maria Poletti, CNR - Naples, 25 June 2019
- WoChem symposium, Vienna (Austria), 24 April 2019.
- Self-assembly of amphiphiles characterized by means of scattering experiments. Prof. Dr. Michael Gradzielski (Technical University of Berlin), 11 April 2019.

- EU project management: from the idea to the dissemination of results. Emilia BELFIORE (Head Of R&D Office, IRCCS, Neuromed) CNR – AdR Naples, 17 January 2019
- “ Project management and leadership for young scientists” by Dr. CJ Fitzsimons from EMBO (2-3 Oct, 2018, CNR IGB, Naples, Italy)
- “Industrial Property Rights: Patents, from RandD to market exclusivity” by Dr. Marco Poletti from Bracco Imaging SpA (10 July, 2018, CNR IGB, Naples, Italy)
- “The role of dioxygen in the biosphere” by Prof. Orjan Hansson from University of Gothenburg, Sweden (3-5 July, 2018, Catania University, Italy)
- “Fundraising and attraction of private investment” by Dr Graciana Diez-Roux (23 May, 2018, TIGEM Naples, Italy)
- “Safety issues for INCIPIT PhD fellows” by Dr. Pietro Ragni (24 April 2018, CNR IGB, Naples, Italy)
- “ Animal experiments: Regulatory framework, ethical issues and 3Rs principle application by Dr. Patrizia Costa (19 April 2018, CNR IGB, Naples, Italy)
- "How to write for biomedical journals and how to present scientific data at meetings- Scientific communication” by Jean Ann Gilder (23 March 2018, CNR IGB, Naples, Italy)
- “Project Writing and Neurobiological Basis of Drug Dependence” by Prof. Jerzy Silberring from Krakow University, Poland (20-22 March 2018, Catania University, Italy)

4. Research Stage

Research Stage from 1-Feb, 2020 until 31-May,2020 Supervised by Berta Cillero Pastor in the lab of Ron Heeren, at the University of Maastricht, Maastricht MultiModal Molecular Imaging Institute (M4I) for research in Native mass spectrometry.

Supplementary material

This section will consist on supplementary data that were utilized to achieve the final analysis as reported in the main body of this report. The supplementary materials will be divided into three sections: Carbonylation assay, Proteasome 20S and IDE, Insulin and Nociceptin section. Each section is related to the experiments reported at chapter 2 and chapter 3. Symbol guide for some of the data: m/z = mass to charge ratio, z = charge, RT= retention time.

A. Carbonylation assay

Table S1. Adducts identified through simulation of deconvoluted spectra after 4 h reaction. M stands for Michael adduct (+56 Da), S for Schiff base adduct (+38).

Species	Experimental Mass	Theoretical Mass	Error (ppm)
α Syn	14459.2383	14459.2421	0.3
α Syn+O	14476.2598	14476.2401	-1.4
α Syn·S	14496.2549	14496.2441	-0.7
α Syn·M	14516.2500	14516.2711	1.5
α Syn·M·H ₂ O	14534.2969	14534.2821	-1.0
α Syn·M·S	14552.2412	14552.2821	2.8
α Syn·2M	14571.3135	14571.3051	-0.6
α Syn·M·2S	14591.3086	14591.2982	-0.7
α Syn·2M·S	14611.3037	14611.3641	4.1

Table S2. List of all the identified α -syn tryptic peptides and their LC-MS features. The carbonylated residue is reported in parentheses (Abbreviation column) or in bold and underlined (Amino acid sequence column).

Abbreviation	Amino acid sequence	Measured m/z	Calculated m/z	z	MW	Δm (ppm)	RT (min)
1-6	MDVFMK	770.3586	770.3575	1	769.36	1.4	17.30
11-21	AKEGVVAAAEK	536.8040	536.8035	2	1071.6	0.9	12.75
11-21 (K12)	<u>A</u> KEGVVAAAEK	565.8252	565.8244	2	1129.7	1.4	12.92
13-21	EGVVAAAEK	437.2385	437.2374	2	872.48	2.5	13.63
13-23	EGVVAAAEKTK	551.8098	551.8088	2	1101.6	1.8	12.83
13-23 (K21)	EGVVAAAE <u>K</u> TK	580.8304	580.8297	2	1159.7	1.2	13.57
22-32	TKQGVAAEAGK	530.2943	530.2933	2	1058.6	1.9	11.65
22-32 (K23)	<u>T</u> KQGVAAEAGK	559.3154	559.3142	2	1116.6	2.1	11.87
24-32	QGVAAEAGK	415.7232	415.7220	2	829.44	2.9	12.30
24-34	QGVAAEAGKTK	530.2941	530.2933	2	1058.6	1.5	11.90

24-34 (K32)	QGVAEAAAG K TK	559.3154	559.3142	2	1116.6	2.1	12.15
33-43	TKEGVLYVGSK	590.8336	590.8322	2	1179.7	2.4	14.86
33-43 (K34)	T KEGVLYVGSK	619.8543	619.8532	2	1237.7	1.8	14.92
35-43	EGVLYVGSK	476.2627	476.2609	2	950.52	3.8	16.27
35-45 (K43)	EGVLYVGS K TK	413.5720	413.5712	3	1237.7	1.9	14.91
44-58	TKEGVVHGVATVAEK	508.9520	508.9509	3	1523.9	2.2	14.16
44-58 (K45)	T KEGVVHGVATVAEK	528.2993	528.2982	3	1581.9	2.1	14.20
46-58	EGVVHGVATVAEK	648.3516	648.3513	2	1294.7	0.5	14.77
46-58 (H50)	EGVV H GVATVAEK	677.3724	677.3723	2	1352.7	0.1	14.73
46-58 (H50)	EGVV H GVATVAEK	677.3734	677.3723	2	1352.7	1.6	14.92
46-60	EGVVHGVATVAEKTK	508.9523	508.9509	3	1523.9	2.8	14.67
46-60 (K58)	EGVVHGVATVAE K TK	528.2990	528.2982	3	1581.9	1.5	14.71
59-80	TKEQVTNVGGAVVTGVTAVAQK	719.7352	719.7340	3	2156.2	1.7	18.07
59-80 (K60)	T KEQVTNVGGAVVTGVTAVAQK	739.0825	739.0813	3	2214.2	1.6	18.11
61-80	EQVTNVGGAVVTGVTAVAQK	643.3554	643.3531	3	1927.1	3.6	19.28
81-96	TVEGAGSIAAATGFVK	739.8968	739.8961	2	1477.8	0.9	18.89
81-97	TVEGAGSIAAATGFVKK	536.2994	536.2982	3	1605.9	2.2	17.42
81-97 (K96)	TVEGAGSIAAATGFV K K	555.6466	555.6454	3	1664.0	2.2	17.53

Table S3. Modification percentage of the main ACR-linked tryptic peptides after 30, 60- and 90-min reaction, as a function of the Cu: α Syn molar ratio. The carbonylated residues are shown in parentheses.

Reaction time	30 min				60 min				90 min			
	0:1	1:1	2:1	4:1	0:1	1:1	2:1	4:1	0:1	1:1	2:1	4:1
35-45 (K43)	2.7±0.4	2.4±0.5	3.2±0.3	4.3±0.5	3.4±0.5	3.5±0.4	4.6±0.8	5.7±0.8	2.4±0.4	3.2±0.4	4.3±0.5	5±0.7
44-58 (K45)	7.5±0.8	6.5±0.8	6.9±0.9	6.7±0.8	12±2	8±1	9±1	10±2	14±2	9±1	12±2	9±2
81-97 (K96)	5.5±0.6	5.7±0.6	5.1±0.5	6.3±0.9	8.7±0.9	8±1	8±2	9±2	10±2	9±1	8±1	11±2
22-32 (K23)	3.9±0.4	3.9±0.4	4.0±0.6	4.7±0.7	7±1	5.4±0.9	6±1	7±1	9±1	5.7±0.8	7.3±0.8	7±1
24-34 (K32)	2.9±0.4	3.4±0.4	2.7±0.4	3.3±0.6	4.7±0.7	4.0±0.5	3.6±0.4	4.7±0.9	6.2±0.9	4.0±0.8	5.1±0.6	5.0±0.8
11-21 (K12)	4.2±0.6	4.1±0.6	4.2±0.5	5.3±0.9	7.3±0.9	5.1±0.9	5.2±0.7	7.1±0.8	8.5±0.9	5.2±0.6	7±1	7.3±0.8
13-23 (K21)	4.4±0.8	4.4±0.8	3.8±0.5	4.7±0.7	7±1	5.6±0.9	5.3±0.8	7±1	9±1	6±1	6.9±0.8	7±1
33-43 (K34)	2.5±0.4	2.5±0.3	3.0±0.6	4.0±0.5	3.7±0.6	3.5±0.5	4.4±0.7	5.0±0.6	2.8±0.3	3.3±0.5	4.1±0.4	5.0±0.8
46-58 (H50)	6.5±0.7	5.3±0.8	2.8±0.3	0.6±0.1	14±2	9±2	4.8±0.9	1.3±0.2	23±3	12±2	8.9±0.8	1.5±0.3
59-80 (K60)	6.1±0.7	7.2±0.9	6.1±0.9	6.9±0.8	10±2	10±1	8±2	11±1	11±2	12±2	11±1	12±2

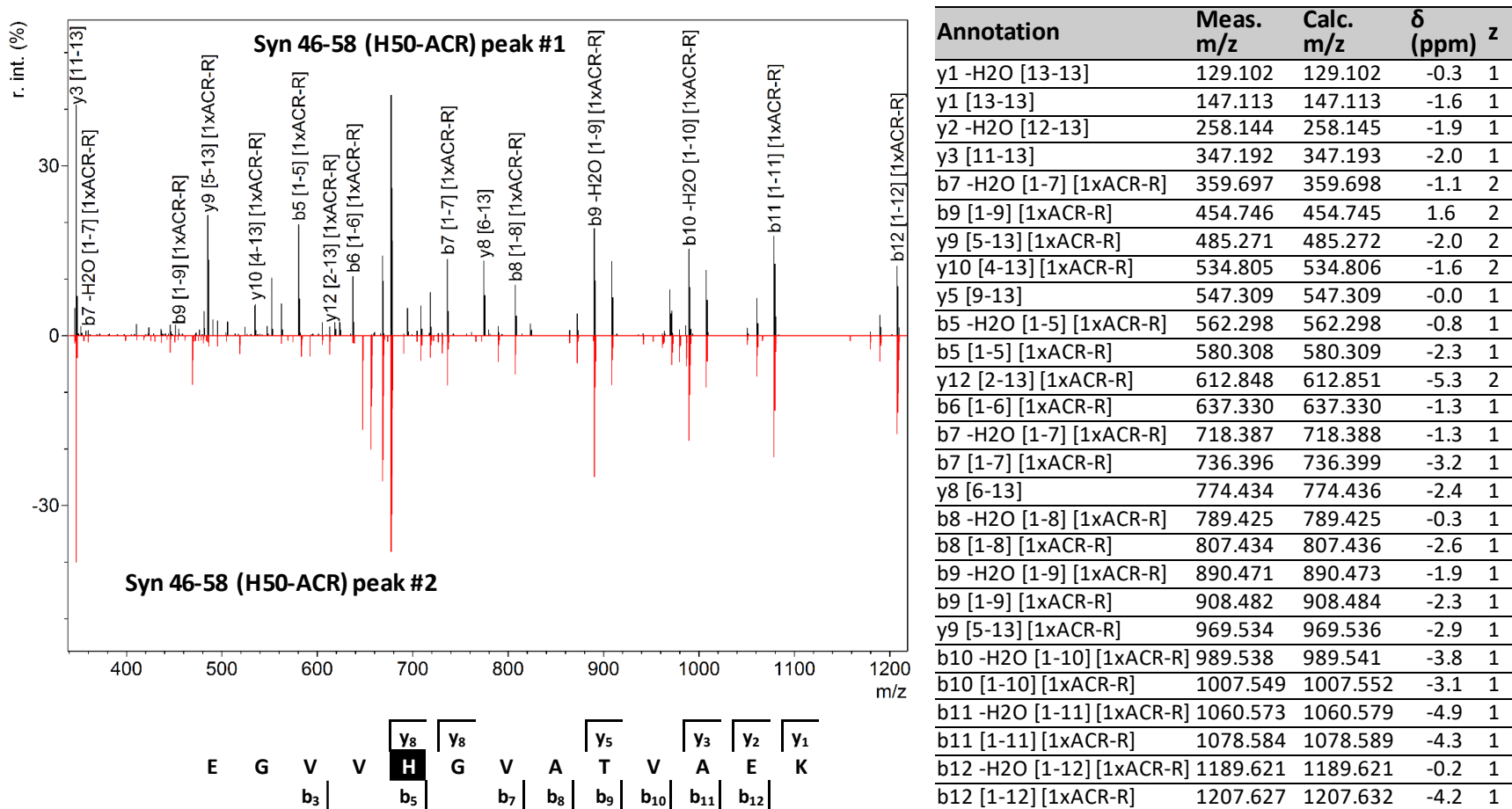
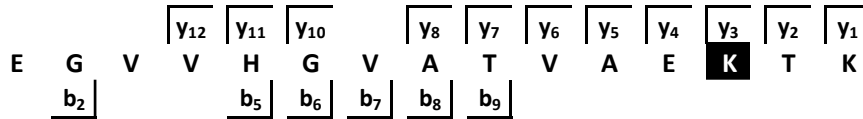
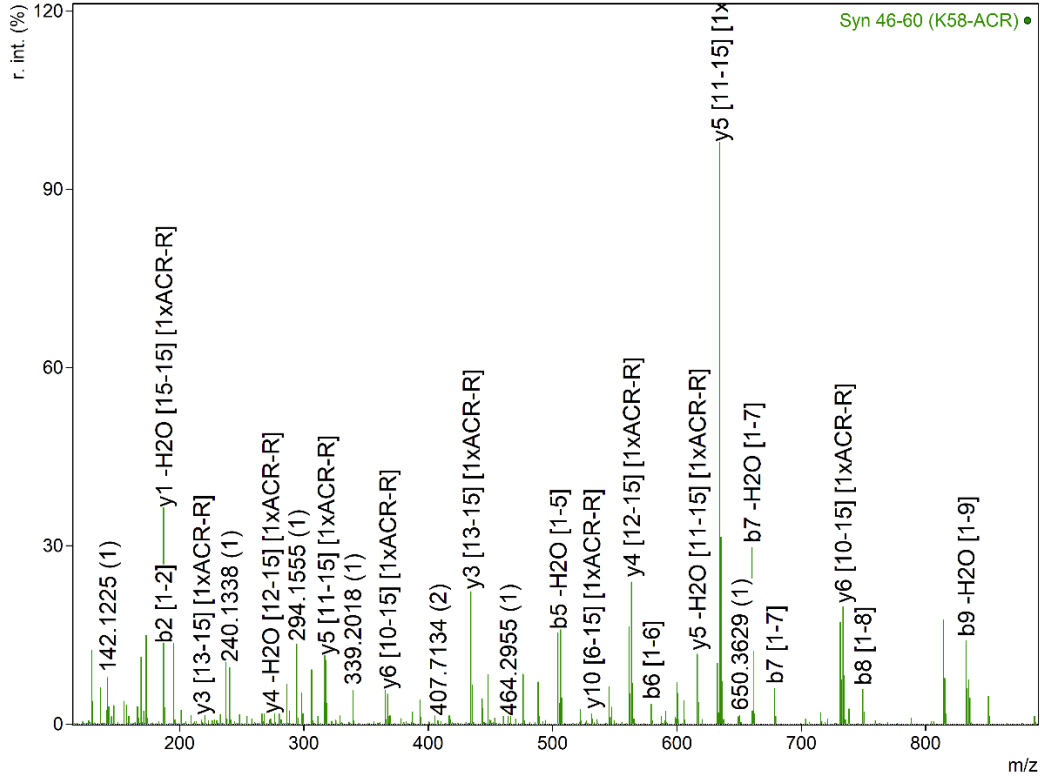
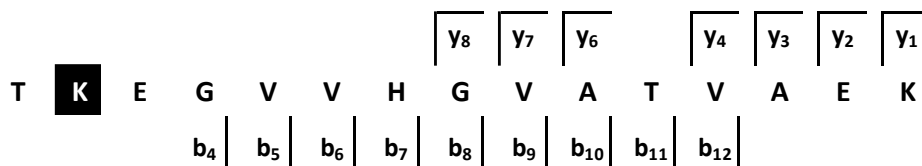
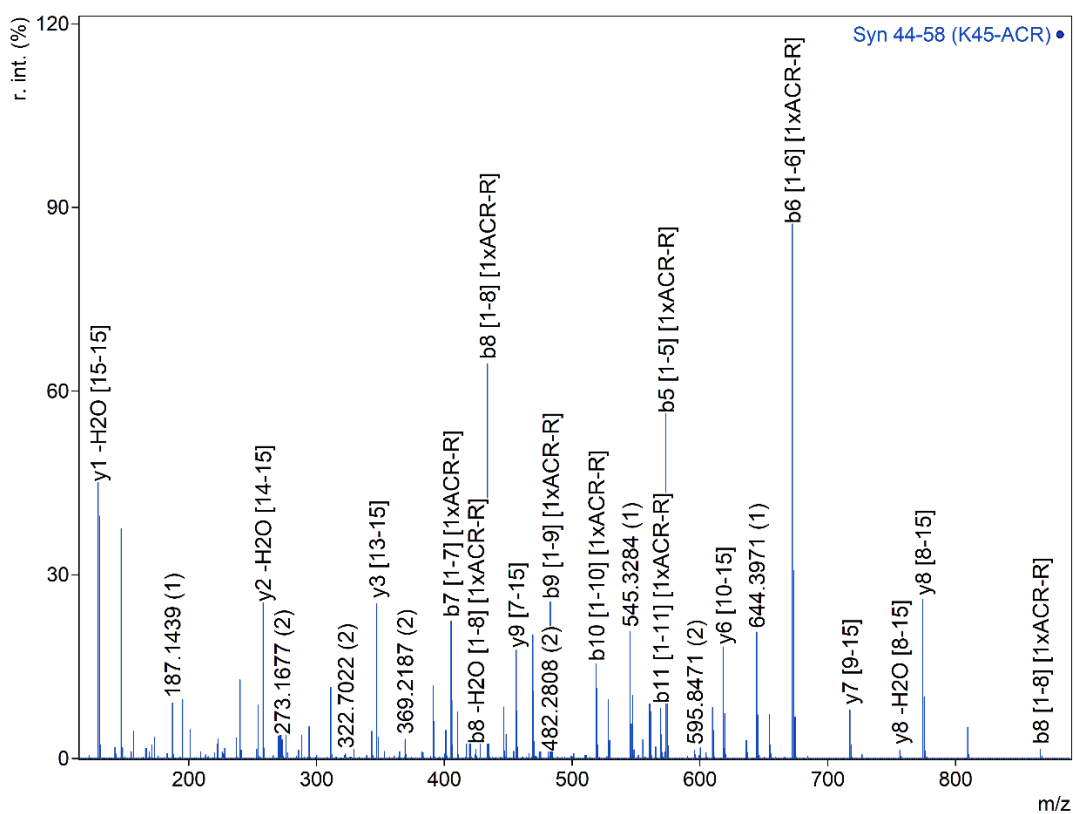


Figure S1. MS/MS acquisition of the tryptic peptide α -syn 46-58 modified by acrolein (ACR) upon reduction with NaBH₄ (ACR-R), related to the chromatographic peaks (#1 and #2). All the fragment of the b and y series are the labeled by the MS/MS and their chemical features have been reported in the table.



Annotation	Meas. m/z	Calc. m/z	δ (ppm)	z
b2 [1-2]	187.071	187.071	-1.2	1
y1 -H2O [15-15] [1xACR-R]	187.144	187.144	-1.2	1
y3 [13-15] [1xACR-R]	217.652	217.652	-2.8	2
y4 -H2O [12-15] [1xACR-R]	273.167	273.168	-4.5	2
y2 [14-15] [1xACR-R]	306.201	306.202	-2.8	1
y5 [11-15] [1xACR-R]	317.692	317.692	-0.4	2
y6 [10-15] [1xACR-R]	367.226	367.226	-1.3	2
y3 [13-15] [1xACR-R]	434.297	434.297	-1.4	1
y4 -NH3 [12-15]	488.270	488.271	-2.2	1
b5 -H2O [1-5]	504.256	504.257	-1.6	1
b5 [1-5]	522.265	522.267	-3.6	1
y10 [6-15] [1xACR-R]	531.313	531.314	-1.5	2
y4 -H2O [12-15] [1xACR-R]	545.328	545.329	-2.8	1
b6 -H2O [1-6]	561.277	561.278	-2.0	1
y4 [12-15] [1xACR-R]	563.338	563.340	-2.5	1
b6 [1-6]	579.287	579.289	-2.2	1
y11 [5-15] [1xACR-R]	599.842	599.843	-1.3	2
y5 -H2O [11-15] [1xACR-R]	616.365	616.366	-2.3	1
y5 [11-15] [1xACR-R]	634.376	634.377	-1.7	1
y12 [4-15] [1xACR-R]	649.376	649.377	-1.3	2
b7 -H2O [1-7]	660.345	660.346	-2.2	1
b7 [1-7]	678.355	678.357	-2.8	1
y6 -H2O [10-15] [1xACR-R]	715.433	715.435	-3.3	1
b8 -H2O [1-8]	731.382	731.383	-2.4	1
y6 [10-15] [1xACR-R]	733.443	733.445	-2.7	1
b8 [1-8]	749.391	749.394	-4.0	1
b9 -H2O [1-9]	832.430	832.431	-1.9	1
y7 [9-15] [1xACR-R]	834.494	834.493	0.9	1
b9 [1-9]	850.441	850.442	-1.4	1
y8 [8-15] [1xACR-R]	905.528	905.530	-2.1	1
y10 [6-15] [1xACR-R]	1061.617	1061.620	-2.6	1

Figure S2. MS/MS acquisition of the tryptic peptide α -syn 46-60 modified by acrolein (ACR) upon reduction with NaBH₄ (ACR-R). All the fragment of the b and y series are the labeled by the MS/MS and their chemical features have been reported in the table.



Annotation	Meas. m/z	Calc. m/z	δ (ppm)	z
y1 -H2O [15-15]	129.102	129.102	-0.4	1
y1 -NH3 [15-15]	130.086	130.086	-0.9	1
y1 [15-15]	147.113	147.113	-1.3	1
y2 -H2O [14-15]	258.144	258.145	-2.0	1
y2 [14-15]	276.156	276.155	2.3	1
y3 [13-15]	347.192	347.193	-2.1	1
b7 [1-7] [1xACR-R]	405.229	405.229	-1.1	2
b8 -H2O [1-8] [1xACR-R]	424.735	424.735	0.5	2
b8 [1-8] [1xACR-R]	433.739	433.740	-1.6	2
y4 [12-15]	446.260	446.261	-2.9	1
y9 [7-15]	456.250	456.251	-1.6	2
b4 [1-4] [1xACR-R]	474.255	474.256	-2.3	1
b9 [1-9] [1xACR-R]	483.274	483.274	-1.8	2
y10 -H2O -NH3 [6-15]	488.266	488.267	-1.8	2
b10 -H2O [1-10] [1xACR-R]	509.787	509.788	-1.6	2
b10 [1-10] [1xACR-R]	518.792	518.793	-2.1	2
b11 -H2O [1-11] [1xACR-R]	560.311	560.311	-1.4	2
b11 [1-11] [1xACR-R]	569.316	569.317	-1.0	2
b5 [1-5] [1xACR-R]	573.323	573.324	-2.1	1
b12 -H2O [1-12] [1xACR-R]	609.845	609.846	-1.7	2
y6 [10-15]	618.344	618.346	-2.1	1
b12 [1-12] [1xACR-R]	618.851	618.851	-0.2	2
b6 [1-6] [1xACR-R]	672.392	672.393	-1.4	1
y7 [9-15]	717.413	717.414	-2.1	1
y8 -H2O [8-15]	756.422	756.425	-4.5	1
y8 [8-15]	774.434	774.436	-2.1	1
b8 [1-8] [1xACR-R]	866.470	866.473	-3.9	1

Figure S3. MS/MS acquisition of the tryptic peptide Syn 44-58 modified by acrolein (ACR) upon reduction with NaBH₄ (ACR-R). All the fragment of the b and y series are the labeled by the MS/MS and their chemical features have been reported in the table.

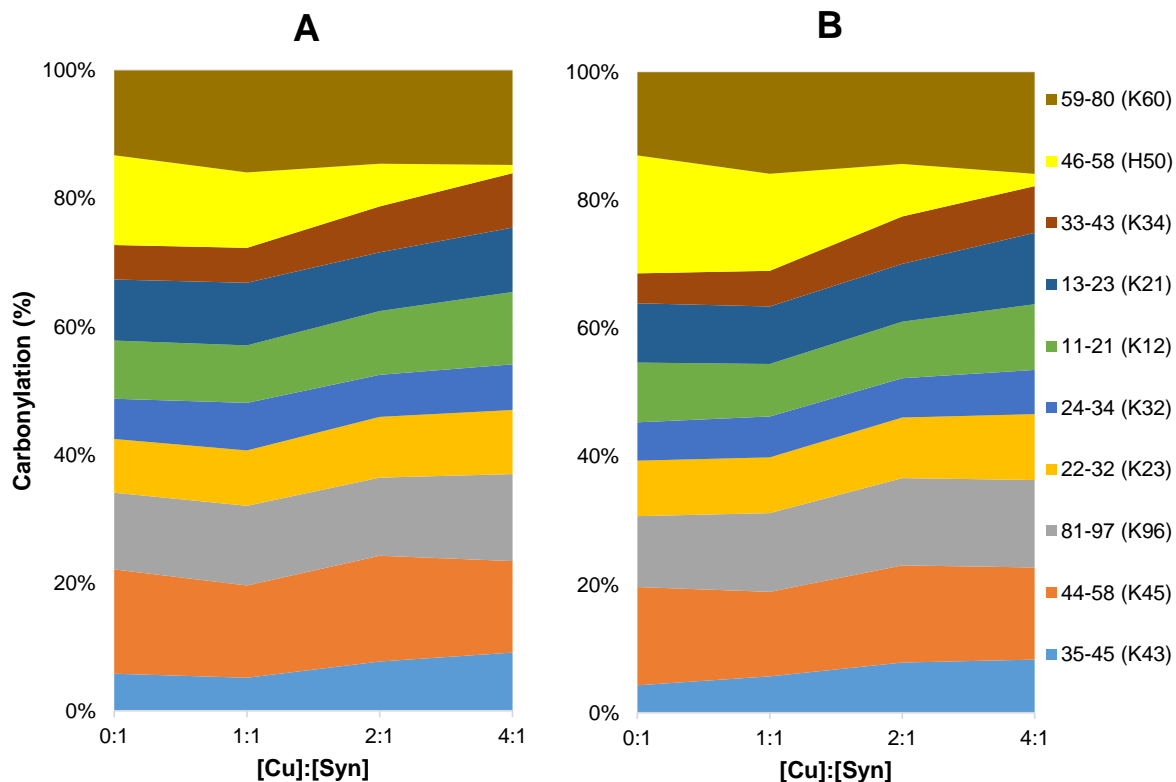


Figure S4. Modification percentage of the main ACR-linked tryptic peptides after 30 (A) and 60 (B) min reaction, as a function of the Cu^{2+} : α -syn molar ratio. The carbonylated residues are shown in parentheses.

Table S4. Main ACR adducts (detected by ESI-MS analysis) of the reaction mixture of P2/ACR.

Species	Chemical Formula	Calculated m/z	Measured m/z	z	Δm (ppm)	Relative Area (%)
$[\text{P2}+\text{ACR}+\text{H}_2\text{O}]\cdot\text{H}^+$	$\text{C}_{28}\text{H}_{46}\text{N}_8\text{O}_{10}$	655.3410	655.3414	1	0.6	61.5
$[\text{P2}+\text{ACR}]\cdot\text{H}^+$	$\text{C}_{28}\text{H}_{44}\text{N}_8\text{O}_9$	637.3304	637.3309	1	0.8	23.6
$[\text{P2}+2\text{ACR}+2\text{H}_2\text{O}]\cdot\text{H}^+$	$\text{C}_{31}\text{H}_{52}\text{N}_8\text{O}_{12}$	729.3777	729.3769	1	-1.1	7.0
$[\text{P2}+2\text{ACR}+\text{H}_2\text{O}]\cdot\text{H}^+$	$\text{C}_{31}\text{H}_{50}\text{N}_8\text{O}_{11}$	711.3671	711.3664	1	-1.0	6.1
$[\text{P2}+2\text{ACR}]\cdot\text{H}^+$	$\text{C}_{31}\text{H}_{48}\text{N}_8\text{O}_{10}$	693.3566	693.3558	1	-1.2	1.8

Table S5. MS/MS peptide fragments of the species [P2+ACR+H₂O]·H⁺.

m/z	Sequence [Modification]	Fragment type	Δm (ppm)
129.1025	e.GV.v	int-a	-2.2
148.0870	v.H. [1xACR; 1xAmide]	im5 -NH ₃	-0.5
166.0977	v.H. [1xACR+H ₂ O; 1xAmide]	im5 -NH ₃	-1.4
172.0613	.E.g [1xAcetyl]	c1 -NH ₃	-5.0
184.1084	v.H. [1xACR+H ₂ O]	im5	-1.7
211.1193	v.H. [1xACR+H ₂ O; 1xAmide]	y1 -H ₂ O	-1.6
229.0818	.EG.v [1xAcetyl]	b2	0.4
229.1297	v.H. [1xACR+H ₂ O; 1xAmide]	y1	-1.0
282.1452	.EGV.v [1xAcetyl]	a3 -H ₂ O	-1.4
293.1614	v.VH. [1xACR+H ₂ O; 1xAmide]	z2 -H ₂ O	-2.1
294.1458	v.VH. [1xACR+H ₂ O; 1xAmide]	z2 -NH ₃	-3.3
300.1559	.EGV.v [1xAcetyl]	a3	-1.7
310.1881	v.VH. [1xACR+H ₂ O; 1xAmide]	y2 -H ₂ O	-2.4
311.1722	v.VH. [1xACR+H ₂ O; 1xAmide]	y2 -NH ₃	-2.5
328.1506	.EGV.v [1xAcetyl]	b3	-0.8
328.1925	v.VH. [1xACR+H ₂ O; 1xAmide]	y2	16.5

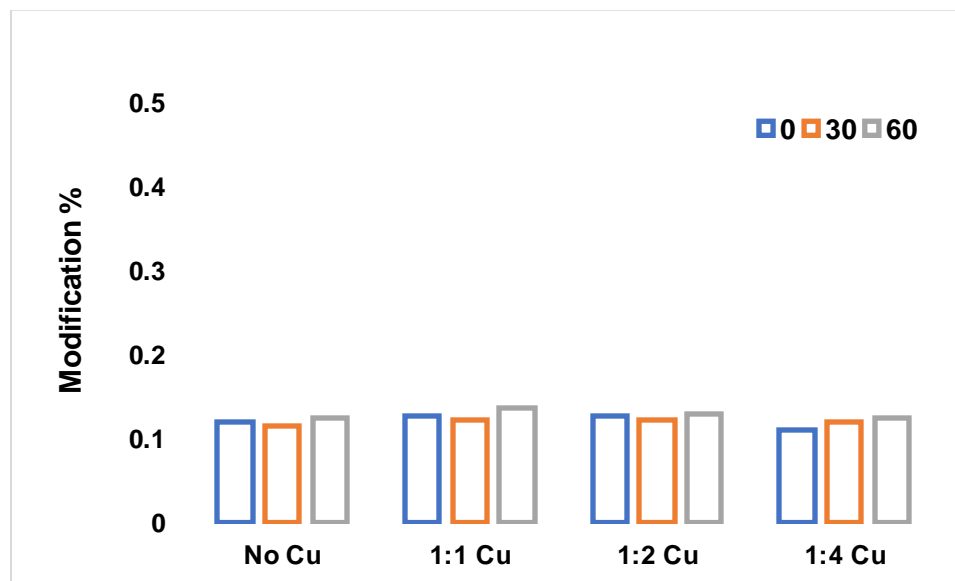


Figure S5. Schiff base formation in the presence of different copper(II) concentrations between peptide P2 and ACR at pH 7.4.

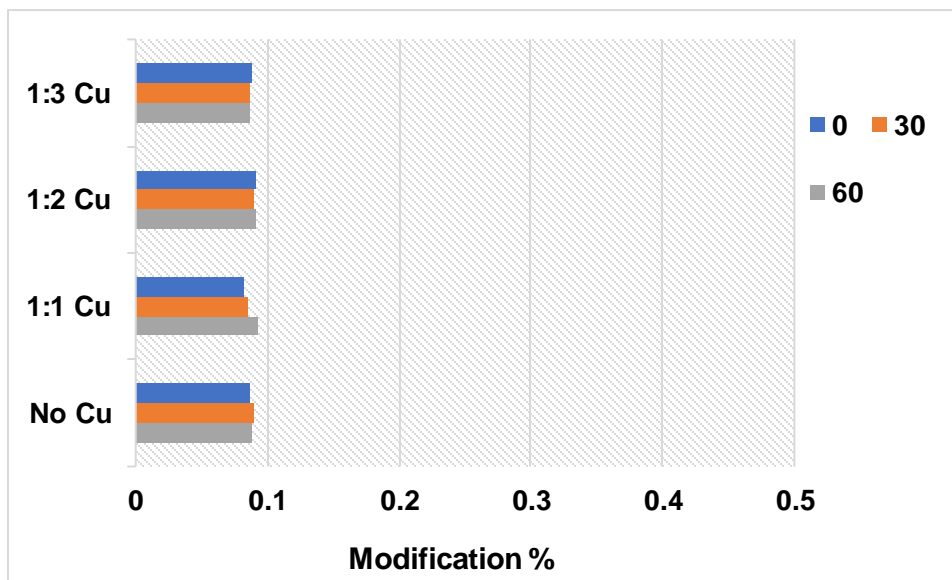


Figure S6. Schiff base formation in the presence of different copper(II) concentrations between peptide P2 and ACR at pH 6.

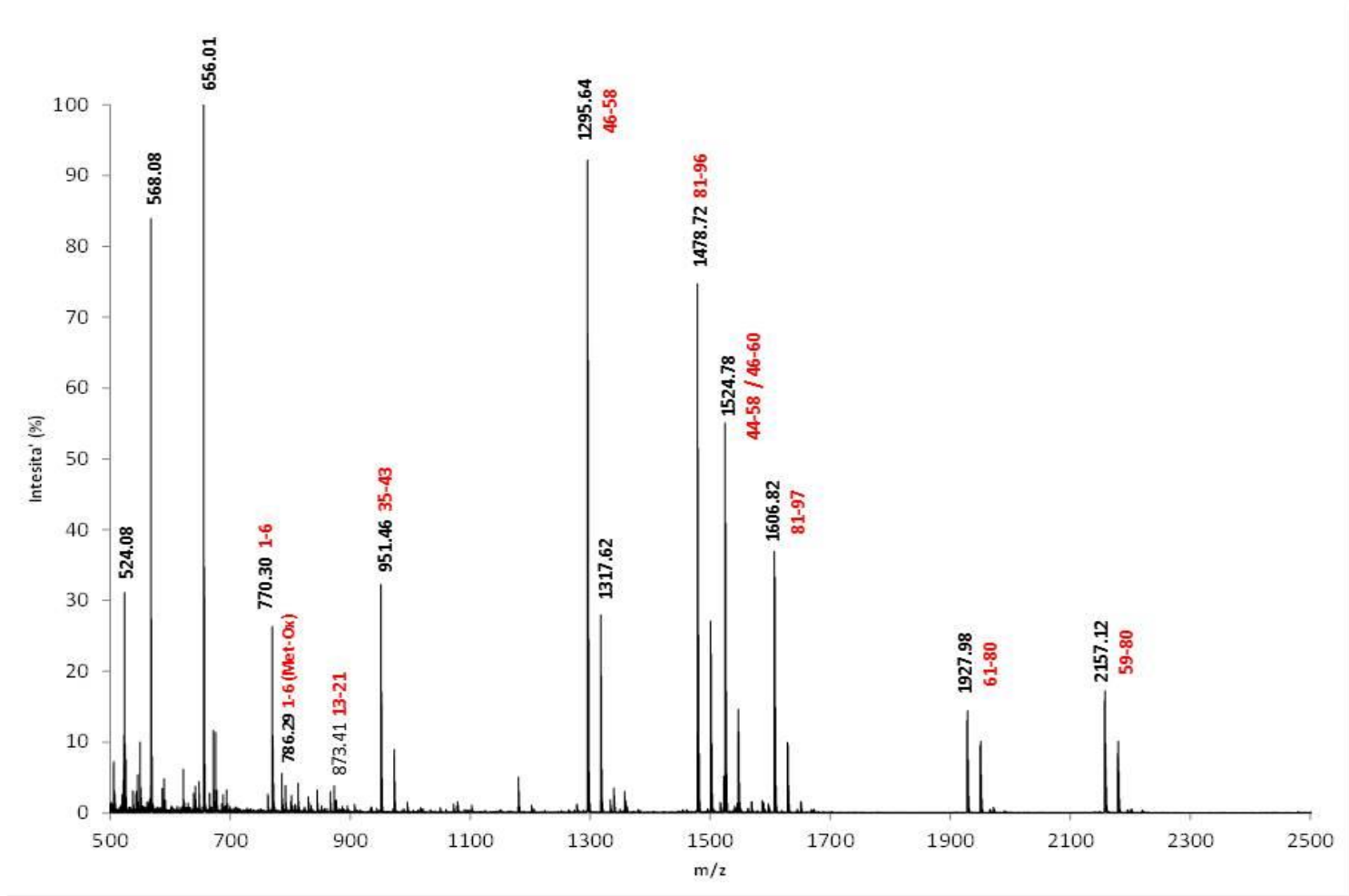


Figure S7. Peptides produced from tryptic digestion of α -Syn, in red attribution corresponding to peptide.

Table S6. Peptides produced from tryptic digestion of α -Syn as detected by MALDI

Specie	Sequence	m/z	m/z	δ	Δ
		exp.	theoretical	(Da)	(ppm)
[1-6] H ⁺	.MDVFMK.g	770.3580	770.3575	0.0005	0.6
[13-21] H ⁺	k.EGVVAAAEEK.t	873.4671	873.4676	-0.0005	-0.6
[35-43] H ⁺	k.EGVLYVGSK.t	951.5122	951.5146	-0.0023	-2.5
[46-58] H ⁺	k.EGVVHGVATVAEK.t	1295.6935	1295.6954	-0.0019	-1.5
[46-58] Na ⁺	k.EGVVHGVATVAEK.t	1317.6859	1317.6773	0.0086	6.5
[59-80] H ⁺	k.TKEQVTNVGGAVVTGVTAVAQK.t	2157.1860	2157.1874	-0.0014	-0.6
[59-80] Na ⁺	k.TKEQVTNVGGAVVTGVTAVAQK.t	2179.1722	2179.1693	0.0028	1.3
[61-80] H ⁺	k.EQVTNVGGAVVTGVTAVAQK.t	1928.0385	1928.0447	-0.0063	-3.2
[61-80] Na ⁺	k.EQVTNVGGAVVTGVTAVAQK.t	1950.0315	1950.0267	0.0048	2.5
[81-96] H ⁺	k.TVEGAGSIAAATGFVK.k	1478.7808	1478.7849	-0.0042	-2.8
[81-96] Na ⁺	k.TVEGAGSIAAATGFVK.k	1500.7735	1500.7669	0.0066	4.4
[81-97] H ⁺	k.TVEGAGSIAAATGFVKK.d	1606.8732	1606.8799	-0.0067	-4.2

B. Native MS

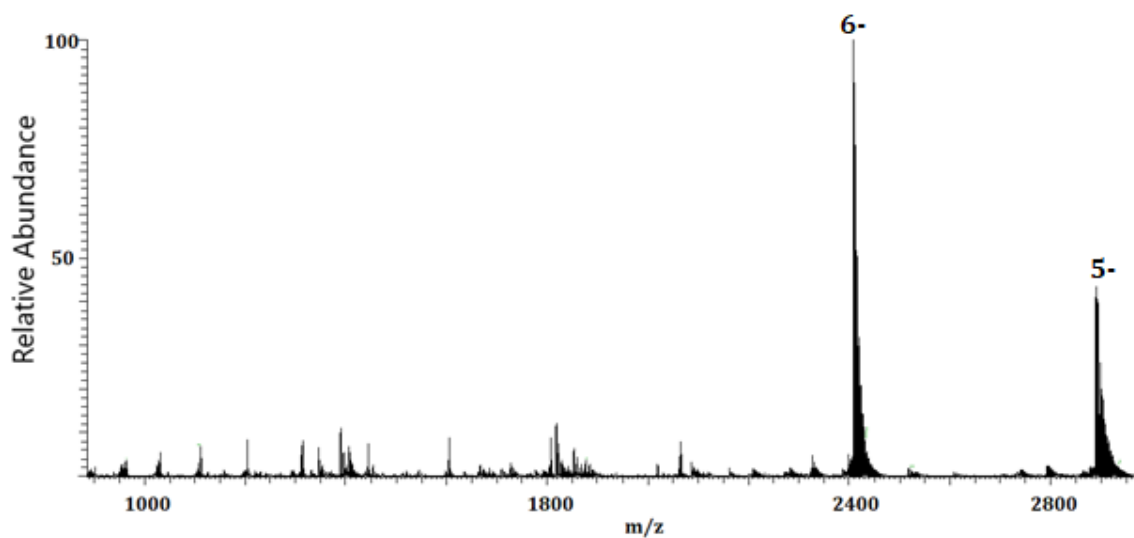


Figure S8. Negative mode native mass spectrometry of α -Syn.

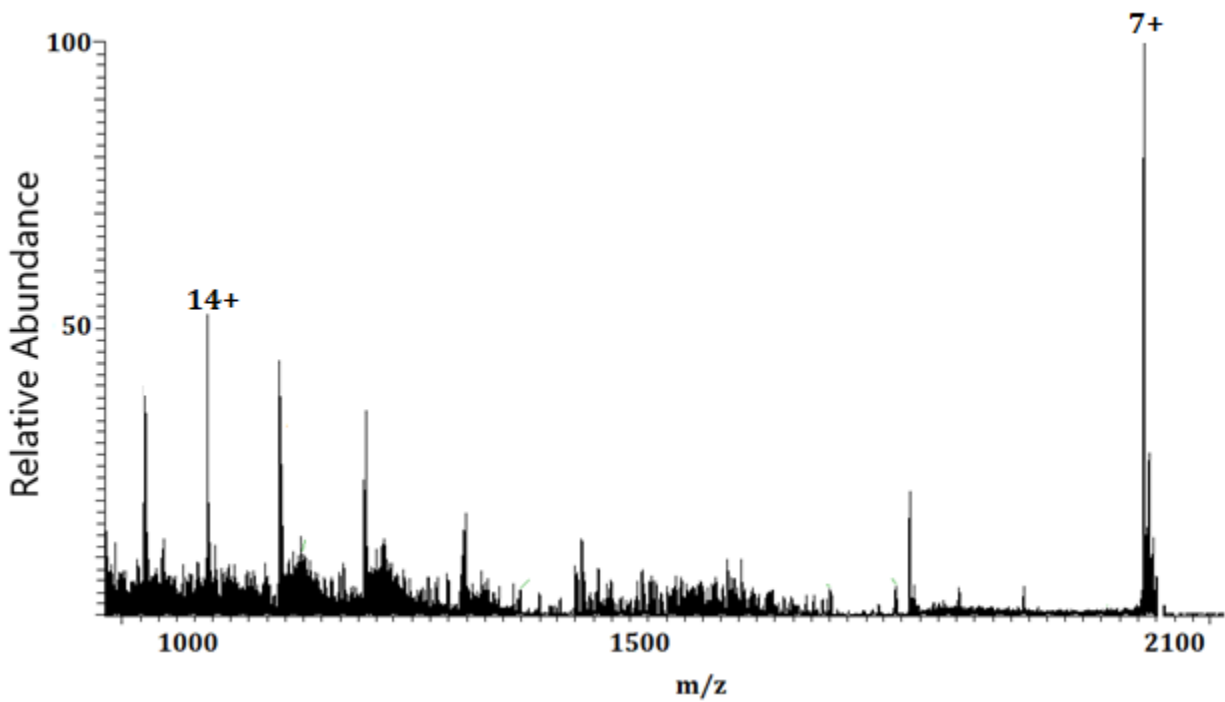


Figure S9. Native mass spectrometry of α -Syn at pH 3.

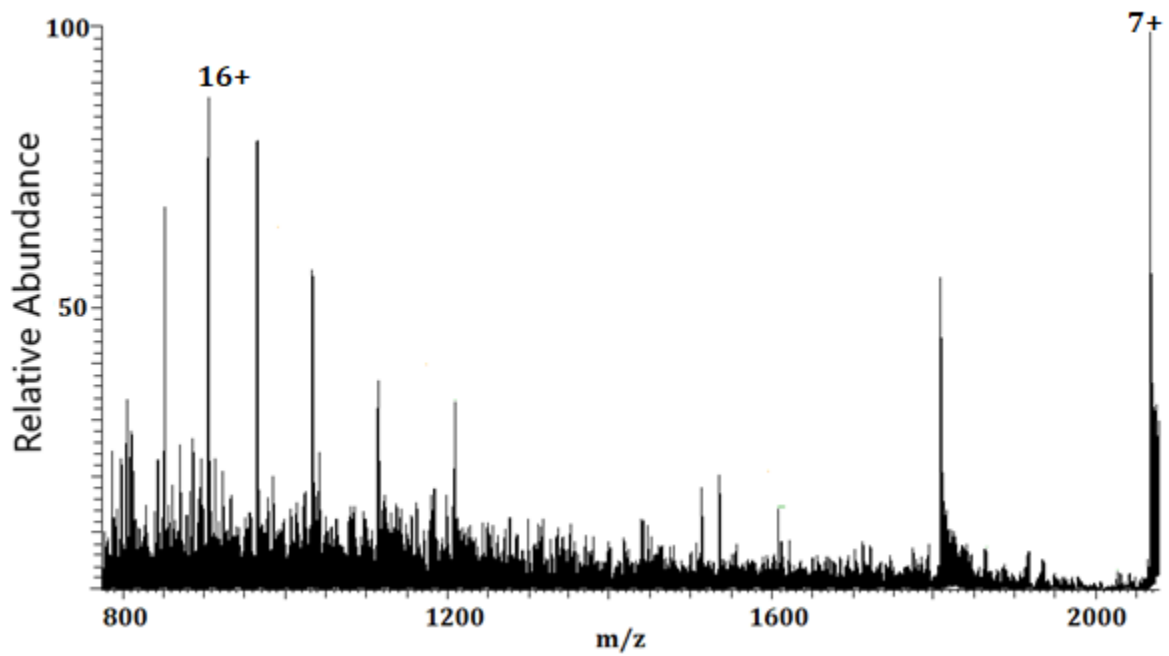


Figure S10. Native mass spectrometry of α -Syn at pH 6.5.

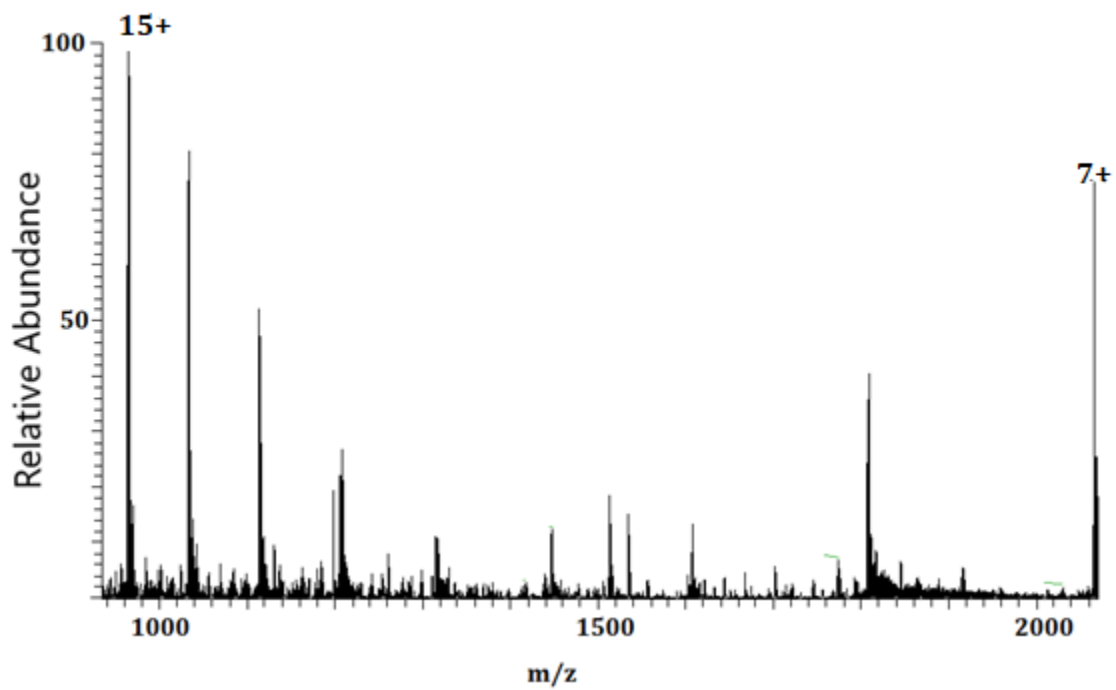


Figure S11. Native mass spectrometry of α -Syn at pH 7.4.

Table S7. Calculated m/z for α -Syn in the presence of different molecules.

Charge state		6+	7+	11+	12+	13+	14+	15+
m/z	Molecular weight	2411	2066.71	1315.55	1206	1113.31	1033.86	965
Rifampicin	822.95	2548.16	2184.27	1390.36	1274.58	1176.61	1092.64	1019.86
CarHQ	397.38	2477.23	2123.48	1351.68	1239.12	1143.88	1062.24	991.49
CDHQ	1305.2	2628.53	2253.17	1424.2	1314.77	1213.71	1127.09	1052.01
ABCDHQ	1475.1	2656.85	2277.44	1439.65	1328.93	1226.78	1139.22	1063.34
HQ	188.18	2442.36	2093.59	1332.66	1221.68	1127.79	1047.3	977.55

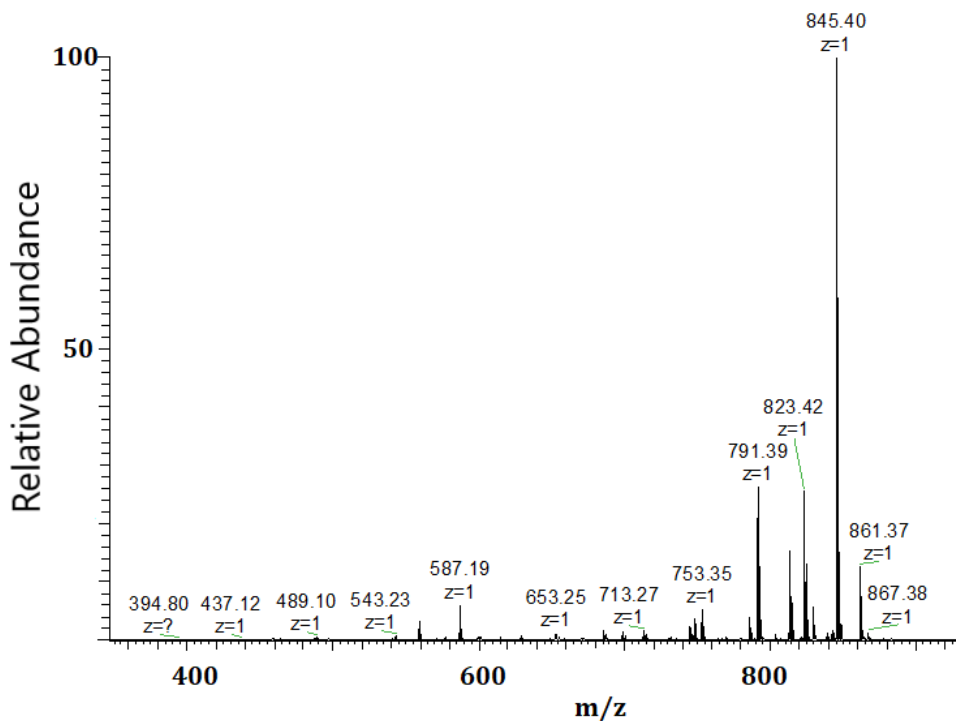


Figure S12. Native mass spectrometry spectra of Rifampicin in ammonium acetate.

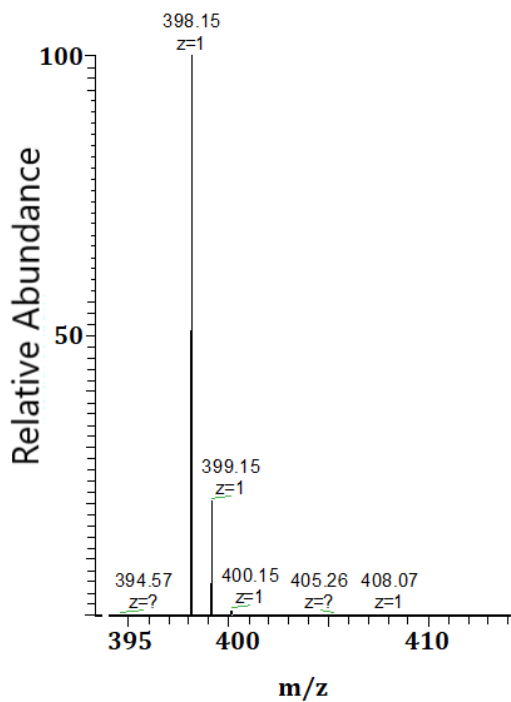


Figure S13. Native mass spectrometry spectra of CarHQ in ammonium acetate.

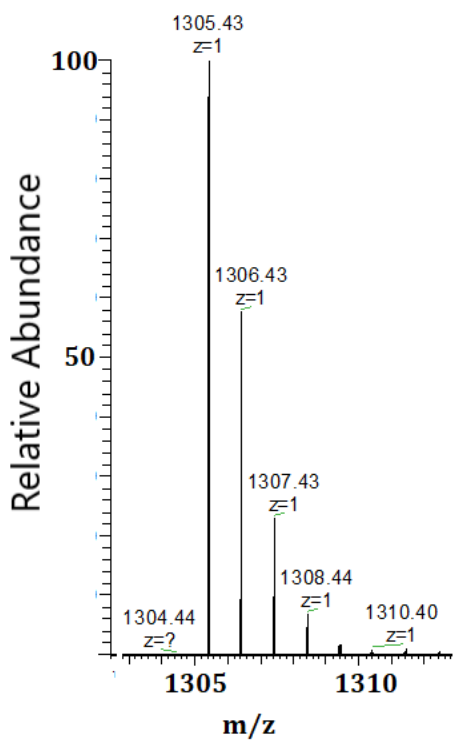


Figure S14. Native mass spectrometry spectra of CDHQ in ammonium acetate.

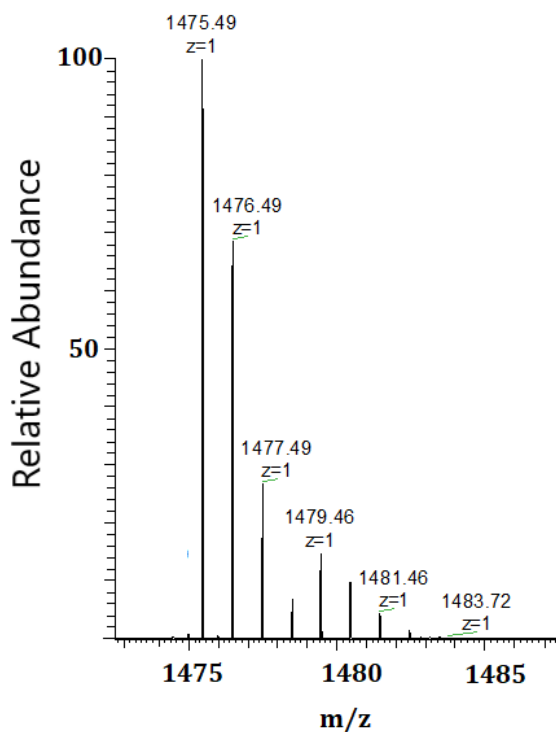


Figure S15. Native mass spectrometry spectra of ABCDHQ in ammonium acetate.

C. PICUP approach

One of the main issues that need to be addressed about the aggregation process of IDPs is the chance to detect and quantify the amount of the oligomeric species, such monomers dimers, trimers, tetramers, etc., by using sensitive and soft analytical approaches. The PICUP⁶⁷ experimental approach allows for the formation of cross links between the protein chains of oligomeric species through the interaction with a Ru-bpy complex and APS (electron acceptor). The reaction is quick (1 sec) and requires small amounts of reagents, differently from other higher molecular weight detection techniques which mostly require a high concentration of the protein sample. Our experimental approach is new since the samples are analyzed with MALDI-TOF as opposed to the traditional analysis with gel electrophoresis. Higher molecular weight species of α -syn were formed after 1s of irradiation. The species included the monomer (~15 KDa), dimer (~30 KDa), trimer (~45 KDa) and the tetramer (~60 KDa) (Figure S16, shows a graphic representation of the species and Table S8). Table S8 shows a significance increase in the oligomeric species after irradiation in comparison to a non-irradiated control. For example, without irradiation the dimer species is 25.8%, but it increases to 61.0% post-irradiation.

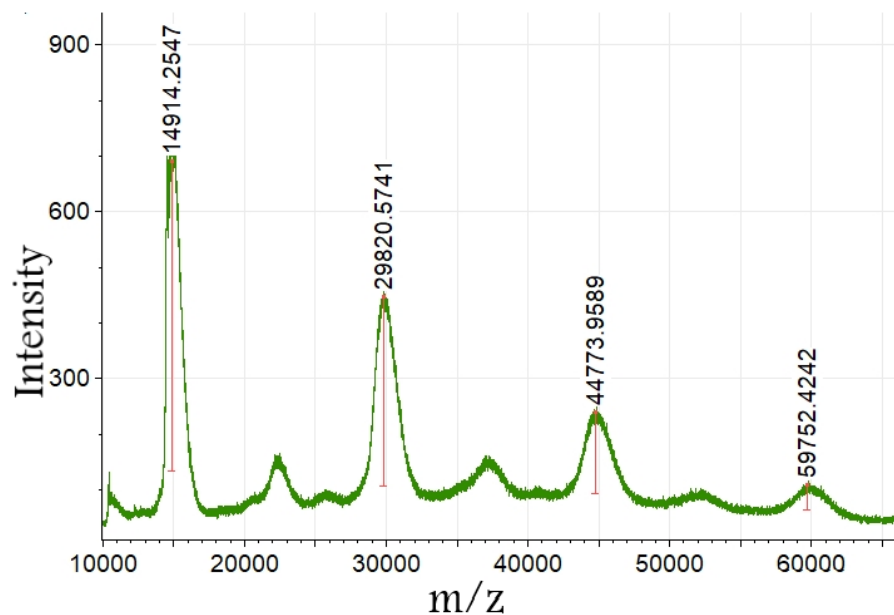


Figure S16. The higher species of α -syn, monomer to tetramer (from left to right), detected by PICUP approach.

Table S8. The formation levels of α -syn oligomers in the absence and presence of irradiation.

α -Syn species	m/z	Control (Rel. intensity)	After irradiation (Rel. intensity)
Monomer	14494	100	100
Dimer	29366	25.8	61.0
Trimer	44349	7.74	26.6
Tetramer	59802	2.59	8.12

D. Proteasome 20S

Table S9. $A\beta_{1-40}$ fragments from proteasome 20S digestion in 60 minutes, significant peptides in **bold**.

RT	m/z	z	MW	Sequences	0 min	30 min	60 min
11.46	682.80830	2	1363.6010	5-15	0	1095923	7987111
11.72	474.22520	2	946.4348	21-30	0	1684419	5278040
12.81	387.68090	2	773.3462	1-6	916393	32627519	89102577
13.07	445.19360	2	888.3716	1-7	17109878	31478078	61857897
13.13	402.20360	4	1604.7832	5-17	0	10495101	84298325

13.83	489.47550	4	1953.8708	1-16	309165	4422463	23323756
13.99	481.71950	2	961.4234	5-12	0	838497	3181280
14.13	599.30440	2	1196.5932	8-17	0	4873027	19605630
14.84	656.81770	2	1311.6198	7-17	0	9486958	39390127
14.97	457.45390	4	1825.7844	1-15	341094	26149320	122913291
15.1	425.43710	4	1697.7172	1-14	216780	7088705	27295143
15.24	488.98970	4	1951.9276	2-17	0	1714451	7976391
15.87	517.74740	4	2066.9584	1-17	5218456	668711473	3366171511
16.23	521.22760	3	1560.6594	1-13	383475	7135037	28480753
16.87	542.51390	4	2166.0244	1-18	0	6868028	39777916
18.5	481.19350	1	480.1857	1-4	1504004	69011919	234889561
18.61	712.80840	2	1423.6012	1-12	0	8391706	28482276
19.07	463.63000	5	2313.1110	1-19	747330	28898585	489700601
19.29	500.50580	4	1997.9920	5-20	493038	16669923	211560427
19.75	352.53180	3	1054.5720	13-20	0	4108654	22973380
20.07	561.30770	1	560.2999	35-40	3055902	416142070	1323550219
20.46	470.03510	5	2345.1365	4-22	0	368908	27585094
20.68	664.51920	5	3317.5570	1-29	347946	517082	76653019
20.66	533.05690	5	2660.2455	1-22	0	0	40053828
20.81	678.72700	5	3388.5960	1-30	122131	555513	139914048
21.25	616.04880	4	2460.1640	1-20	9100143	117873546	11485579039
22.21	512.85480	5	2559.2350	4-24	0	289985	73017995
22.4	569.28410	3	1704.8289	7-20	357306	25646065	229992133
22.48	672.36450	2	1342.7134	21-34	4599520	691160142	2386821825
23.47	572.32400	2	1142.6324	23-34	1814966	78600578	291983672
24.14	674.3918	1	673.3840	34-40	1240453	3291072	9084813
24.41	737.8837	2	1473.7518	21-35	0	4732038	27100527
24.37	781.4622	1	780.4544	15-20	0	2929055	11189268
24.5	412.2239	1	411.2161	18-20	0	62253495	317680461
24.49	653.4029	1	652.3951	16-20	0	7115655	39426746
24.63	745.8979	2	1489.7802	20-34	0	15018244	76074483

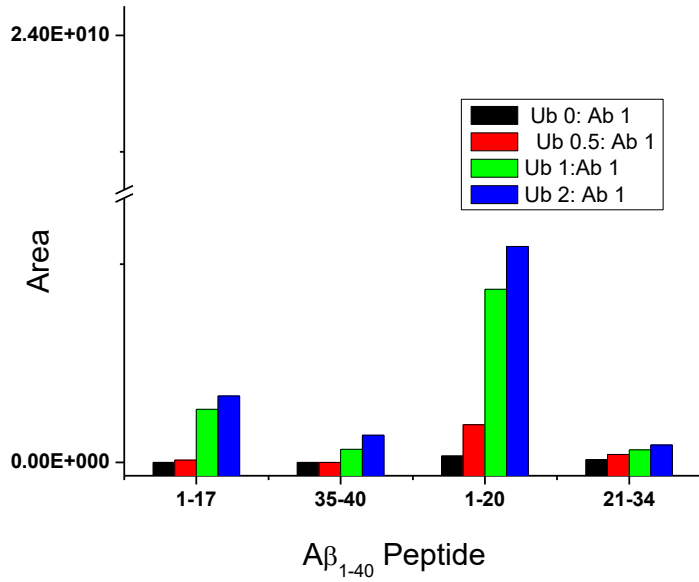


Figure S17. The effect of Ub on the formation of A β ₁₋₄₀ peptides after 0 min of incubation.

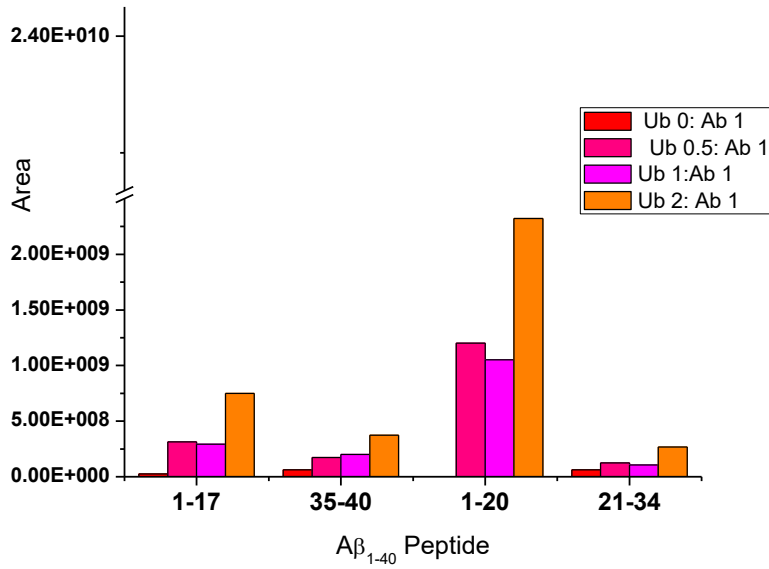


Figure S18. The effect of Ub on the formation of A β ₁₋₄₀ peptides after 20 min of incubation.

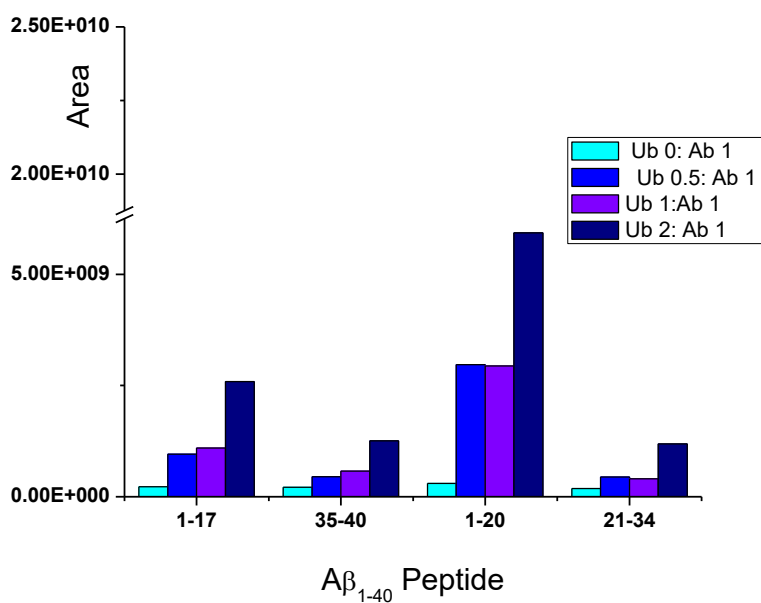


Figure S19. The effect of Ub on the formation of Aβ₁₋₄₀ peptides after 60 min of incubation.

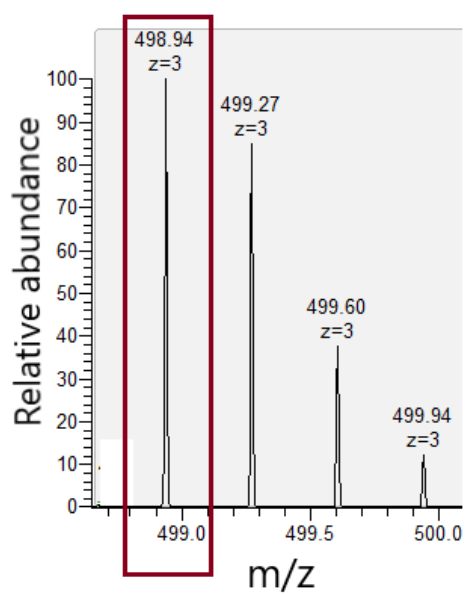


Figure S20. Ab₁₆₋₂₈ detection on LC-MS, m/z value is easily converted to molecular weight value by a mathematical equation.

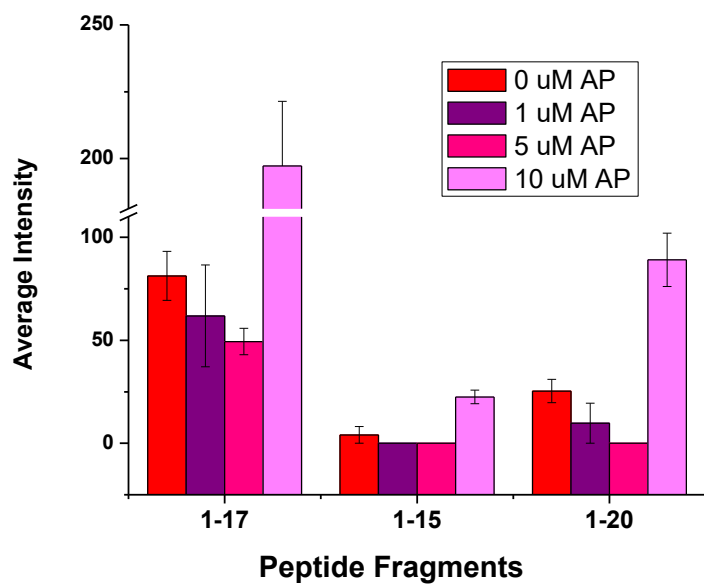


Figure S21. Formation of three representative hydrolytic peptides of Aβ₁₋₂₈ and the effect of aminopyrine (AP) different concentrations at 60 min.

E. IDE, Insulin and Nociceptin

Table S10. The calculated human insulin values are based on amino acid differences with published calculated bovine values⁶⁴.

Insulin IDE fragments	calculated bovine	calculated human
A(1–13) + B(1–9)	2313	2357.06
A(1–13) + B(1–10)	2450.1	2494.16
A(1–13) + B(1–13)	2791.3	2835.36
A(1–13) + B(1–14)	2862.3	2906.36
A(1–13) + B(1–16)	3138.5	3182.56
A(1–14) + B(1–9)	2476	2520.06
A(1–14) + B(1–10)	2613.1	2657.16
A(1–14) + B(1–13)	2954.3	2998.36
A(1–14) + B(1–14)	3025.3	3069.36
A(1–14) + B(1–16)	3301.5	3345.56
A(14–21) + B(10–24)	2749.2	2749.2
A(14–21) + B(10–25)	2896.3	2896.3
A(14–21) + B(10–30)	3456.6	3486.63
A(14–21) + B(11–24)	2612.2	2612.2
A(14–21) + B(11–25)	2759.3	2759.3
A(14–21) + B(11–30)	3319.6	3349.63
A(14–21) + B(14–24)	2271	2271
A(14–21) + B(14–25)	2418.1	2418.1
A(14–21) + B(14–30)	2978.4	3008.43
A(14–21) + B(15–24)	2200	2200
A(14–21) + B(15–25)	2347	2347
A(14–21) + B(15–30)	2907.3	2937.33
A(14–21) + B(17–24)	1923.8	1923.8
A(14–21) + B(17–25)	2070.9	2070.9
A(14–21) + B(17–30)	2631.2	2661.23
A(15–21) + B(10–24)	2586.1	2586.1
A(15–21) + B(10–25)	2733.2	2733.2
A(15–21) + B(10–30)	3293.5	3323.53
A(15–21) + B(11–24)	2449.1	2449.1
A(15–21) + B(11–25)	2596.2	2596.2
A(15–21) + B(11–30)	3156.5	3186.53
A(15–21) + B(14–24)	2107.9	2107.9
A(15–21) + B(14–25)	2255	2255
A(15–21) + B(14–30)	2815.3	2845.33
A(15–21) + B(15–24)	2036.9	2036.9
A(15–21) + B(15–25)	2183.9	2183.9
A(15–21) + B(15–30)	2744.2	2774.23
A(15–21) + B(17–24)	1760.7	1760.7
A(15–21) + B(17–25)	1907.8	1907.8
A(15–21) + B(17–30)	2468.1	2498.13

Table S11. Insulin peptides digested by IDE based on LC-MS analysis.

Insulin	RT	m/z	z
Full length	24.98	1162.34	5
A14-21 B17-24	19.82	641.95	3
A14-21 B14-30	22.95	752.86	4
A1-13 B1-9	21.66	785.68	3
A14-21 B17-25	21.94	690.97	3
A14-21 B14-24	22.42	757.68	3
A14-21 B14-25	23.38	806.7	3
A14-21 B10-30	24.09	872.42	4

Table S12. Nociceptin peptides digested by IDE based on LC-MS analysis.

Nociceptin	RT	m/z	z
1-16	16.01	420.98	4
1-9	16.52	470.75	2
1-11	16.56	366.86	3
1-8	18	406.7	2
2-11	16.55	476.25	2
1-12	15.81	418.89	3
1-10	16.43	343.18	3

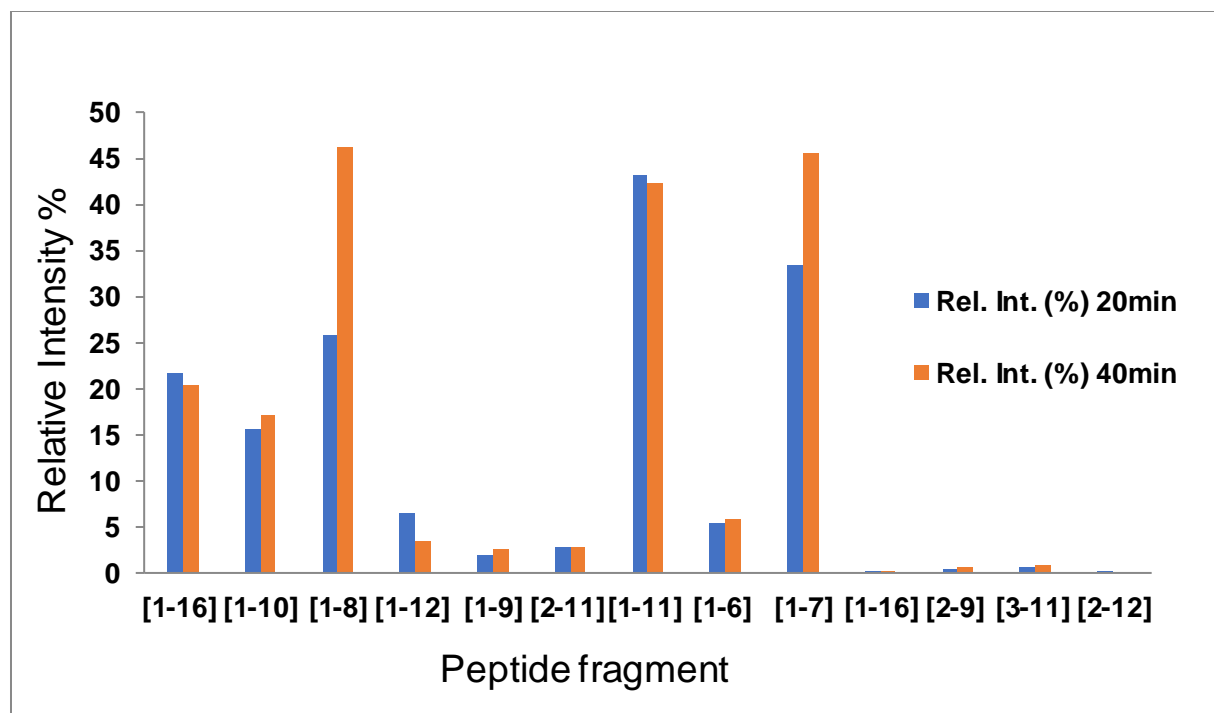


Figure S22. Nociceptin peptides production after 20- and 40-minutes incubation with IDE.

F. SPR measurements

IDE, α -Syn and A β interplay one to each other in vitro. The interaction between IDE and α -Syn was investigated using SPR measurements. Different concentrations of α -Syn were flowed onto a sensor with IDE previously immobilized on the surface. Data coming from the first and second sets of concentrations are reported in Figure S23 and Figure S24, respectively. The interaction curves showed a very steep dissociation phase, this means that the protein binds to IDE but is released quickly. Next, the curves were extracted and analyzed with the software TraceDrawer. The best kinetic evaluation models that compare the theoretical trend to the experimental curves were the "OneToOne" (Figure S26) and "OneToOne Two state" (Figure S25). When using OneToOne Two state kinetic evaluation model, the fitted curves of Figure S25 (Black) were produced. OneToOne Two state model is an interaction model which assumes that the initial interaction is weak, but as the protein partners come together the binding affinity

increases. Table S13 is also generated from this model. B_{max} is the maximum signal which depends on the number of receptors, BI describes the mass effect and is often specific for each curve, ka_1 [$1/(M \cdot s)$] is the association rate constant for the first association, kd_1 [$1/s$] is a constant of the dissociation rate for the first association, ka_2 [$1/s$] is a constant association rate for the second association and kd_2 [$1/s$] is the dissociation rate constant for the second association. In the OneToOne TwoState interaction model equation (see below), Y is the recorded signal, $A1B$ is the primary complex, which turns into the $A2B$ secondary complex. B is the unbound target and c is the concentration of ligand.

$$\frac{dB}{dt} = - (ka_1 \cdot B \cdot c - kd_1 \cdot A1B)$$

$$\frac{dA1B}{dt} = (ka_1 \cdot B \cdot c - kd_1 \cdot A1B) - (ka_2 \cdot A1B - kd_2 \cdot A2B)$$

$$\frac{dA2B}{dt} = (ka_2 \cdot A1B - kd_2 \cdot A2B)$$

$$Y = A1B + A2B$$

$$A1B(t = 0) = A2B(t = 0) = 0, B(t = 0) = B_{max}$$



Figure S23. α -Syn injections 10 μ M, 20 μ M, 5 μ M and 2.5 μ M with reference channel.

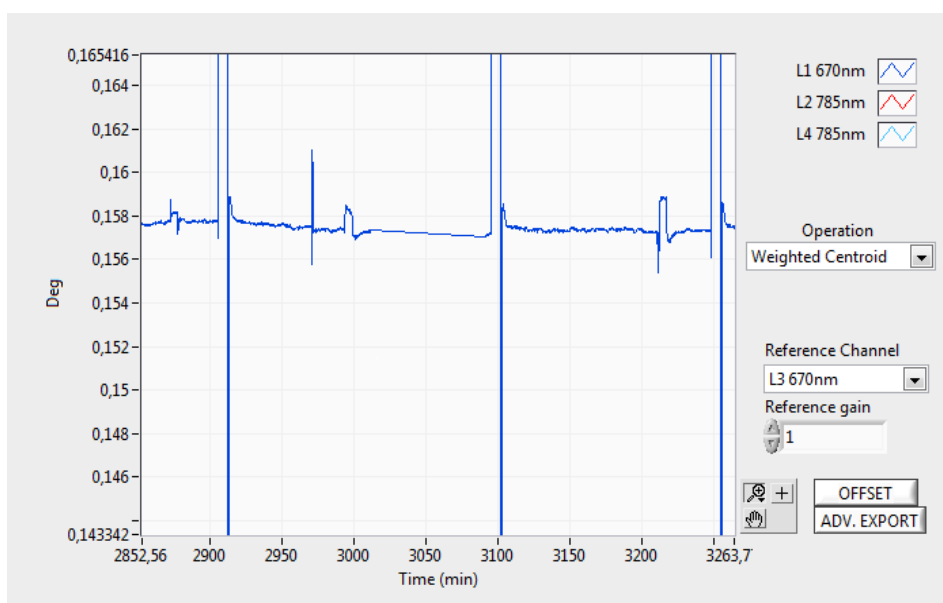


Figure S24. α -Syn injections 1 μ M, 15 μ M and 40 μ M with reference channel.

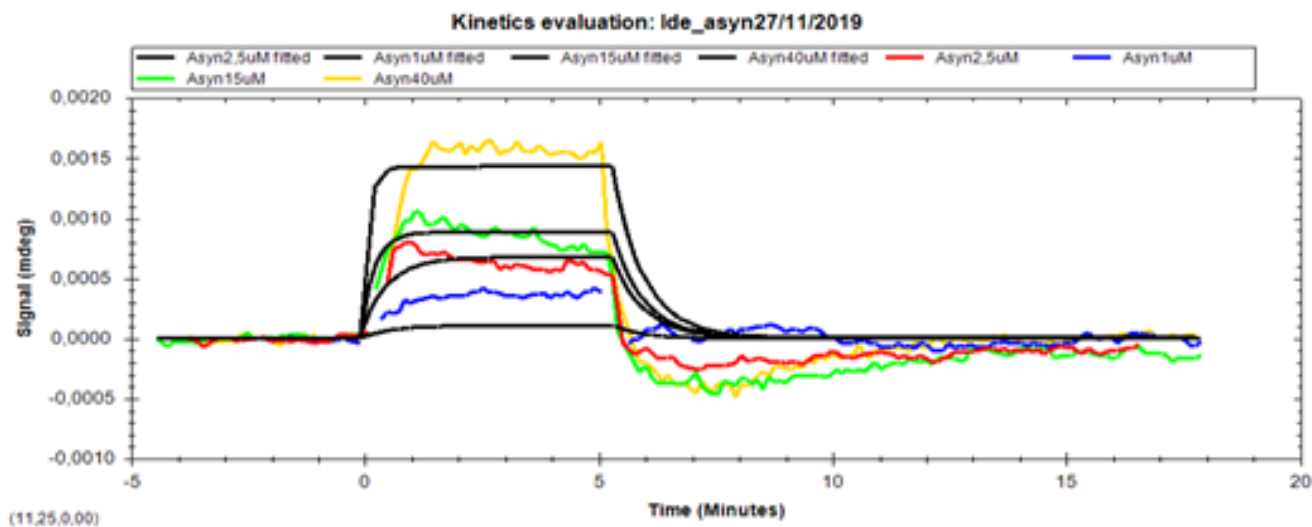


Figure S25. Fit of the experimental curves using the "OneToOneTwoState" kinetic evaluation mode

Table S13. "OneToOneTwoState" model for α -Syn with IDE.

α -Syn (μ M)	ka_1 (1/(M·s))	kd_1 (1/s)	KD (M)	ka_2 (1/(M·s))	kd_2 (1/s)
2,5	2,14e3	2,51e-2	5,88e-5	1,90e-5	9,51e-5
40,0	2,14e3	2,51e-2	5,88e-5	1,90e-5	9,51e-5
1,0	2,14e3	2,51e-2	5,88e-5	1,90e-5	9,51e-5
15,0	2,14e3	2,51e-2	5,88e-5	1,90e-5	9,51e-5

Alternatively, the OneToOne model was used (Figure S26), producing a better fitting of the experimental curves. OneToOne creates a normal 1: 1 interaction for a monovalent ligand binding on a target. It is the simplest model of an interaction; in many cases it is close to reality. Table S14 is generated from this model were the parameters are similar to that of OneToOneTwo state model except there is only one association/dissociate constant. The OneToOne interaction model equation is:

$$\frac{dY}{dt} = (ka \cdot c - kd) \cdot Y$$

$$Y(t = 0) = 0, \text{ saturated target signal} = B_{max}$$

The calculated values of K_D in the OneToOne is $2.03e-4$ M, while in the OneToOneTwoState is $5.88e-5$ M. As the curves are better fitted by using the OneToOne model, it is possible that $2.03e-4$ M is a more reliable value for the K_D of this interaction at these experimental conditions.

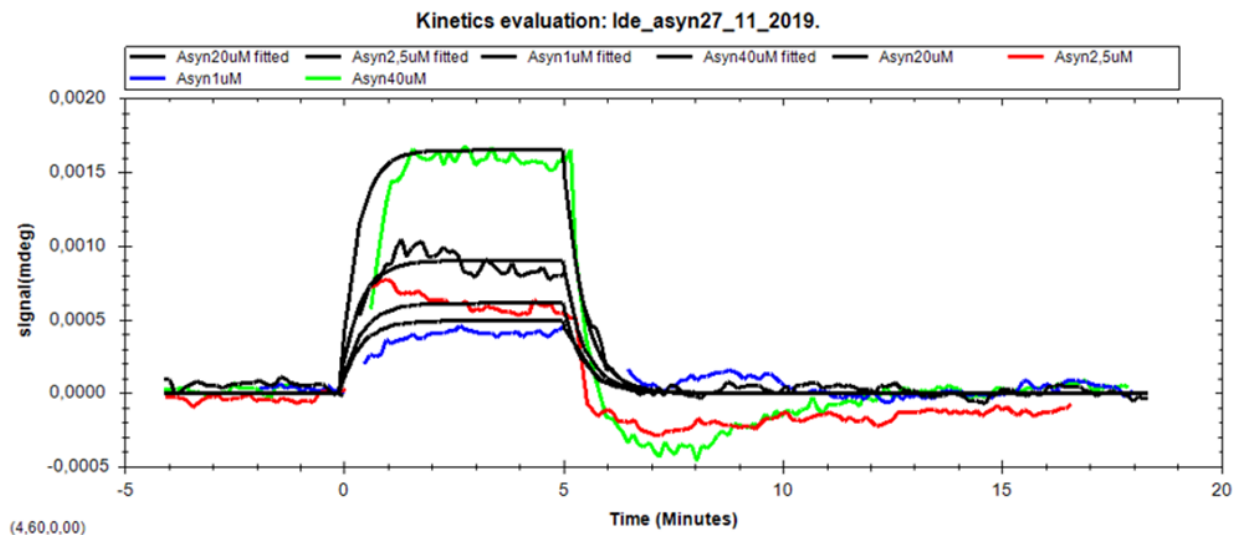


Figure S26. Fit of the experimental curves using the "OneToOne" kinetic evaluation method.

Table S14. OneToOne model for α -Syn with IDE.

α -Syn (μ M)	B_{max} ([signal(mdeg)])	k_a ($1/(M \cdot s)$)	k_d (1/s)	K_D (M)
1,0	0,10	$1,77e2$	$3,58e-2$	$2,03e-4$
2,5	0,05	$1,77e2$	$3,58e-2$	$2,03e-4$
20,0	0,01	$1,77e2$	$3,58e-2$	$2,03e-4$
40,0	0,01	$1,77e2$	$3,58e-2$	$2,03e-4$